Carbon Dioxide Physical Foaming of Polymer Blends:

-Blend Morphology and Cellular Structure-

Rahida Wati Binti Sharudin

2012

Contents

Chapter IV

Preparation of Microcellular Thermoplastic Elastomer Foams from Polystyrene-b-polybutadiene-b-polystyrene (SEBS) and their Blends with Polystyrene

Chapter I

General Introduction

1.1. Polymer Foam

Polymer foam is defined as a gaseous void surrounded by matrix phase, generally liquid or solid phase.[1] Nowadays, a broad range of cellular materials based on polymers, are readily available and their structures are as versatile as their application. An increased in demand on foamed products led to the necessity to improve the cell structure, especially to reduce the cell size from microcellular to nanocellular-scaled size. As the properties of polymer foams are closely related to their cell structures and densities, controlling the cell size at nano-scaled, nanocellular foam promises a significant reduction in thermal conductivity, and an improvement in toughness and light weight.[2]

1.2. Foaming Process

Polymers are foamed by using thermodynamic instability of a polymer/gas system. This process is necessary to promote bubble in the polymer matrix via physical and chemical foaming. Physical and chemical foaming involve four basic steps which are polymer/gas solution formation, bubble nucleation, suppression of cell coalescence and cell growth as shown in Figure 1.1.[3] These basic steps are applied to batch and continuous foaming processes.

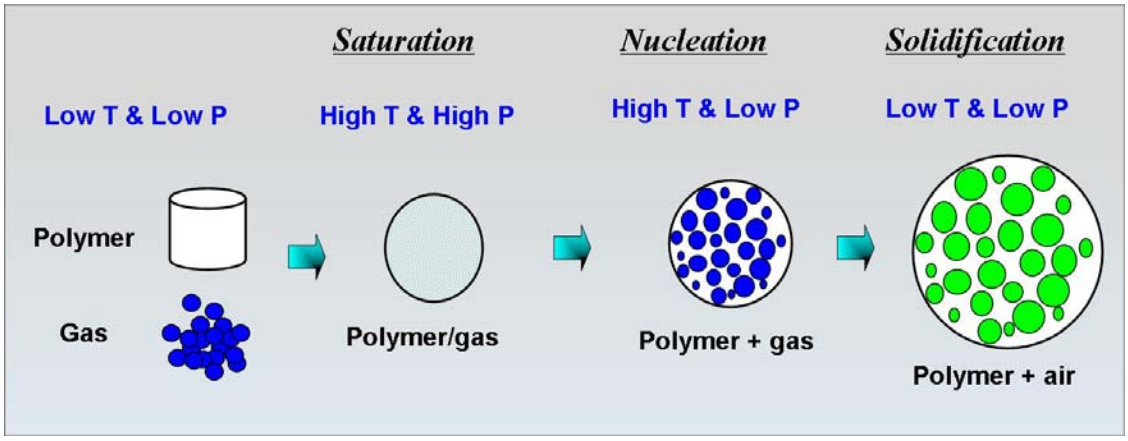

Figure 1.1 Schematic diagram of basic steps in polymer foaming.

1.2.1. Physical Foaming

The knowledge of physical phenomena governing microcellular processing of polymer led to the implementation of microcellular batch process and continuous process. In batch foaming, as shown in Figure 1.2, polymer is first placed in a high pressure vessel where the sample is saturated with physical blowing agent under high pressure and ambient temperature. Then, a thermodynamic instability is induced by rapidly dropping the solubility of gas in the polymer sample. This is accomplished by releasing the pressure (pressure quench) or heating the sample (temperature quench).

In the continuous foaming process which usually takes place by extrusion process, a soluble amount of blowing gas is initially injected into a polymer melt stream to form polymer/gas homogeneous solution. Then, the large injected gas bubbles are broken into smaller bubbles and stretched through shear mixing. Eventually, the polymer is foamed when the single phase mixture is passed through a die by sudden drop in pressure.[1]

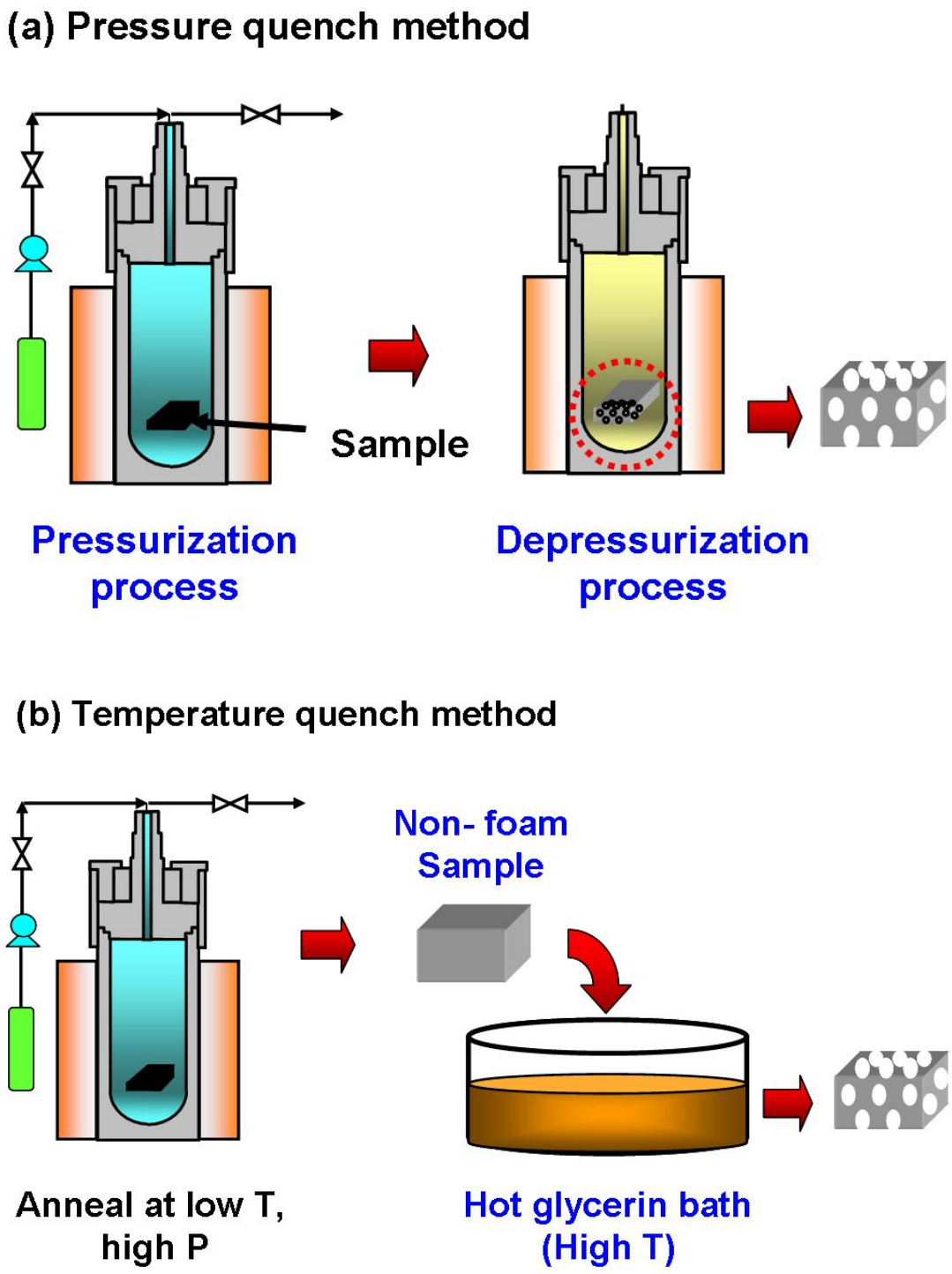

Figure 1.2. Schematic diagram of batch foaming process.

1.2.2. Chemical Foaming

Chlorofluorocarbons (CFCs) and some hydrochloroflourocarbons (HCFCs) were banned because they deplete ozone layer and consequently contribute to greenhouse effect. Therefore the use of chemical blowing agent (CBA) has gained interest because they are more environmental friendly as compared to CFCs and HCFCs. In chemical foaming, CBAs are usually added into a polymer in solid form and activated through addition of heat by releasing gas mainly nitrogen (N_2), carbon dioxide (CO_2) and water.[4]

Rubber is widely foamed via chemical foaming process. Ariff *et al.*[5] and Najib *et al.*[6] prepared natural rubber foams using sodium bicarbonate as blowing agent. Liu *et al.*[7] utilized azobisformamide to produce silicone rubber foam. Another examples of CBAs are azodicarbonamide[8-10] and celogen[11] which have been widely reported in numerous studies.

1.3. Blowing Agent for Foaming

A blowing agent expands the polymer upon reduction of gas solubility through heating or reducing the pressure. In the early years of the foaming technology, the most popular blowing agents are CFC, hydrocarbons, and chlorinated hydrocarbons.[3] CFCs are good blowing agents for preparing high cell density and narrow size distribution of cells.[12] However, they are more expensive than hydrocarbons and harmful to ozone layer. The destruction of ozone layer was due to the presence of chlorine (Cl_2) and bromine (Br_2) from degradation of CFCs compounds.[13] Over the years, many types of blowing agents have been utilized to replace the used of CFC and HCFC such as PBA, CBA and hydrocarbon.[14]

CBAs are compounds in solid and liquid phases that decompose to form gases. They are simply compounded with polymer matrix and do not require any modification of the existing equipment.[3] Sodium carbonates is one of the earliest CBAs used to produce polymer foam since 1900's.[4]

Since the foaming process with CBA is complicated, PBA is more favorable choice because it is non toxic and nonflammable.[15] PBAs are generally comprised of low boiling volatile liquids such as halogenated hydrocarbons, ethers and alcohols. Hydrocarbons like *n*-butane, isobutene and *n*-heptane are also largely used as PBAs. Different type of physical blowing gas affected the cell properties of final foam product. Kim *et al.*[16] for example, studied the effect of various physical blowing agents on thermoplastic vulcanizate (TPV) foams in extrusion foaming process. They claimed that N_2 and CO_2 produced TPV foams with small cell size as well as uniform cell structure as compared to *n*-butane and water. Gendron *et al.*[17] studied the effect of HCFC-142b, *n*-pentane and CO_2 on various types of polyolefin resins; PP, low density polyethylene (LLDPE) and high density polyethylene (HDPE). They found that the degree of plasticization in polyolefin resins is proportional to the ratio between molecular weight of the repeat unit of the resin and the molecular weight of the physical blowing agent. Kim *et al.*[18] make used of *N, N'-dinitroso pentamethylene tetramine* (DPT) as blowing agent to prepare good cell properties of natural rubber foam.

However, CO_2 remains the most commonly blowing agent used in foam industry. Supercritical CO_2 ($scCO_2$) known as ''tuneable solvent'' can be used to plasticize and to reduce the viscosity of polymer.[19-21] Besides, $scCO_2$ provides a solution to problems associated with the use of biopolymers due to its inertness.[12]

There are also studies reported on the use of a mixture of blowing agents for foaming. Since single blowing gas may not perform adequately in some cases, a mixture of blowing gases probably more suitable to match the desired cell properties.[12]

1.4. Homopolymer Foaming

In the last decades, many studies have been devoted on homopolymer foaming. Significant efforts have led to the production of foamed materials, in many applications and have enabled developments in foaming area. Most commercial thermoplastic foams deals with the foaming of homopolymer while with blend foaming is still limited.[2] As reported in literature, homopolymer foaming usually produced poor cell properties like large cell size, low cell density and non-uniform cell structure due to poor properties of polymer itself.[25] For example, Corre *et al.*[26] claimed that a narrow foaming window of PLA is due to its poor melt viscosity and elasticity. They proposed a modification of neat PLA through chain extension with epoxy additive to enhance the elasticity prior foaming. At the same time, Mihai *et al.*[27] showed that PLA foams exhibited low cell uniformity. Kim *et al.*[9] pointed out that EVA/ NR blend foam has lower density, improved rebound resilience and greater tear strength as compared to EVA foam. This is achieved through monitoring crosslinking behavior between EVA and NR.

Semicrystalline polymer like PP, high density polyethylene (HDPE), poly (ethylene terephthalate) (PET) and polybutylene (PB) offer good mechanical properties, high melting point, excellent chemical resistance and acceptable range of mechanical properties. Semicrystalline polymers are relatively cheaper than other polymers. Therefore they are favorable in many applications.[28] However, they are not easy to be foamed. High degree of crystallinity of semicrystalline polymers contributes to poor melt

strength and low melt drawability.[29] It is difficult to control the cellular structure of semicrystalline polymer foams because blowing gases do not dissolve in the crystalline phase. Thus, cell nucleation is inhomogeneous due to the heterogeneous nature of the semicrystalline polymer.[30]

Naguib *et al.*[31] also studied on PP foaming. Their foamed PP products showed high open-cell content which unsatisfactory for many applications. They claimed that cell walls are ruptured easily during foaming due to weak melt strength possessed by PP. Lee *et al.*[32] incorporated long chain branches for isotactic PP to enhance its melt elasticity. This to ensure the foaming of PP progressed well.

In addition to PP, low viscosity of neat PET is also not suitable for foaming. Branching and cross linking are needed to be carried out on PET prior to foaming process.[33]

1.5. Polymer Blend

Basically, polymer blend is a mixture of two or more polymers in which the second polymer should be higher than 2 wt%. Below that level, the second polymer is considered as an additive.[12] Recently, polymer blend gains considerable interest among researchers due to its advantages can be obtained from blending different polymers such as;[34-36]

i. Providing materials with desired properties at the lowest price compared to a cost needed for developing new polymer;
ii. improving specific properties which are not possessed by homopolymer alone; and,
iii. offering useful and economic means for municipal plastics waste recyling.

The addition of one macromolecular species to another via physical means yields polymer blend that can form a wide variety of morphologies. Polymer blend can generally be classified as compatible or incompatible. Compatible polymer blends are composed of chemically dissimilar macromolecules that are combined to produce miscible or immiscible mixture. In contrast, incompatible polymer blend consists of species that are strongly repulsive which cannot be made miscible by thermal means alone.[37] Generally, when two polymers are blended together, the resulting morphology will be composed of a major phase (matrix) and a minor phase (dispersed domain).[38] The blend maybe either compatible or incompatible type.

Blend morphology plays a critical role in foaming.[12] However, this morphology depends on the viscosity of polymer. For the case of incompatible binary blend system, the viscosities of each polymer will determine which one forms the matrix phase and dispersed domain regardless of the amount of constituent polymers present. The less viscous polymer forms the matrix phase while the more viscous polymer tends to form the dispersed domain as shown in Figure 1.3 (a). The dispersed domain usually appears spherical in shape as it tries to minimize the surface energy.[34] When the concentration of polymer which formed the dispersed domain increases, the morphology is changed to co-continuous type as shown in Figure 1.3 (b).

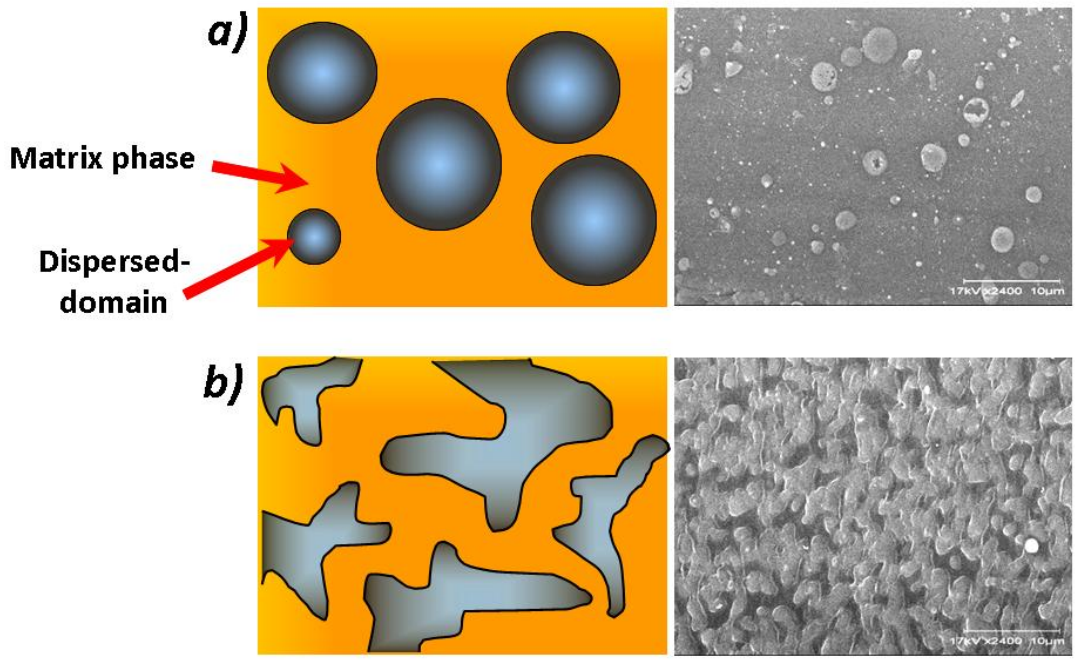

Figure 1.3 Binary blend morphology: (a) Droplet-type and (b) Co-continuous type.

1.5.1. Polymer Blend Foaming

Foaming of polymer blend is considered to be a solution to problems associated with the homopolymer foaming. To date, there are several studies done on the utilization of polymer blend to improve the foaming processability by enhancing the rheological properties,[39] to work as nucleating agent,[40,41] and manipulate the mechanical strength.[42-45]

Based on the basic idea, heterogeneous nucleation is induced at the interface when foreign body is added into one polymer. Nucleating agents are used for providing large number of nucleation sites.[46-51] Many papers discussed about the usage of inorganic particles such as rubber particle,[40,41] talc[52-55] or nanoclay[56-61] to induce heterogeneous nucleation. Guo *et al.*[62] claimed that carbon nanofiber (CNF) and activated carbon (AC) successfully enhanced the bubble nucleation in PS foaming.

At the same time, Ema *et al.*[63] found that incorporation of nano-clay induced heterogeneous nucleation lowered the activation energy barrier as compared to homogeneous nucleation. Regardless of type of nucleating agent used, the same conclusion was drawn out where the small amount of nucleating agent promotes the heterogeneous bubble nucleation. However, the uses of these traditional nucleating agents are often led to the non-uniform cell structures of final foam products. This is because their sizes are too large and prone to agglomeration.[64] Due to this aggregation problem, nanocomposites synthesis is performed to control the dispersion and distribution of nanoparticle on a polymer matrix. However, this approach is still under research.[1]

Block or graft copolymers which can form micelles have been studied as heterogeneous nucleation sites for enhancing the cell properties in one polymer. Spitael *et al.*[49] investigated the use of spherical block copolymer micelles to aid bubble nucleation in PS matrix. They found that none of the PS/ diblock copolymer blend showed a significant increase in cell density compared to neat PS foam. Three main factors which hindered the effectiveness of these block copolymer micelles are identified; i.e. aggregation of micelles, high surface tension of more core components of diblocks and the size of micelles is near the critical size of nucleating bubble. Systematic study of diblock copolymers' effects on bubble nucleation is still needed.

1.6. Aim of Tailoring the Foaming Behavior via Different Pairs of Polymer Blend

An increased in demands on foamed products often led to the necessity to improve the cell structure, especially to reduce the cell size. Thus, the uses of additives become

attractive in foaming process. It is believed that the addition of such additives like inorganic particle lowers the free energy barrier for bubble nucleation in polymer[46]. As reported by previous studies, the improvement of cell properties in polymer could be achieved by blending with second constituent either polymer or inorganic particle. However, there are some limitations of using second constituent as nucleating agent. For the case of traditional nucleating agent, aggregation problem tend to be a key factor in reducing their effectiveness to aid bubble nucleation. In spite of that, the use of diblock copolymers in polymer foaming still new and a clear understanding on their role in the bubble nucleation process is lacking.[49]

This thesis deals with topics closely related to foaming of polymer blends. For polymer blend foaming, the improvement of cell properties is not simply taking the advantage of adding second polymer as nucleating agent. It is a process of controlling the bubble location and nucleation based on different physical properties possess by each polymer. The understanding of controlling the bubble nucleation would facilitates future development of new blend foam product. In fact, choosing the appropriate pairs of polymers is also essential to facilitate the controllability of both bubble location and nucleation in polymer blend.

The selection of foam products is made in accordance to its properties and resulted cell structures. These cell properties and cell structures however, are determined by controlling the bubble location and nucleation. Therefore, it is believed that a thorough study on controlling the bubble nucleation is indispensable in polymer blend foaming. Despite that, only a few studies have been reported on preparing polymer blend foam with consideration of controlling the bubble location. The aim of present work is to

exploit different type of polymer blend for preparing foam product with improved cell properties by controlling the bubble location and nucleation.

This work deals with two-phases blend systems where droplet-type morphology is exploited as a template for foaming. As shown in Figure 1.4, the aim of this work is to control the location of bubble either in dispersed domain, matrix phase or at the interface. In order to control the location of bubble in binary blend system, the following key factors have to be considered;

i. Rheological properties;

ii. solubility and diffusivity of CO_2 in each polymer; and

iii. the interfacial properties between the blend components

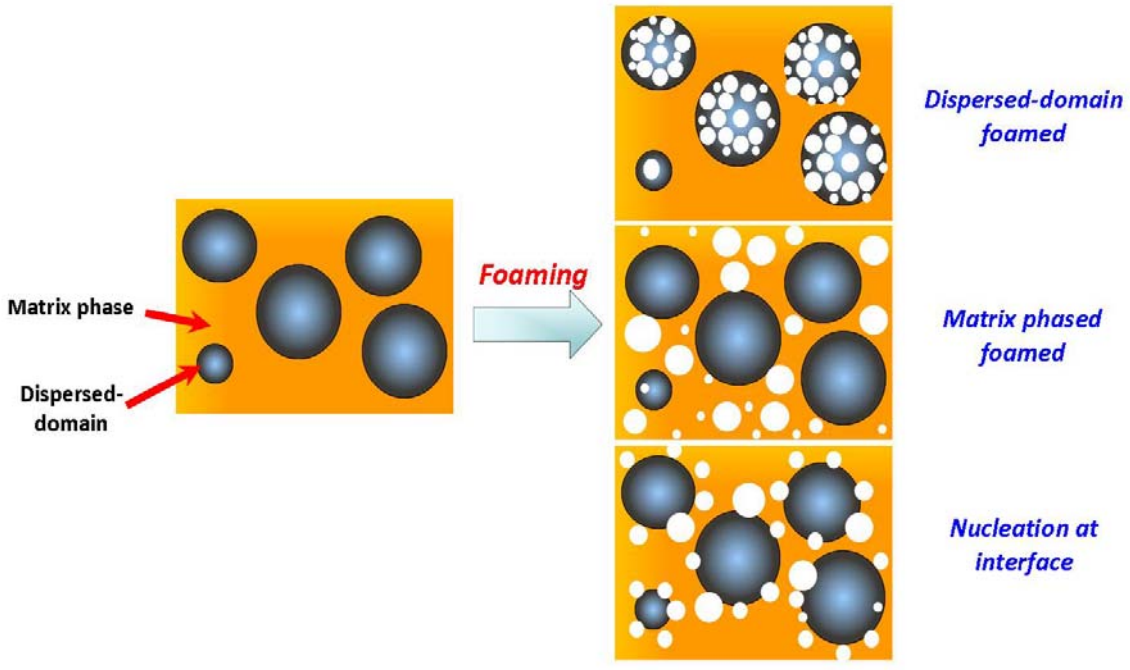

Figure 1.4 A target location of nucleated bubble based on binary blend system.

In regards to the mentioned factors, the controllability of bubble nucleation and location in binary blend system will be introduced. Relationship between cell structure, foaming condition and polymers' properties will be explained in all blend systems.

1.7. Strategies for Controlling the Bubble Nucleation in Polymer Blend System.

The controllability of bubble nucleation and location is depending on type of blend system. For the case of blend system which consists of polymer and inorganic particle, the location of nucleated bubble is controllable only in polymer. Even though blending polymer with inorganic particle allows improvement of cell density, the foaming of polymer/inorganic particle system has some drawbacks. The presence of agglomerated particle usually inhibits bubble nucleation or act as disturbance for polymer foaming. For example, clay particle contains crystallite layers which stacking together to form the agglomerated clay. Special approaches such as nanocomposite synthesis and development of surface chemistry are needed to separate these crystallite layers.[1] Besides, several studies reported that polar interaction between polymer and clay surface is the key factor in achieving particle dispersion on polymer matrix.[1]

As a result of non-uniform dispersion of inorganic particle in polymer matrix, the overall cell uniformity still remains as a crucial problem for development of novel cellular material. This problem leads to the deterioration of foamability which reflects the overall foam homogeneity and final cell properties. In order to overcome these drawbacks, the following approaches are proposed for controlling the bubble nucleation and location in polymer blend systems;

i. Using blend morphology as a template for foaming by appropriately choosing the polymer pair;
ii. controlling the dispersibility of dispersed domain in polymer matrix by viscosity and temperature;
iii. utilizing nano-scaled dispersed domain for reducing cell size from macro-scaled to nano-scaled cell size;
iv. selecting suitable foaming conditions; and
v. performing batch foaming to control the gas sorption into polymer.

1.8. Aim of the Thesis

The aim of this thesis is to control the bubble nucleation and location in polymer blend based on different physical properties of polymers as well as foaming conditions like temperature, pressure and depressurization rate. This work considers four blend systems namely polystyrene (PS)/ polypropylene (PP), poly (methyl methacrylate) (PMMA)/ PP, PP/ polystyrene-b-polybutadiene-b-polystyrene (SEBS) and PS/ SEBS blends in attempt to understand how controlling the bubble location and nucleation affects the properties and cellular structure of blend foams. The fundamental relationship between blends' properties and selective blending system on the foaming behavior is investigated to control the location of nucleated bubble.

1.9. Outline of the Thesis

Polymer blending posses many advantages over the homopolymer foaming where some of the polymer functionalities like foamability could be improved by blending. Besides, the weakness of one polymer could be compensated by other polymer. In

addition, the enhancement in cell density could be achieved through heterogeneous nucleation. Polymer blend offers a solution to the problem faced by homopolymer foaming like low foamability, non uniform cell structure, narrow processing condition, foam shrinkage and etc.

In order to overcome the problem related to homopolymer foaming, the addition of second constituent like polymer, inorganic particle or diblock copolymer appears advantageous. However, as demonstrated by the literature, polymer blend foaming with inorganic particle unable to achieve desired cell uniformity, as reflected by poor dispersibility of particle on polymer matrix. In addition, the location of nucleated bubble cannot be controlled neither by viscosity nor temperature. Therefore, the present work aims to introduce a novel concept to enhance the foamability of polymer blend system by controlling the bubble nucleation and location based on the polymers' physical properties as well as processing parameters.

The controllability of bubble nucleation is the main focus in each chapter. In chapter 2, the bubble nucleation was controlled at the polymer interface. The impacts of high interfacial tension between PS/PP and PMMA/PP blends in lowering the stability of bubbles in matrix as well as in dispersed domain are discussed. In particular, this study addresses the role of PP dispersed domain as nucleating agent in inducing heterogeneous bubble nucleation in PS and PMMA solid-state foaming.

In chapter 3, the nano-scaled dispersed domain of SEBS is utilized for preparing nanocellular foam and the exploitation of SEBS in templating the foaming of PP/SEBS blend system is further studied. The bubble nucleation is aimed to be located in SEBS dispersed domain to reduce the cell size from micro-scaled to nano-scaled cell size. Small

cell and high cell uniformity of foam is expected to be prepared by taking the advantage of controlling bubble location in nano-scaled SEBS dispersed domain together with its well dispersibility on PP matrix. Foam with reduced cell size, improved cell uniformity, a potentially higher bubble nucleation in SEBS dispersed domain, and enhanced mechanical strength improved the performance of PP/SEBS blend foam product.

Chapter 4 is focusing on the reduction of foam shrinkage in elastomer foaming. The aim of this study is to control the bubble location in SEBS matrix. In order to ensure the foaming is taken place in SEBS matrix, high viscous polymers like PS and PP are blended into SEBS. These kinds of polymers are chosen to restrict the bubble to nucleate in PS or PP dispersed domains as compared to in SEBS matrix. While combining polymer blending and foam processing potentially allows the reduction of foam shrinkage in SEBS, controlling the bubble nucleation and location are still needed.

In summary, controlling the bubble nucleation and location in selective blending system allows for enhancement of cell properties as stated follows;

i. Improving the cell uniformity through well dispersibility of dispersed domain on polymer matrix;
ii. increasing the cell density by heterogeneous nucleation induced at the polymer interface; and
iii. reducing the foam shrinkage in elastomer foam.

These results show that controlling the bubble nucleation is beneficial for preparing improved cell properties of polymer blend foams.

Summary of thesis

	Chapter 2	***Chapter 3***	***Chapter 4***
Title	PP dispersed-domain as nucleating agent for PS and PMMA solid-state foaming.	CO_2-induced reinforcement of mechanical properties of polyolefin-based nanocellular foams.	Preparation of microcellular thermoplastic elastomer foams from polystyrene-b-polybutadiene-polystyrene (SEBS)/ and their blends.
Expectation result	Enhancement of cell densities in PS and PMMA through heterogeneous nucleation at the interface.	Improvement of cell density, cell uniformity and widened the foaming window of PP.	Reduction of foam shrinkage in SEBS foam.
Scheme structure (target location of bubble)	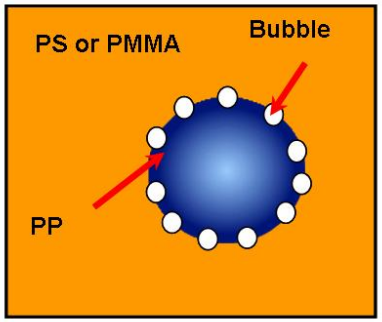	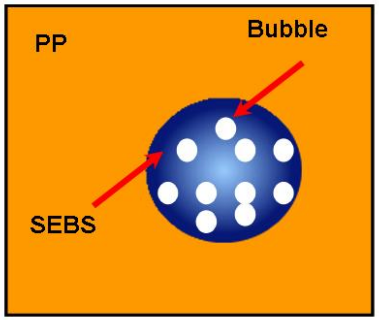	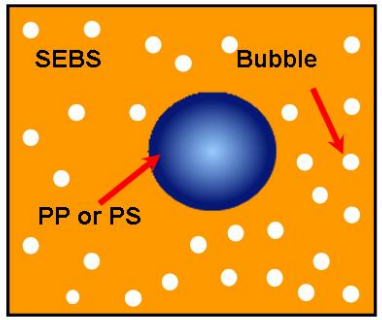

1.10. References

[1] L. J. Lee, C. Zeng, X. Cao, X. Han, J. Shen, G. Xu, *Composites and Tech.* **2005**, 65, 2344.

[2] H. Ruckdashcel, P. Gutmann, V. Alstadt, H. Schmalz, A. H. E. Muller, *Adv. Polym. Sci.*, **2010**, 227, 199.

[3] S. T. Lee, *Foam Extrusion: Principles and Practices*, **2000**, Technomic Publishing Co. Inc.

[4] S. T. Lee, D. P. K. Scholz, *Polymeric Foams: Technology and Development in Regulation, Process and Products*, CRC Press, **2008**, 10.

[5] Z. M. Ariff, Z. Zakaria, L. H. Tay, S. Y. Lee, *J of App. Polym. Sci.*, **2008**, 107, 2531.

[6] N. N. Najib, Z. M. Ariff, A. A. Bakar, C. S. Sipaut, *Materials and Design*, **2011**, 32, 505.

[7] P. Liu, D. Liu, H. Zhou, P. Fan, W. Xu, *J of App. Polym. Sci.*, **2009**, 113, 3590.

[8] H. J. Tai, *J of Polym. Research*, **2005**, 12, 457.

[9] M. S. Kim, C. C. Park, S. R. Chowdhury, G. H. Kim, *J of App. Polym. Sci.*, **2004**, 94, 2212.

[10] R. Gendron, C. Vachon, *J of Cellular Plastics*, **2003**, 39, 71.

[11] R. P. Ilier, K. H. Lee, C. B. Park, *J. of Cellular Plastics*, **2006**, 42, 139.

[12] R. B. McClurg, *Chem. Eng. Sci.*, **2004**, 59, 5779.

[13] R. Gendron, *Thermoplastic Foam Processing: Principles and Development*, **2005**, CRC Press.

[14] S. N. Leung, A. Wong, Q. Guo, C. B. Park, J. H. Zhong, *Chemical Eng. Sci.*, **2009**, 64, 4899.

[15] X. Min, J. Shen, H. Huang, D. L. Tomasko, L. J. Lee, *Polym. Eng. and Sci.*, **2007**, 104.

[16] S. G. Kim, C. B. Park, M. Sain, *J. of Cellular Plastics*, **2008**, 44, 53.

[17] R. Gendron, M. F. Champagne, *J of Cellular Plastics*, **2004**, 40, 131.

[18] J. H. Kim, K. C. Choi, J. M. Yoon, *J Ind. Eng. Chem.*, **2006**, 12(5), 795.

[19] I. Kikic, F. Vecchione, *Current Opinion in Solid State and Material Sci.*, **2003**, 7, 399.

[20] T. L. Sproule, J. A. Lee, H. Li, J. J. Lannutti, D. L. Tomasko, *J of Supercritical Fluids*, **2004**, 28, 241.

[21] H. Zhou, J. Fang, J. Yang, X. Xie, *J. of Supercritical Fluids*, **2003**, 26, 137.

[22] W. Zhai, Y. Ko, W. Zhu, A. Wong, C. B. Park, *Int. J. Mol. Sci.*, **2009**, 10, 5381.

[23] N. Naga, Y. Yoshida, M. Inui, K. Noguchi, S. Murase, *J of App. Polym. Sci.*, **2011**, 119, 2058.

[24] A. V. Gonzalez, P. S. Paternault, A. M. L. Periago, C. A. G. Gonzalez, C. Domingo, *European Polym. Journal*, **2008**, 44, 1081.

[25] S. Pilla, S. G. Kim, G. K. Auer, S. Gong, C. B. Park, *Material Sci. and Eng. C*, **2010**, 30, 255.

[26] Y. M. Corre, A. Maazouz, J. Duchet, J. Reignier, *J of Supercritical Fluids*, **2011**, 58, 177.

[27] M. Mihai, M. A. Huneault, B. D. Favis, H. Li, *Macromolecular Bioscience*, **2007**, 7, 907.

[28] C. B. Park, L. K. Cheung, *Polym. Eng. and Sci.*, **1997**, 37(1), 1.

[29] Y. Jahani, M. Barikani, *Iranian Polym. Journal*, **2005**, 14 (4), 361.

[30] Z. M. Xu, X. L. Jiang, T. Liu, G. H. Hu, L. Zhao, Z. N. Zhu, W. K. Yuan, *J. of Supercrit. Fluid*, **2007**, 41, 299.

[31] H. E. Naguib, C. B. Park, N. Reichelt, , *J of App. Poly. Sci.*, **2004**, 91(4), 2661.

[32] P. C. Lee, H. E. Naguib, C. B. Park, J. Wang, *Polym. Eng. and Sci.*, **2005**, 1445.

[33] S. T. Lee, C. B. Park, N. S. Ramesh, *Polymeric Foam: Technology and Science*, **2007**, CRC Taylor & Francis.

[34] L. A. Utracki, *Polymer Blends Handbooks*, **2002**, 1, Kluwer Academic Publihers.

[35] T. S. Valera, A. T. Morita and N. R. Demarquette. *Macromolecules,* **2006**, 39, 2663.

[36] V. Rek, N. Vranjes, M. Slouf, I. Fortelny, Z. Jelcic, *J. of Elastomers and Plastics*, **2008**, 40, 237.

[37] T. A. Walker, D. J. Frankowski, R. J. Spontak, *Adv. Mater.*, **2008**, 20, 879.

[38] M. Hemmati, H. Nazokdast, H. S. Panahi, *J. of App. Polym. Sci.*, **2001**, 82(5), 1129.

[39] M. Yamaguchi, K. I. Suzuki, *J. Polym. Sci. Part B : Polym. Phys.*, **2001**, 39, 2159.

[40] N. S. Ramesh, D. H. Rasmusen, G. A. Campbell, *Polym. Eng. Sci.*, **1994**, 34, 1685.

[41] N. S. Ramesh, D. H. Rasmussen, G. A. Campbell, *Polym. Eng. Sci.*, **1994**, 34, 1698.

[42] Z. Chen, X. Liu, T. Li, R. Lu, *J. of Applied Polym. Sci.*, **2006**, 101, 967.

[43] M. Nikazar, B. Safari, B. Bonakdarpour, Z. Milani, *Iranian Polym. Journal*, **2005**, 14(12), 1050.

[44] S. I. Hirota, T. Sato, Y. Tominaga, S. Asai, M. Sumita, *Polymer*, **2006**, 47, 3945.

[45] C. H. Ho, C. H. Wang, C. I. Lin, Y. D. Lee, *Polymer*, **2008**, 49, 3902.

[46] D. Garcia, *Journal of Polym. Sci.*, **1984**, 22, 2063.

[47] W. Zhai, J. Yu, L. Wu, W. Ma, J. He, *Polymer*, **2006**, 47, 7580.

[48] K. Taki, K. Nitta, S. Kihara, M. Ohshima, *J. of App. Polym. Sci.*, **2005**, *97*, 1899.

[49] P. Spitael, C. W. Macosko, R. B. McClurg, *Macromolecules*, **2004**, 37, 6874.

[50] T. Nemoto, J. Takagi, M. Ohshima, *Macromol. Mater. Eng.*, **2008**, 293, 991.

[51] J. Tatiboue, R. Gendron, A. Hamel, A. Sahnoune, *J. of Cellular Plastics*, **2002**, 38, 203.

[52] Y. Moon, S. W. Cha, *Fibers and Polymers*, **2007**, 8(4), 393.

[53] H. E. Naguib, C. B. Park, P. C. Lee, D. Xu, *J of Polym. Eng.*, **2006**, 26(6), 565.

[54] C. Wang, S. N. Leung, M. Bussmann, W. T. Zhai, C. B. Park, *Ind. Eng. Chem. Res.*, **2010**, 49, 12783.

[55] Y. H. Lee, C. B. Park, K. H. Wang, *J. of Cellular Plastics*, **2005**, 41, 487.

[56] C. C. Ibeh, *J of Cellular Plastics*, **2008**, 44, 493.

[57] Y. H. Lee, K. H. Wang, C. B. Park, M. Sain, *J. of Applied Polym. Sci.*, **2007**, 103, 2129.

[58] C. Jo, H. E. Naguib, *J. of Physics*, **2007**, 61, 861.

[59] J. Shen, X. Cao, L. J. Lee, *Polymer*, **2007**, 47, 6303.

[60] P. H. Nam, P. Maiti, M. Okamoto, T. Kotaka, *Polym. Eng. Sci.*, **2002**, 42, 1907.

[61] K. Taki, T. Yanagimoto, E. Funami, M. Ohshima, *Polym. Eng. Sci.*, **2004**, 44. 1004.

[62] Z. Guo, J. Yang, M. J. Wingert, D. L. Tomasko, L. J. Lee, *J. of Cellular Plastics*, **2008**, 44, 453.

[63] Y. Ema, M. Ikeya. M. Okamoto, *Polymer*, **2006**, 47, 5350.

Chapter II

Polypropylene Dispersed Domain as Potential Nucleating Agent in PS and PMMA Solid-State Foaming

2.1 Introduction

Although various new foam products have been developed recently, improving the cell structure is still important because smaller and more uniform cells can provide good mechanical properties[1-3] as well as significant reduction of the amount of plastics materials[4]. Fine cell structure and high cell density have been shown to be dependent on the bubble nucleation rate in polymers. The nucleation of bubbles can take place via two mechanisms: one is homogeneous and the other heterogeneous[5]. Nucleating agents, such as talc and nano-clay, can be used to induce heterogeneous nucleation for producing a large number of nucleation sites. The addition of a nucleating agent increases the bubble nucleation rate, which enables better control of the cell morphology, cell density, cell size and cell size distribution. The effect of nucleating sites on the cell morphology may depend on the type and size of the nucleating agent[6]. Small-sized and uniformly distributed particles in a polymer matrix would be the most suitable nucleating agents for producing high cell density and small cell size in polymeric foams. There have been many reports on the use of inorganic particle as nucleating agents. In the last decade, the use of nano-sized inorganic particles has been investigated. Wentoa *et al.*[7] indicated that nano-silica aggregates dramatically increased the bubble nucleation rate in PC/nano-silica composites. A pioneering study investigating the use of nano-clay as a bubble nucleating

agent in polymer foam was reported by Nam *et al.*[8]. They found that the addition of nano-clay to polypropylene (PP) drastically reduced the cell size and increased the cell density in PP foam. However, the use of inorganic materials as nucleating agents, especially nano-sized particles such as nano-clay, creates difficulty in terms of dispersibility in the polymer. Organic modification on the surface of inorganic nucleating agents may improve the dispersion, but it reduces the performance of the nucleating agent. Taki *et al.*[9] pointed out that the bubble nucleation could not be drastically improved, but the bubble growth rate was suppressed to keep the cell size small by the addition of an organomodified nano-clay into polymer. The nucleating agent must be uniformly dispersed in the polymer matrix and provide a heterogeneous interface for bubble nucleation. However, both are often competitive and difficult to achieve at the same time[9,10]. An organic nucleating agent could be well dispersed at high temperatures by melt mixing, but it would be immiscible and segregated from the matrix polymer at lower temperatures, so it could be used as an efficient nucleating agent by designing the appropriate processing conditions. Pieter *et al.*[11] reported that micelles with a polydimethylsiloxane (PDMS) core component increase the cell density in blend foaming while polystyrene-b-poly (ethylene propylene) and PS-b-PMMA diblocks were not effective as a nucleating agent. They attributed the improvement in the cell density to the size of the micelles, which is near the critical bubble size, the aggregation of micelles and the high surface tension of the core components. N.S. Ramesh *et al.*[12] studied the effect of a rubber component on the heterogeneous nucleation in high impact polystyrene foams. They claimed existing microvoid in rubber could enhance the bubble nucleation. Recently, Nemoto *et al.*[13] controlled the bubble nucleation sites and size in PP/rubber

blends and prepared a nanocellular foam by using their blend morphology as a template for bubble nucleation where the rubber domain plays the role of bubble nucleating site.

In this study, the potential of using a dispersive polymer domain in blend polymer as a bubble nucleating agent was investigated by exploiting its dispersibility of domain polymer in the matrix polymer in the molten state and its immiscibility in the solid state. We investigated polypropylene as a bubble nucleating agent in polymer blend foams. PP is easily obtained, and its dispersibility in other polymers can be controlled by viscosity and temperature. Due to the higher solubility and diffusivity of CO_2 and N_2, which are often used as physical foaming agents, PP can also be used as a CO_2 reservoir and releaser. Furthermore, PP possesses high interfacial tension with other polymers such as PS and PMMA. Thus, PP can be used as an efficient bubble nucleating agent if the foaming conditions are chosen appropriately. Several experiments on the pressure quench batch foaming in solid-state PS/PP and PMMA/PP polymer blends were conducted to observe the effect of PP dispersed domains on the cell density, cell size and cell structure. This study focused especially on the relationship between the cell morphology and interfacial tension of PP with PS and PMMA.

2.2 Experimental

2.2.1 Materials

Homo-Polypropylene (PP, Mw= 410,000) was supplied by Mitsubishi Chemical. Polystyrene (PS, Mw= 192,000) and Poly (methyl methacrylate) (PMMA, Mw= 120,000) were obtained from Aldrich Chemical Co. All polymers were used as received.

2.2.2 Blend Sample Preparation

The PS/PP and PMMA/PP blends were prepared with a twin-screw extruder (ULT nano05, TECHNOVEL, Japan) at various blend ratios. The details of the processing scheme are as follows. Polymer resins were dry-blended prior to being fed into the hopper. Blending was carried out by twin screws, and the polymer resins were compounded at 220°C for 5 minutes. The screw rotor speed was kept constant at 38 rpm during the extrusion process. The extrudate was then grinded and compression-molded into a disc-shaped sample, 25 mm in diameter and 1 mm in thickness using a hot press at 200°C and 10 MPa for 10 minutes.

2.2.3 Foaming Process

The polymer samples were foamed by a pressure quench method. Samples were first placed in a pressure vessel and heated to the desired temperature. When the temperature reached the desired level, the autoclave was pressurized by CO_2 at a given pressure, and the samples were saturated with supercritical carbon dioxide ($scCO_2$) for 6 hours. After a predetermined sorption time, $scCO_2$ in the pressure vessel was released from the saturation pressure to ambient pressure within 10 seconds. Samples were then removed from the vessel, and the cell structure of the foamed samples was analyzed by SEM (Tiny- SEM, Technex Co. Ltd., Japan). The cell density and cell size were determined from the SEM images with the aid of a software program (Image J). The number of cells per unit volume of foamed sample is determined by

$$N_f = [nM / A]^{3/2} \quad (2.1)$$

where *n* is the number of cells in a micrograph, *A* is the area of the micrograph, and *M* is the magnification factor. The average diameter was calculated by manually measuring the diameter of at least 100 cells on the micrographs. For the cell diameter measurements, the standard deviation is also calculated.

2.2.4 Rheological Characterization

The dynamic storage modulus, G', of each polymer as a function of strain rate was evaluated using a rheometer (ARES). A dynamic temperature ramp test was performed in a rectangular torsion mode in a temperature range from 30 to 200°C. The strain percentage was 10% in the temperature range from 30 to 100°C, 2% for 140°C to 160°C and reduced to 0.1% for 160 to 200°C. The heating rate was 2°C/min at every temperature.

2.3 Results and Discussion

2.3.1 Blend Morphology of PS/PP blend

Figure 2.1 shows the blend morphology of PS/PP at different blend ratios: 90/10, 80/20 and 70/30. In every PS/PP sample, a sea and island morphology, which has spherical shaped dispersive domain of PP in the PS matrix, was observed. As the PP content increased, the number of PP spherical domain increased while the average diameter of the domain remained about 4 μm as listed in Table 2.1.

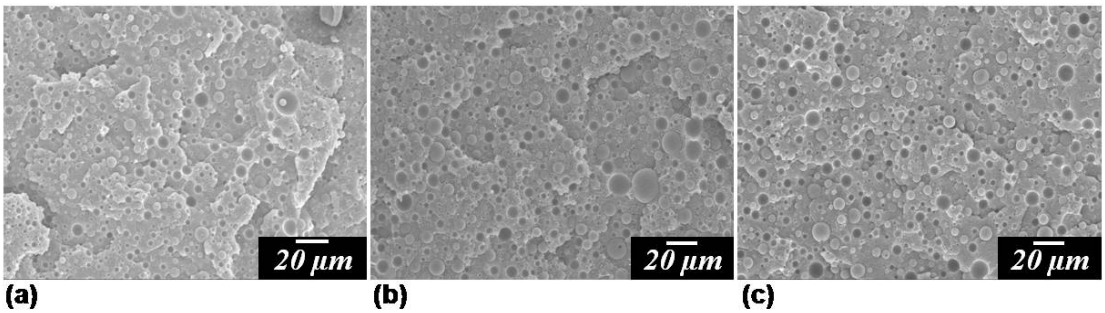

Figure 2.1. SEM micrographs of PS/PP blend morphology at different PP content; (a) 90/10; (b) 80/20, and (c) 70/30

Table 2.1. Average diameter of PP- dispersed domain

Blend ratio (PS/PP)	**d_v of PP in PS/PP blend (μm)**	**d_v of PP in PMMA/PP blend (μm)**
70/30	3.9±1.3	8.6±4.2
80/20	3.8±1.9	6.0±2.6
90/10	3.5±0.8	3.1±1.4

2.3.2 Effect of Foaming Conditions on PS/PP blends

To investigate the effect of foaming temperature, batch foaming experiments were conducted on the PS/PP (80/20) blend at different foaming temperatures, 80, 100 and 120°C, and at a given saturation pressure of 15 MPa. The resulting cell structures were illustrated in Figure 2.2. The temperature dependence was clearly observed in the cell structures; the cell densities of the PS/PP blends foamed at 100°C and 120°C were lower than that of the PS/PP foamed at 80°C. With the increase of foaming temperature, PP/PS blend foam shows the decrease in cell density. As the foaming temperature increases, the diffusivity of CO_2 in polymer increases and the viscosity of the polymer matrix decreases. At high temperature, polymer molecule has high mobility and allows CO_2 to diffuse into

the growing bubbles rapidly. Then, the cell growth rate is increased by the increase in the diffusion rate. As a result, the bubbles grow faster and create cells of larger size at high foaming temperatures. Furthermore, bubbles coalescence rate increases at the temperatures above T_g of PS. The increase in bubble coalescence rate makes the cell size larger.

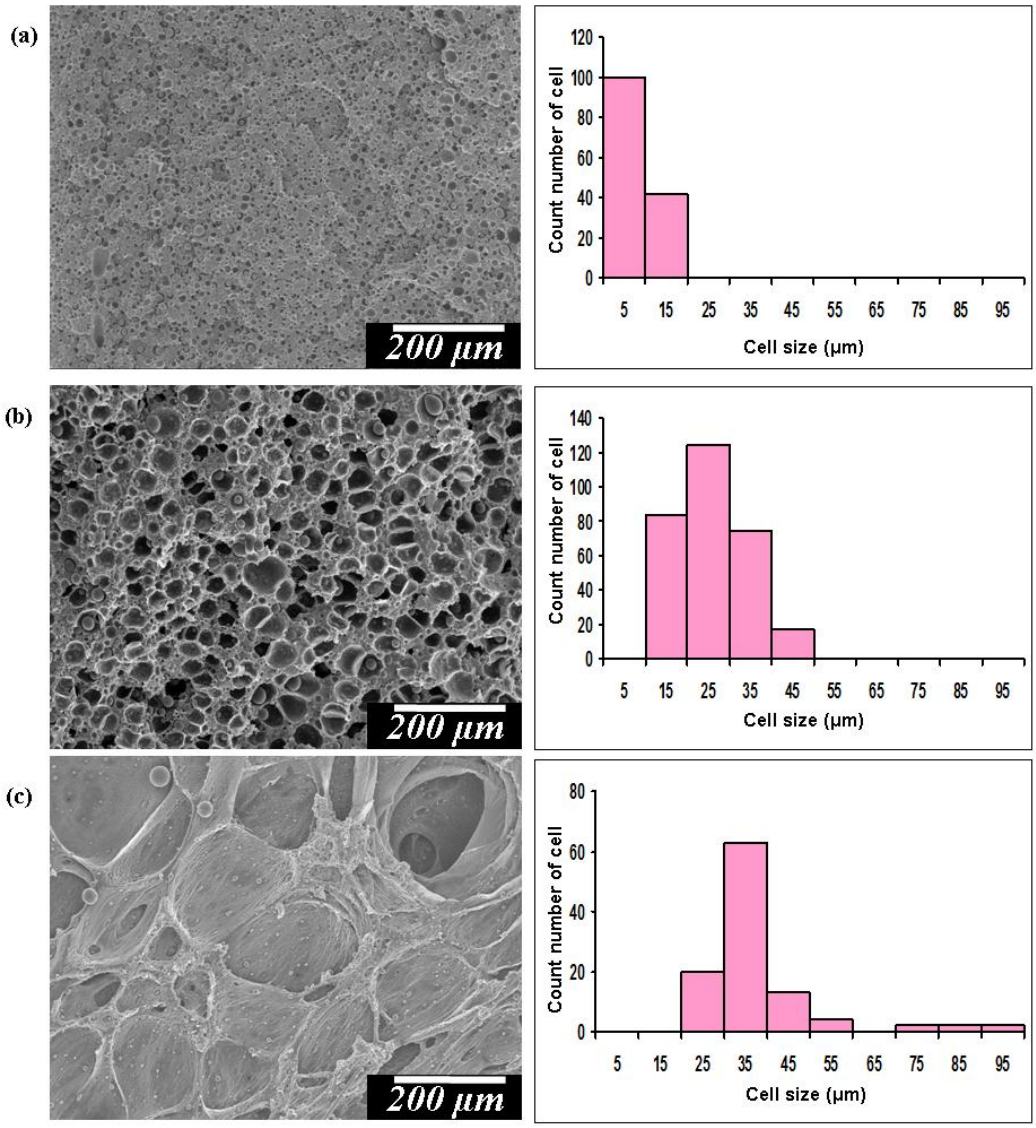

Figure 2.2. SEM images and cell size distribution of PS/PP foams at; (a) 80°C (b) 100°C, and (c) 120°C.

The saturation pressure and pressure release rate have considerable influence on the cell density, which could be observed in Figure 2.3. It shows the SEM images of PS/PP (80/20) foams prepared at the same temperature, 100°C, but different sorption levels of 8, 10 and 15 MPa. The pressure was released within 10 s. Thus, the pressure release rates were approximated to be 0.8, 1 and 1.5 MPa/s for each experiment. It has been reported that the increase in the saturation pressure resulted in a higher cell density[15]. The increase in the saturation pressure resulted in a higher solubility of CO_2 in polymer and a higher cell density. The high concentration of CO_2 in polymer would increase bubble nucleation rate. In Figure 2.3, it is clearly seen that PS/PP foams obtained at higher saturation pressure attained a much smaller cell size with higher cell density.

The effect of the pressure release rate on the PS/PP bubble density and cell size can be clearly seen in Figure 2.4 The PS/PP (80/20) foams were prepared by changing the pressure release rate while keeping the foaming temperature at 100°C and the saturation pressure at 10 MPa. The cell density decreased, and the cell size increased with the decrease in the pressure release rate. Table 2.2 summarizes the experimental data of cell size and density of PS/PP foams at various foaming conditions. The results concur with those in the previous studies[9-16], i.e a lower foaming temperature, higher saturation pressure, and higher depressurization rate lead to a higher cell density with a smaller cell size.

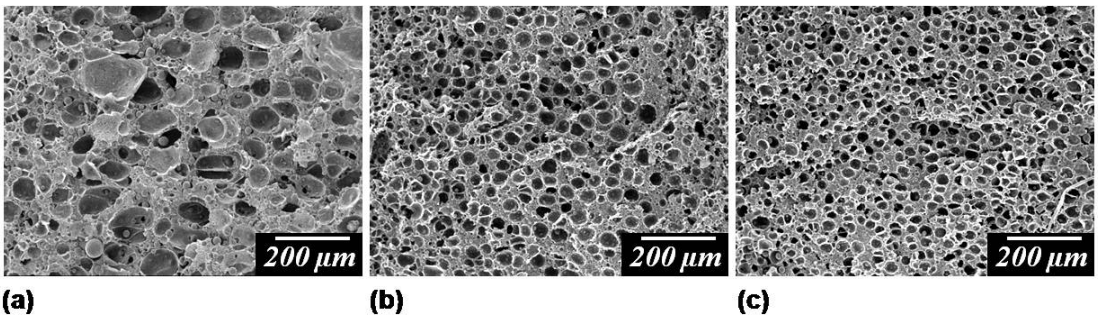

Figure 2.3. Cell morphologies of PS/PP (80/20) foams at 100°C and depressurization rate of 10 MPa/s. Saturation pressure: (a) 8 MPa; (b) 10 MPa; and (c) 15 MPa.

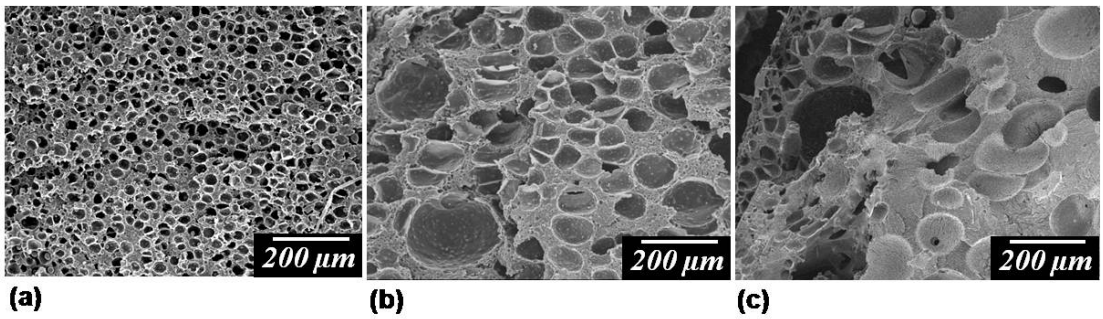

Figure 2.4. Cell morphologies of PS/PP (80/20) foams at 100°C and saturation pressure of 15 MPa. Pressure release time: (a) 10s; (b) 120s; and (c) 300s.

2.3.2 Effect of PP Contents on PS/PP blend foams

The influence of PP dispersed domain on PS foams was investigated by foaming both neat PS and PS/PP blends. Figure 2.5 illustrates the SEM micrographs and histograms of the cell size distribution of both neat PS and PS/PP blend foams with different blend ratios. They were foamed by the pressure quench method at the same pressure and temperature condition, i.e., 10 MPa and 100°C. The resulting cell structure of the PS/PP blend was quite different from that of the PS homopolymer foam. The uniformity of cell size was increased by the addition of PP. The cell size of the PS foam shows a broad

distribution with cell size in a range from 13 to 78 μm. On the other hand, the cell size distribution of the PS/PP blend foams become narrower than that of neat PS foam and they are in a range from 11 to 48 μm.

In addition to the improvement in the uniformity of cell size, an increase in the cell density was clearly observed in all PP contents over the PS homopolymer. It could be said that the presence of PP domains enhanced the bubble nucleation and suppressed the bubble growth. This is because the increase in the interfacial area between PS and PP could enhance the heterogeneous bubble nucleation at the interface between two polymers and increase the cell density. These results indicated the feasibility of PP as a nucleating agent for PS solid-state foaming.

Figures 2.5b-d show that all the blend ratios have a similarly unique cell structure, wherein PP particles were surrounded by empty space and located inside the cells. The formation mechanism of this unique cell structure will be described further in the discussion section. The PP dispersed domains remained as non-foamed particle due to its high stiffness and hard to foam at 100°C. It is highly possible that the strong suppression for the bubble nucleation in the PP domain was originated from the higher stiffness and higher viscoelasticity of PP at this foaming temperature, which is illustrated in Figure 2.6. The higher elasticity increases the energy barrier for bubble nucleation and results in suppression of foaming.

Table 2.2 Summary of the cell properties of PS/PP foams at various foaming conditions

Sample	PP content (wt%)	Foaming condition			Cell density (10^6 cells/cm^3)	Average cell size (μm)
		T (°C)	P (MPa)	dp time (s)		
Effect of PP content						
PS/PP	10	100	10	10	6.94	31.5±18.3
PS/PP	20	100	10	10	12.30	25.9±8.2
PS/PP	30	100	10	10	16.00	23.9±8.1
Effect of Foaming Temperature						
PS/PP	20	80	15	10	138.00	9.14±2.7
PS/PP	20	100	15	10	29.70	22.2±4.9
PS/PP	20	120	15	10	0.45	178.5±107.2
Effect of Saturation Pressure						
PS/PP	20	100	8	10	1.59	50.6±18.3
PS/PP	20	100	10	10	12.30	25.9±8.2
PS/PP	20	100	15	10	29.70	22.2±4.9
Effect of Pressure Release Time						
PS/PP	20	100	10	10	12.30	25.9±8.2
PS/PP	20	100	10	120	1.82	49.2±20.7
PS/PP	20	100	10	300	1.54	119.7±62.7

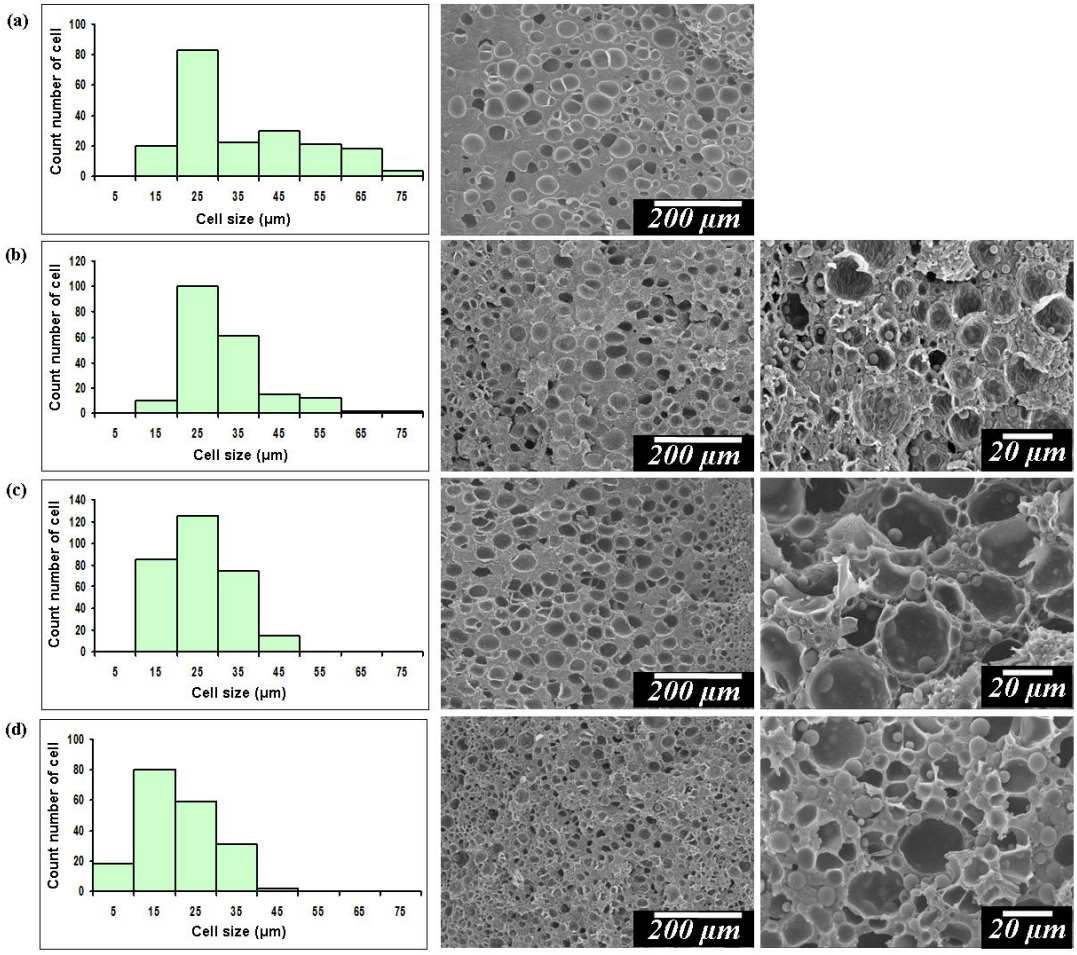

Figure 2.5. SEM micrographs and cell size distribution of samples foamed at 100°C, 10 MPa and depressurized at 1 MPa/s; (a) PS homopolymer, (b) PS/PP (90/10) blend, (c) PS/PP (80/20), and (c) PS/PP (70/30) blend.

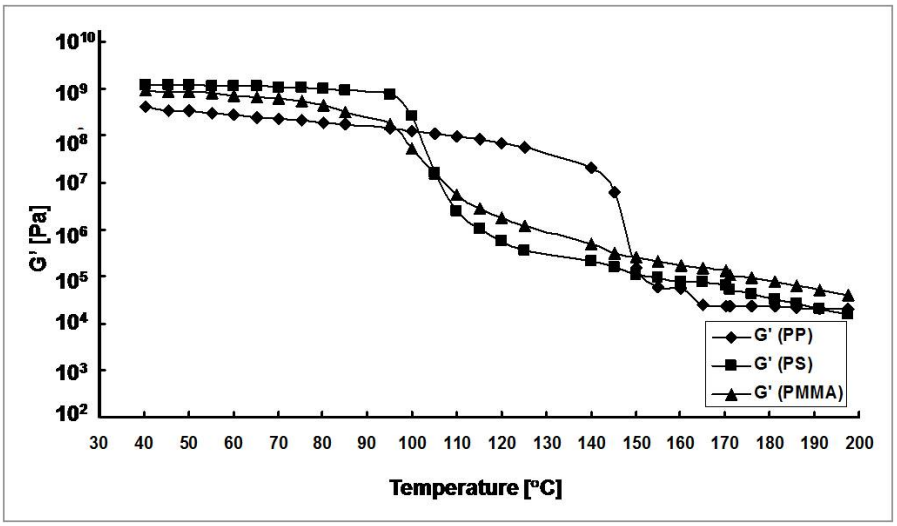

Figure 2.6. Storage modulus of PP, PS and PMMA homopolymers at different temperatures.

2.3.4 Foaming Behavior of PMMA/PP blends

The foaming experiments with PMMA/PP blends were also conducted to verify the role of the PP domains in polymer blend foaming. PMMA/PP blends were prepared with different blend ratios of 90/10, 80/20 and 70/30. Their blend morphologies were characterized before foaming, as the morphologies of the PS/PP blends had been. The effect of PP content on the morphology of PMMA/PP blends is illustrated in Figure 2.7. For all PP contents, a sea and island morphology was observed. However, when the PP content increased over 10 wt%, the dispersed PP domains coalesced. Large non-spherical PP domains were observed when the PP content was 30 wt%, as illustrated in Figure 2.7c. These morphologies showed that the PMMA/PP blend is an incompatible polymer pair, and the PP domain size increases with increasing PP content. According to Clavio *et al.*[17], coalescence occurs due to the high interfacial tension and the large viscosity ratio of the two polymers in a blend system.

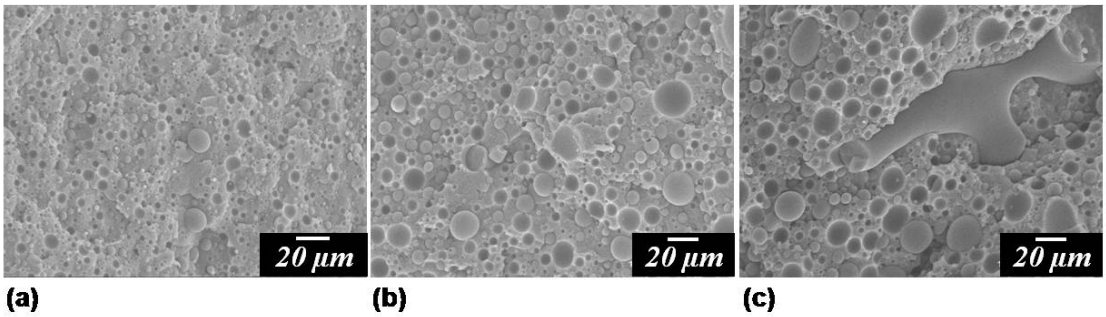

Figure 2.7. SEM micrographs of PMMA/PP blend morphology at different PP content; (a) 90/10; (b) 80/20; and (c) 70/30.

Figures 2.8 and 2.9 show the PMMA/PP (70/30) cell structures obtained for different foaming conditions: one was foamed at 80°C with a saturation pressure of 15 MPa, and the other was foamed at 100°C with a pressure of 10 MPa. The cell morphology of the dispersed PP domains enclosed by cells in the PS matrix were also observed in all PMMA/PP blends, as shown in Figures 2.8d-f and Figures 2.9d-f. To show the effect of PP content on cell density in PS/PP and PMMA/PP blend foams, the cell densities of the neat PS and PMMA foams as well as PS/PP and PMMA/PP blend foams are plotted against the PP content.

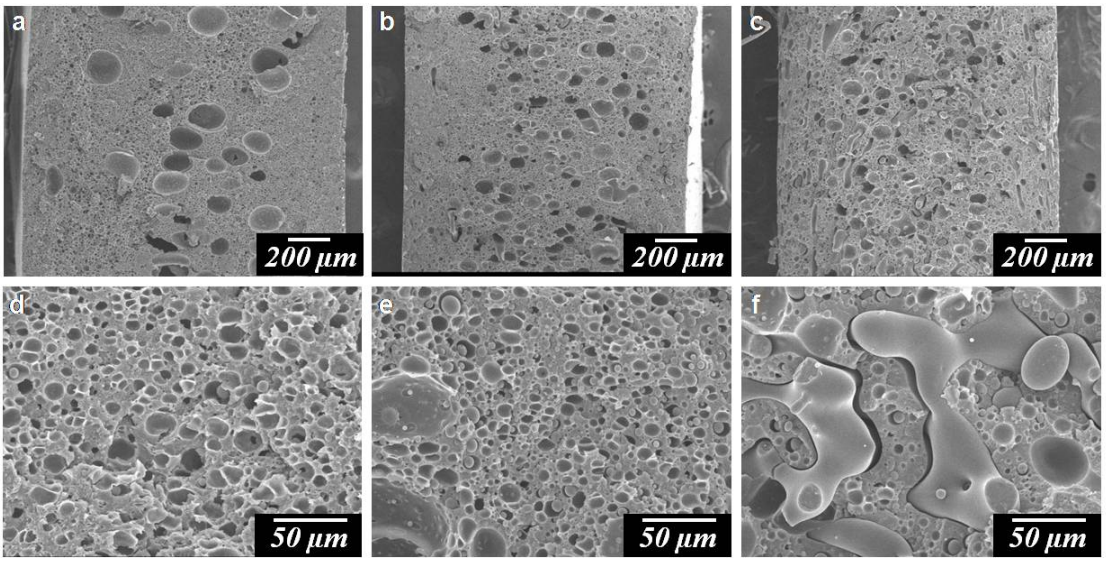

Figure 2.8. SEM images of PMMA/PP foams at 80°C and 15 MPa. Blend ratio: (a) and (d) 90/10; (b) and (e) 80/20; and (c) and (f) 70/30.

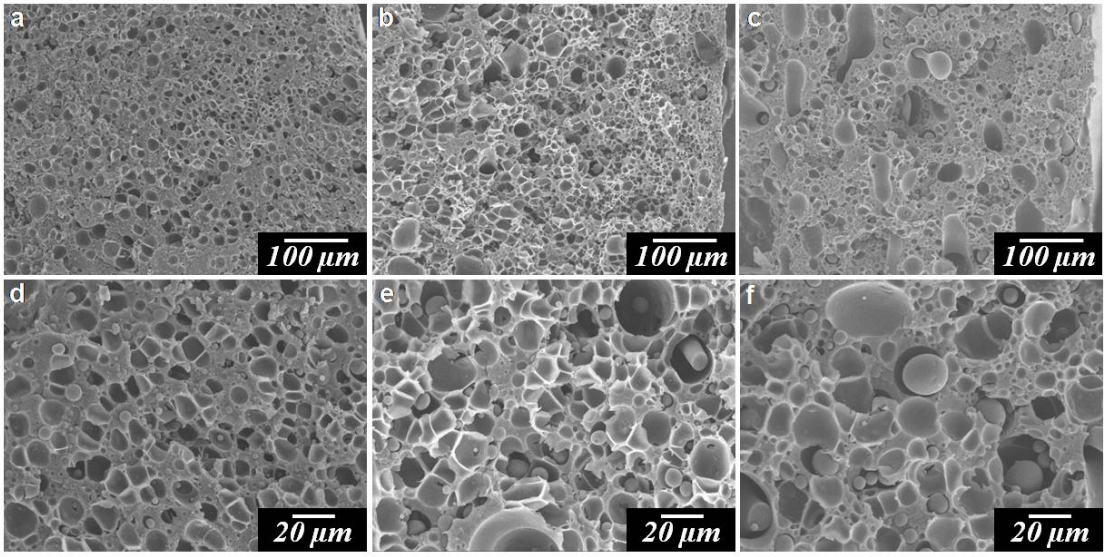

Figure 2.9. SEM images of PMMA/PP foams at 100°C and 10 MPa. Blend ratio: (a) and (d) 90/10; (b) and (e) 80/20; and (c) and (f) 70/30.

Figures 10 and 11 respectively shows the plots of the cell density of the PS/PP and the PMMA/PP blend foams against the PP content. The cell density of the PS/PP blend foam increased with the increase in the PP content while it showed a maximum value at 10% of PP content in PMMA/PP blend foam. The dispersed PP domains increased the cell density in PMMA/PP blend with 10 wt% of PP content. However, a drop in cell density with increasing PP content was observed in PMMA/PP blends over a 10 wt% blend ratio of PP. This reduction was caused by the coalescence of PP domains.

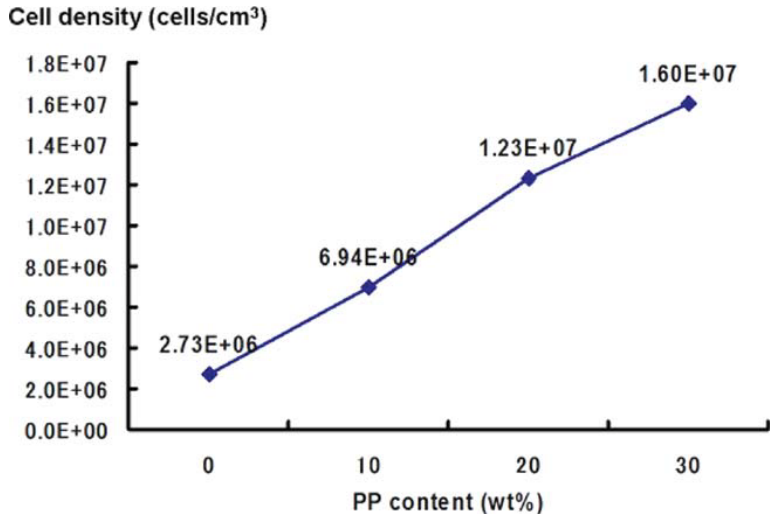

Figure 2.10. Plots of cell density of PS homopolymer and PS/PP blends at different PP content foamed at 100°C and 10 MPa.

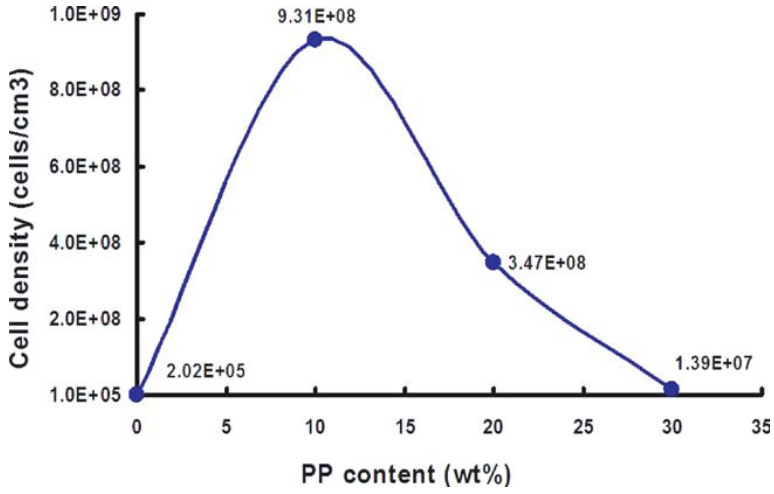

Figure 2.11. Plots of cell density of PMMA homopolymer and PMMA/PP blends at different PP content foamed at 100°C and 10 MPa.

2.3.5 Discussion

An improvement in the cell density and cell size reduction was observed in PS/PP and PMMA/PP blends compared to homopolymers. The presence of PS/PP and PMMA/PP interfaces could be effectively reduce the activation energy barrier to bubble nucleation, thereby increasing the bubble nucleation rate. PP could be considered as a nucleating agent because it possesses the characteristic necessary for providing heterogeneous nucleation sites due to its higher interfacial tension in the matrix polymer and function as a CO_2 reservoir. It was also observed that the presence of PP dispersed domain created a unique cell structure, where PP particles were surrounded by empty space and located inside cells. The cell structure was the consequence of weak adhesion between two polymers in blend. CO_2 could easily diffuse into the interface and exfoliate the disperse domain from continuous phase. The interfacial tension between PMMA/PP is 7.5 mN/m and PS/PP is 5.68 mN/m[18] respectively as listed in Table 2.3. Higher interfacial tension

means that a large surface energy is needed to create the interface, and thus the adhesion between two polymers is so low. As a result, at the interface with higher interfacial tension, CO_2 easily diffuses and expands the space between the two polymer interfaces. From the viewpoint of bubble nucleation theory, the relationship between the high interfacial tension of blend polymers and the bubble nucleation can be explained by Blander's model. Blander proposed a thermodynamics model of bubble nucleation at an interface between two immiscible liquids[19]. The bubble nucleation rate, J was described as:

$$J = C\,exp\left[\frac{-16\pi\gamma^3\Theta}{3kT\Delta P^2}\right] \tag{2.2}$$

where C is pre-exponential, γ is surface tension and Θ is the contact angle of the bubble on the nucleating surface.

$$\Theta = \frac{1}{4\gamma_A^3}\left\{\gamma_A^3\left(2-3m_A+m_A^3\right)+\gamma_B^3\left(2-3m_A+m_A^3\right)\right\} \tag{2.3}$$

$$m_A = cos(\pi-\theta) = \frac{\gamma_A^2+\gamma_{AB}^2-\gamma_B^2}{2\gamma_A\gamma_{AB}} \tag{2.4}$$

$$m_B = cos(\pi-\phi) = \frac{\gamma_B^2+\gamma_{AB}^2-\gamma_A^2}{2\gamma_B\gamma_{AB}} \tag{2.5}$$

Based on these nucleation equations, a generalization can be made with respect to the change in the bubble nucleation sites by the relative values of the various interfacial tensions, as illustrated in Figure 2.12.

(1) In the case of $\gamma_B \geq \gamma_A + \gamma_{AB}$, less energy is required to form a bubble in polymer A.

(2) In the case of $\gamma_A \geq \gamma_B + \gamma_{AB}$, the bubble nucleation occurs predominantly in polymer B and tends to detach from the interface.

(3) If both $\gamma_A < \gamma_B + \gamma_{AB}$ and $\gamma_B < \gamma_A + \gamma_{AB}$ hold, the bubbles mostly nucleate at the interface.

In this study, polymer A is PP, and polymer B represents either PS or PMMA, as shown in the schematic diagram of the bubble function at the interface between two immiscible polymers (see Figure 2.12). Given the surface tension of PP to CO_2, γ_A is large at the foaming temperatures of 80 and 100°C due to the existence of the crystalline phase in PP, and the interfacial tension, γ_{AB}, is also large. Cases (2) and (3) can both be applied to PS/PP and PMMA/PP blends. In the case of the PS/PP blend, considering that CO_2-induced reductions of the surface tension of PP and PS in CO_2 at 170°C and 10 MPa[20] are 12 and 13 mN/m respectively, bubbles are more likely to nucleate and become stable at the interface. The situation could hold for case (3). The larger the interfacial tension, γ_{AB} is, the smaller the wetting angles, θ and ϕ become. As a result, more bubbles are nucleated at the interface.

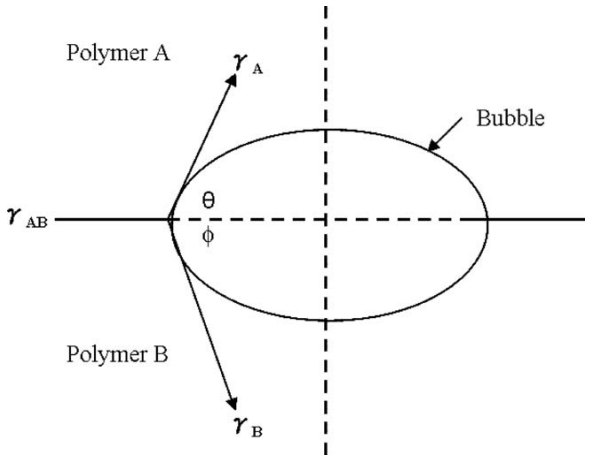

Figure 2.12. Schematic diagram of bubble formation at the interface of two immiscible polymers.

Table 2.3 Interfacial tension of pairs of polymers

Polymers	Literature value (mN/m)
PP/PS	5.68
PP/PMMA	7.50
PS/PMMA	1.69

In the physical foaming, the following rule generally holds; the bubbles that nucleated earlier will grow faster and end up as larger cells. This mechanism with the aforementioned balance of three interfacial tensions at the interface created the void space around the PP domains in the PS as well as PMMA matrix. As listed in Table 2.3, the interfacial tension between PMMA/PP is the largest among the three. Referring to the cell structure of the PMMA/PP (70/30) blend, which had the large void spaces around the PP domains (see Figures 2.9d-f), it could be assumed that bubble nucleation occurs earlier at the interface between PMMA/PP, which is in line with the rule in case (3) condition. The larger void space around the domains in PMMA/PP compared to the PS/PP blend could be explained by this mechanism.

To confirm the bubble nucleation and growth behavior at the interface of the two polymers, a visual observation experiment was also conducted. The details of the experimental setup were given in our previous paper[21]. The bubble nucleation and growth at the interface between PS and PP as well as PMMA/PP were observed, by using a high-pressure view cell. Rectangular films of each polymer, PP, PS and PMMA, were prepared and placed in parallel in the high-pressure view cell for the purpose of creating the interfaces of PS/PP and PMMA/PP.

The visual observation experiment was conducted by releasing the pressure from 10 MPa to atmospheric pressure within 48 s after dissolving CO_2 for 6 hours at 150°C.

Snapshot pictures were taken during the pressure quench foaming experiment as illustrated in Figure 2.13. Due to the limitation of the resolution of the high speed camera, the smallest bubble that could be detected was 10 μm. Thus, the nuclei of bubbles below 10 μm could not be observed. During foaming, however, many bubbles were formed at the PP/PS and PMMA/PP interfaces. As time elapsed, dark portions appeared at the interface between PMMA/PP and expanded along the interface (Figure 2.13a). Then, the spherical bubbles appeared at the interface between PS and PP (Figure 2.13b). That is, the heterogeneous nucleation occurred first at the interface of PMMA/PP and later at the PS/PP interface. Subsequently, bubbles appeared in the PS and PMMA regions (Figures 2.13d and e). There was no bubble formation in PP during the course of foaming. This movie confirms that bubble nucleation is enhanced at the interface of two polymers. Furthermore, the interface with higher interfacial tension induces the heterogeneous nucleation and serves as a preferential site for bubble nucleation.

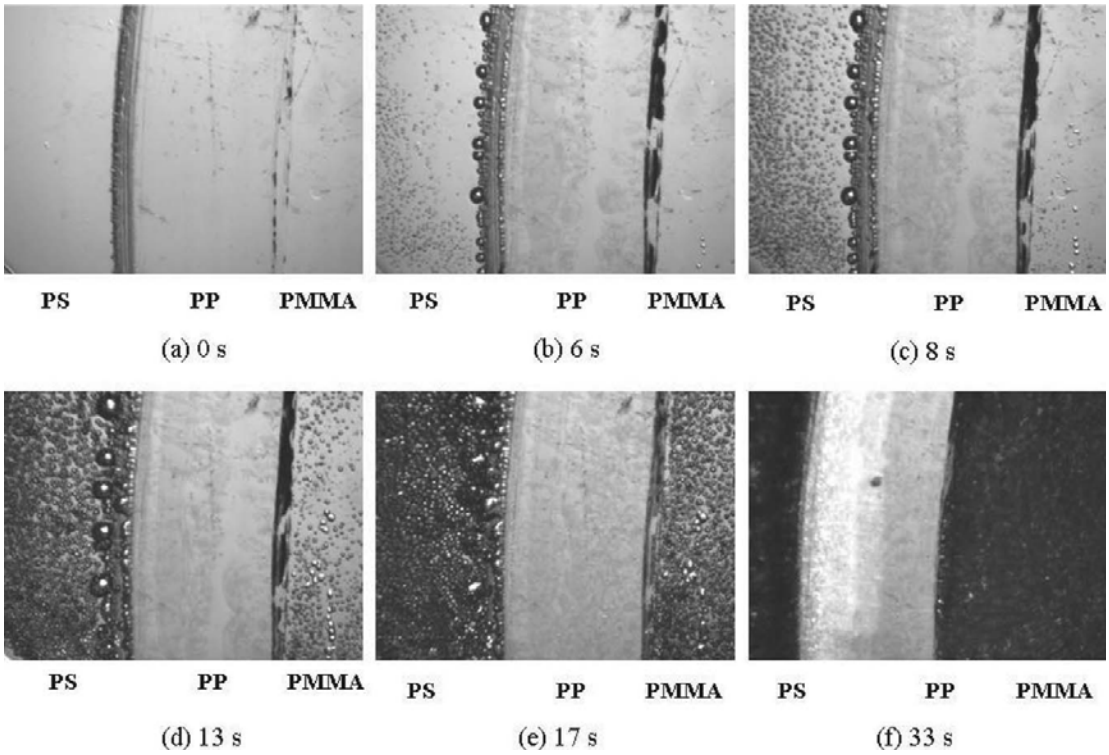

Figure 2.13. Bubble nucleation and expansion evolution processes of the PS/PP and PMMA/PP interfaces observed by visual observation experiment.

2.4 Conclusion

The cell structures of PS/PP and PMMA/PP blend foams were investigated. PP content could improve cell density and cell size over the homopolymers as long as PP had a small domain size and larger surface-to-volume ratio and the foaming was conducted at a temperature lower than the melting temperature, T_m of PP. The bubble nucleation could be enhanced at the interface of two polymers with higher interfacial tension. By manipulating the temperature and blend ratio, PP could be used as a nucleating agent with good dispersibility and high nucleating ability.

2.5 References

[1] Z. Tu, K. Mai, Z. Wu, *J of App. Polym. Sci.*, **2006**, 101, 3915.

[2] X. Han, J. Shen, H. Huang, D. L. Tomasko, L. Lee, *J. Polym. Eng. Sci.*, **2007**, 47, 103.

[3] J. S. Colton, N. P. Suh, *Polym. Eng. Sci.*, **1987**, 27,500.

[4] S. K. Goel, E. J. Beckman, *AIChE Journal*, **1995**, 41, 357.

[5] D. Garcia, *Journal of Polym. Sci.*, **1984**, 22, 2063.

[6] L. J. Lee, C. Zeng, X. Cao, X. Han, J. Shen, G. Xu, *Composites and Tech.*, **2005**, 65.

[7] W. Zhai, J. Yu, L. Wu, W. Ma, J. He, *Polymer*, **2006**, 47, 7580.

[8] P. H. Nam, P. Maiti, M. Okamoto, T. Kotaka, *Polym. Eng. Sci.*, **2002**, 42,1907.

[9] K. Taki, T. Yanagimoto, E. Funami, M. Ohshima, *Polym. Eng. Sci.*, **2004**, 44. 1004.

[10] K. Taki, K. Nitta, S. Kihara, M. Ohshima, *J. of App. Polym. Sci.*, **2005**, 97, 1899.

[11] P. Spitael, C. W. Macosko, R. B. McClurg, *Macromolecules*, **2004**, 37, 6874.

[12] N. S. Ramesh, D. H. Rasmusen, G. A. Campbell, *Polym. Eng. Sci.*, **1994**, 34, 1685.

[13] T. Nemoto, J. Takagi, M. Ohshima, *Macromol. Mater. Eng.*, **2008**, 293, 991.

[14] I. Luzinov, C. Pagnoulle, R. Jerome, *Journal of Polym.*, **2000**, 41, 3381

[15] C. B. Park, L. K. Cheung, *Polym. Eng. Sci.*, **1997**, 37, 1.

[16] D. L. Tomasko, A. Burley, L. Feng, S. K. Yeh, K. Miyazono, S. N. Kumar, I. Kusaka, K. Koelling, *J. Of Supercritical Fluids*, **2009**, 47, 493

[17] P. S. Calvao, M. Yee, N. R. Demarquette, *Polymeric*, **2005**, 46, 2610.

[18] T. S. Valera, A. T. Morita, N. R. Demarquette, *Macromolecules*, **2006**, 39, 2663.

[19] S. Hartland, *Surface and Interfacial Tension: Measurement, Theory and Applications*, Marcel Dekker Inc. **2004**.

[20] K. Taki, T. Murakami, M. Ohshima, *Proc. Of Asian Workshop of Polymer Processing in Singapore*, **2002**.

[21] K. Taki, T. Nakayama, T. Yatsuzuka, *Journal of Cellular Plastics*, **2003**, 39, 155.

Chapter III

CO_2-induced Reinforcement of the Mechanical Properties in Polyolefin-based Nanocellular Foams

3.1. Introduction

Polymeric foams have several unique properties. Their low thermal and electric conductivities[1] and high light reflection[2] have encouraged intensive studies of these properties in order to develop new foams for performance- oriented applications. The major drawback of conventional polymer foams is their weak mechanical properties. Plastic foams with very small pores, characterized by cell sizes smaller than 10 μm and called microcellular foams, were invented to address this drawback.[3] In the early stages of microcellular foam research, it was believed that microcellular foams could reduce the weight of polymers without sacrificing the mechanical properties. For certain application, it was possible for the microcellular foams to have better mechanical properties than solid (non foam) polymers. In fact, there have been some reports that microcellular foams exhibit a higher mechanical strength-to-weight ratio and a higher impact strength than the common structural foams at equivalent densities.[4,5] However, it has not yet been reported that microcellular foaming can actually increase the yield or the ultimate stresses higher than the values achieved prior to foaming.

In practice, crystalline fillers, such as glass fiber and nanoclays, are often used to improve the mechanical properties of polymer products. The mechanical properties of polymer foams could also be improved by glass fiber and clays. However, the yield and

the ultimate stresses could not be recovered to their original values prior to foaming the polymer with the fillers. In the worst case for foaming, the filler works as an inhibitor of the bubble nucleating agents or as a disturbance to preparing a uniform cell structure.[6]

The use of crystallinity for improving the mechanical properties of foams has not been thoroughly investigated. The previous studies on crystallinity in polymer foams have mainly focused on their effect on foamability and cell uniformity. The presence of a crystalline phase makes the polymer matrix structurally heterogeneous, which makes bubble nucleation possible. At the same time, the crystalline phase reduces the foamability and narrows the operating region for foaming because the physical foaming agent cannot be dissolved in the crystalline phase, and a drastic change in elasticity occurs when melting in the crystalline phase. Pioneering work on the microcellular foam of a semi crystalline polymer was conducted by Colton,[7] who set the foaming temperature in the vicinity of the melting temperature. Doroudiani *et al.*[8] conducted batch foaming experiments with high density polyethylene (HDPE), polybutylene (PB), poly(propylene) (PP), and poly(ethylene terephthalate) (PET) to investigate the effects of the crystallinity and the morphology of semi crystalline polymers on the cell structure. They showed that controlling the cooling rate during foaming was a key factor in preparing microcellular foams of semicrystalline polymer and that the crystallization changed the bubble nucleation behavior and made the cell structure different. Park's group[9] has further advanced the study of the effect of crystallinity on foaming. They investigated an HDPE/i-PP blend for physical foaming and showed that HDPE/i-PP polymer blends could produce a finer cell structure than neat HDPE and i-PP polymer. Xu *et al*.[10] thoroughly studied the foaming behavior of PP with CO_2 and showed that at a

high depressurization rate, 15 $MPa \cdot s^{-1}$, a bimodal cell structure was created in the presence of the crystalline phase. They showed that bubble nucleation in the crystalline region occurred when the depressurization rate was set high enough. In a subsequent paper,[11] they found that micro fibrils and microcells were formed by CO_2 foaming at the centers of spherulites and in the amorphous phase located in between spherulites of i-PP. They also determined that the melting temperature was shifted up after foaming i-PP with CO_2 and that γ-crystals were formed at high CO_2 saturation pressures.

This dissolved CO_2 changes the glass transition temperature, the crystallization temperature and the behavior of the polymer foam. Since the mid-1980s, CO_2- induced crystallization in semicrystalline polymers has been reported by several researchers. In earlier works, the attention was mostly directed to the CO_2- induced depression of T_g and T_m. Beckman *et al.*[12] reported that the degree of crystallinity in bisphenol A polycarbonate was increased with CO_2 treatment. Handa *et al.*[13] investigated the poly(ether ether keton, poly(aryl ether ether ketone). They showed CO_2- induced depression of T_g and T_m. The focus of studies in this field then shifted to the effect of CO_2 crystallization kinetics. Mizoguchi *et al.*[14] investigated the crystallization rate of PET in the presence of CO_2, and Handa *et al.*[15] studied syndiotactic polystyrene (sPS). Kalospiros *et al.*[16] proposed a crystallization model based on the assumption that the kinetics rate depends on the degree of swelling in the amorphous regions and the degree of crystallinity itself. They showed the good agreement between the model and experimental data for polymer- CO_2 systems. Takada *et al.*[17] measured the in situ isothermal crystallization rate of i-PP, PET and PLLA in pressurized CO_2 and reported on the crystallization kinetic behaviors: when the magnitude of the CO_2- induced depression

of T_g is far greater than that of the equilibrium melting temperature, T_m°, the crystallization rate is increased by CO_2 in most of the temperature region between T_g and T_m. In contrast, when the magnitude of the CO_2- induced depression of T_g is almost the same as that in T_m°, the crystallization rate is decreased in the presence of CO_2 in the nucleation rate- controlled temperature region, and it is increased in the crystal growth rate- controlled region. Varma-Nair *et al.*[18] also pointed out the CO_2- induced change in the phase behavior and the crystallization kinetics of i-PP: the rate of crystallization decreased at 126°C with the addition of CO_2. Very recently, Shieh *et al.*[19] reported that nonisothermal crystallization from the melt in CO_2 could produce dual melting peak temperatures in PET, which normally shows a single melting peak. Jiang *et al.*[11] also reported the dual melting peaks of i-PP foams, which were foamed with CO_2 at 156°C under pressures in the range of 10.4 to 16.1 MPa. These studies have shown that CO_2 can provide a tuneable technique for controlling crystallinity, crystallization kinetics and morphology, and for improving the mechanical properties.

In this study, the CO_2- induced crystallization effect was combined with the nanocellular foaming technique to increase the yield and the ultimate stresses of the foams to a higher level than that of the solid polymer. Nanocellular foaming techniques have been successfully advanced as a technique for reducing the microscale cell size further down to the nanoscale. Several techniques for preparing nanocellular foam have been proposed: high-T_g polymer,[20] rapid pressure quenching,[21] organoclay-polymer nanocomposites[22] and polymer blends with a disperse nanoscale domain.[23-25] Those methods can successfully provide cellular structures with 1 μm or smaller cell sizes. In this research, we employed our nanoscale dispersed- domain method[23-25] to reduce the

cell size and make the cell structure as uniform as possible. We investigated PP and PP/ SEBS blend systems. SEBS was used to prepare the dispersed phase in order to prepare a uniform fine- scale cell.

3.2. Experimental

3.2.1. Materials

The materials used in this study were a homopolymer PP (M_w= 410,000) supplied by Mitsubishi Chemical and SEBS, with a *styrene* content of 18 % and an *ethylene-butylene* content of 82 %, that was obtained from Asahi Kasei elastomers. The polymers were used as-received.

3.2.2. Blend Sample Preparations

Please refer to preceding chapter.

3.2.3. Foaming Process

Please refer to preceding chapter.

3.2.4. Differential Scanning Calorimeter

The crystallinity and the melting temperature of both solid (non foamed) and foamed PP and PP/SEBS blend samples were measured using DSC (Perkin Elmer Pyris 1). The samples of approximately 3 mg were placed into aluminium pans, heated up to 200°C at the rate of 10°C·min^{-1}, held for approximately 3 minutes to make the sample a crystal-

free melt and then cooled down to 30°C at the rate of -10°C·min^{-1} for the first scan. The procedure was repeated with the same sample for the second scan.

3.2.5. X-Ray Diffraction Analysis

X- ray diffraction (XRD) (RigakuRINT2000) was used to characterize the visual assessment of crystallite orientation of solid and foam samples. The XRD patterns were recorded in the range of 10 to 60° of the diffraction angle 2θ using Ni-filtered Cu Kα radiation (λ= 0.1548) at 40 kV and 20 mA.

3.2.6. Mechanical Measurement

A tensile test was carried out by using Autograph (Shimadzu Autographs AGS-J Series) at ambient temperature with a strain rate of 1 mm·min^{-1} for all solid and foamed samples. The test piece was cut out from the solid or foamed samples to be 1 mm in thickness, 10 mm in width and 6 mm in length.

3.3. Results and Discussion

3.3.1. Effect of CO_2 on the Melting Behavior

We first examined the effect of the sorption (annealing) temperature on the crystallization of PP and PP/SEBS blend with different blend ratios, 70/30 and 90/10, by measuring their thermal behavior via DSC. Figures 3.1 and 3.2 show the resulting DSC heat curves of PP and PP/SEBS blends treated at different sorption temperatures. The heat curve before CO_2 sorption, in other words, the heat curve of the solid sample, shows

a single peak, just as the second scan. Both foamed and non foamed PP samples treated with CO_2 at 10 MPa and 155°C show the dual melting peaks for the first scan and the single peak for the second scan. The first peaks were observed at approximately 160°C and the second peaks were observed at 175°C. It was thought that the dual endothermic peaks were caused by CO_2 sorption. CO_2 sorption at temperatures below the melting point can induce PP crystallization and make the lamellae thicker. As a result, the melting temperature increases. The same trend was observed in the PP/SEBS blend samples: the first peak was observed at approximately 160°C, whereas the second peak was observed above 170°C.

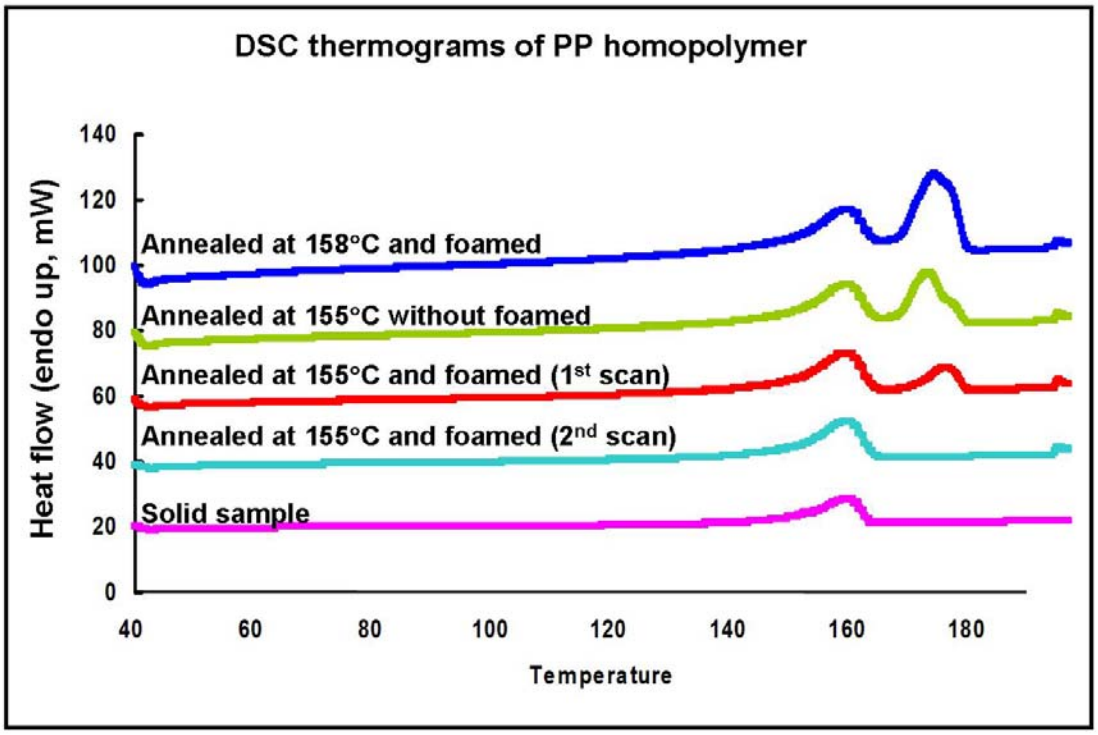

Figure 3.1. DSC thermograms of solid PP and annealed PP at different temperatures and under 10 MPa CO_2.

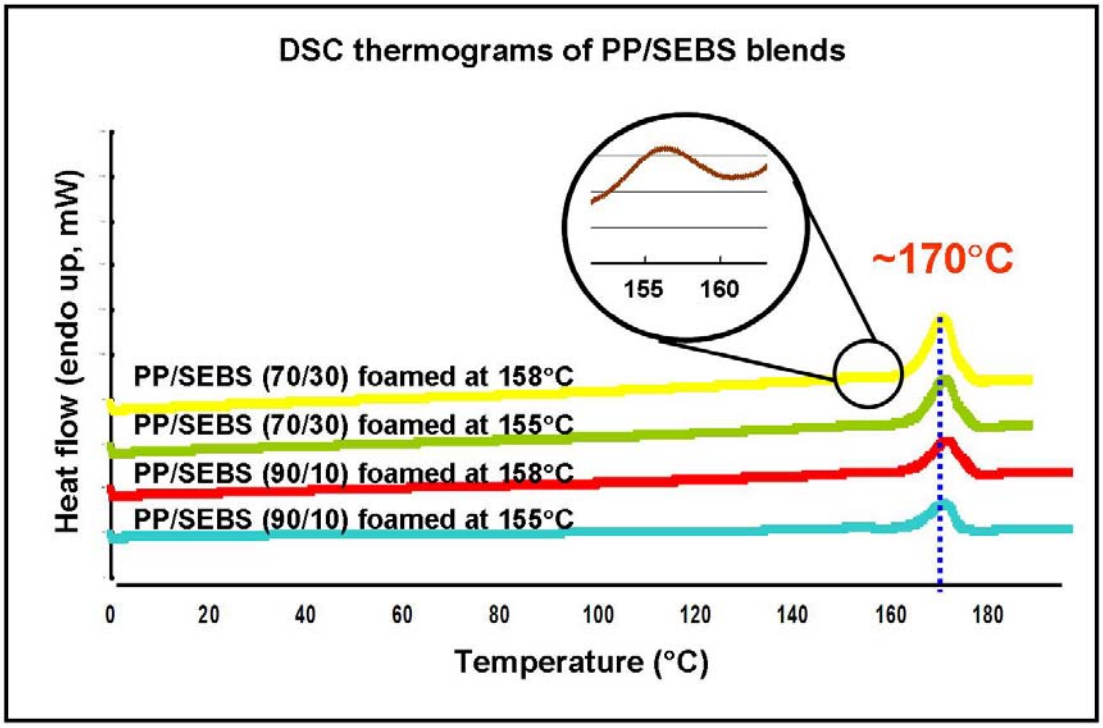

Figure 3.2. DSC thermograms of PP/SEBS (70/30) and (90/10) blend samples foamed at different sorption temperatures and 10 MPa.

Table 3.1 summarizes the melting temperature for the first and second peaks of PP and the PP/SEBS (70/30) blend that were annealed and foamed at different temperatures. When the samples were treated under the temperatures below the T_m of the solid, the dual peaks were obtained for both PP homopolymer and PP/SEBS blends. As the annealing (sorption) temperature increased up to the melting temperature of the solid sample, the melting temperature at the second peak increased, while the one at the first peak did not change. When increasing the temperature to 165°C, both the PP homopolymer and the PP/SEBS blend lost the second peaks. Only one peak remained at 160°C, as the solid sample shows.

Table 3.1. The melting temperature shift of PP and the PP/SEBS (70/30) blend annealed and foamed at different temperatures after DSC measurement.

Samples	Processing temperature (°C) first peak/ second peak				
	150	155	158	160	165
PP homopolymer	145/170	155/178	158/178	160/180	160/-
PP/SEBS (70/30) blend	145/170	155/175	157/178	158/178	160/-

Wang *et al.*[26] showed that the melting behavior of the α-form lamellae is determined by the defects inside the lamellae. Melting and recrystallization occur easily when the lamellae has defects. Al-Raheil *et al.*[6] studied the dual melting peaks of isotactic polypropylene crystallized from the melt. They concluded that the first peak represents the melting of crosshatched lamellae and the second shows the melting of radial and reorganized tangential lamella. It could be speculated from our DSC data that CO_2 treatment could increase the thickness of the radial and tangential lamellae.

Figure 3.3 compares the XRD patterns of solid PP and PP foam. Foams were prepared by pressure quenching at 1 MPa·s^{-1} after treating the solid sample at 155°C and 10 MPa CO_2 for 6 hours. The diffraction peak of foamed PP was sharper than that of solid PP. Comparison of the crystalline content of PP solid with that of PP foam clearly shows that a 4.2% increment in the crystalline content was achieved by the CO_2 treatment at 155^{o}C. This increase in crystallinity was measured by the aid of the enthalpy values taken from DSC measurement. Furthermore, as can be seen in Figure 3.3, the new peak was observed at 20.1, which is a characteristic of γ-form crystals. The XRD data showed that CO_2 treatment changed not only the crystallinity but also the crystalline morphology.

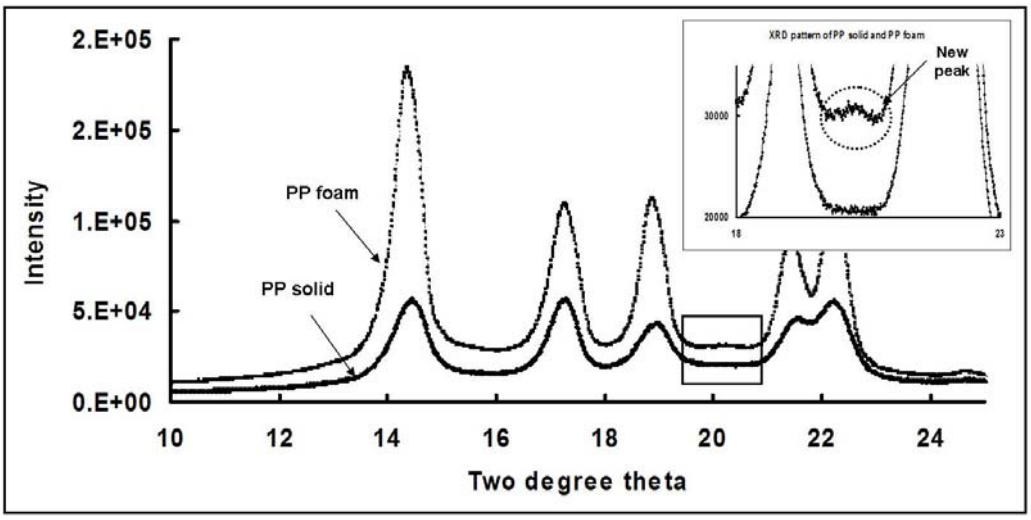

Figure 3.3. XRD patterns of PP solid and foamed PP obtained at 155°C and 10 MPa.

3.3.2. Effect of Temperature on Cell Structure

The effect of the CO_2 sorption temperature on the cell structure is clearly seen in Figure 3.4. The PP samples were foamed at different temperatures, 155, 158 and 160°C, with 10 MPa CO_2. No cell was found when homo PP was foamed at 155°C and at the depressurization rate of 1 $MPa \cdot s^{-1}$ (Figure 3.4a). This is because the high crystallinity restricted the CO_2 to dissolve into the crystalline phase and the overall high elasticity prevented the bubbles from nucleating and growing. The foamability was improved to some degree as the temperature increased to 158°C. Microfibrils around the microcells were observed in Figure 3.4b, as Jiang *et al.* reported [11]. This indicates that bubbles were nucleated in the inter lamellar amorphous region. The larger cell and the non uniform cell structure were observed in the sample treated at 160°C. As the temperature increases, the diffusivity of CO_2 increases and the elasticity decreases. The bubble nucleation occurs in

the amorphous phase, which is non uniformly distributed in the PP matrix. As a result, the bubbles became large and non uniformly distributed.

To improve the foamability and uniformity of the cell structure, SEBS was added in different ratios. The foaming experiments were carried out under the same annealing and foaming conditions as the homo PP foaming experiments. Figures 3.5 and 3.6 show the cell structure of foams of PP/SEBS (70/30) and (90/10) blends, respectively. Blending SEBS apparently increases the cell density and reduces the non foamed part of homo PP foams. This is because the dispersed SEBS domains provide a template for bubble nucleation [24].

According to our previous study[24] on nanocellular foam, bubble nucleation and growth were selectively localized in the SEBS domain at a lower foaming temperature, approximately 120°C, where the elasticity, G', of SEBS was lower than that of PP. Utilizing the blend morphology as a template for bubble nucleation as well as CO_2 solubility and elasticity differences between the matrix and the dispersed phase polymers to control the bubble location and growth, nanocellular foam with a cell size of approximately 200 nm was prepared. In this study, even at higher temperatures near the melting temperature of homo PP, the elasticity of SEBS was far lower than that of PP because of the presence of crystalline PP. Thus, bubble nucleation occurred more easily in the SEBS domain than in PP. In other words, SEBS provides a lower elasticity and a highly dispersed phase to enhance bubble nucleation and suppress bubble growth. As a result, blending SEBS with PP widened the processing windows of foaming. Uniform cell structure was achieved at temperatures below 160°C by adding SEBS.

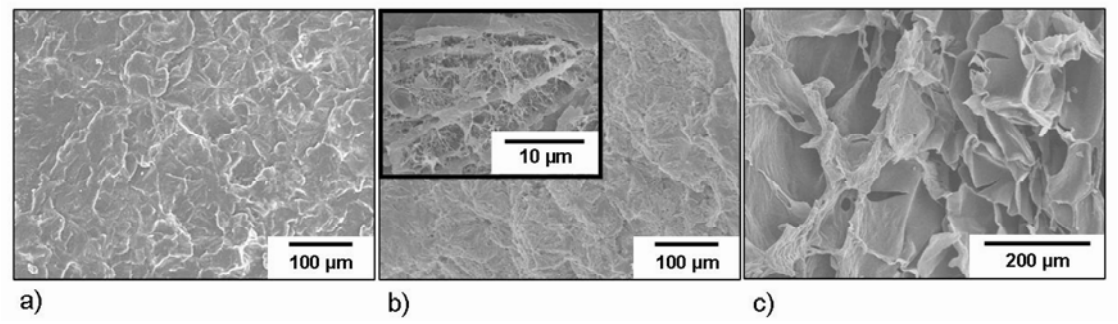

Figure 3.4. SEM micrographs of the cell structures of homo PP foam at various foaming temperatures (a) 155°C (b) 158°C and (c) 160°C.

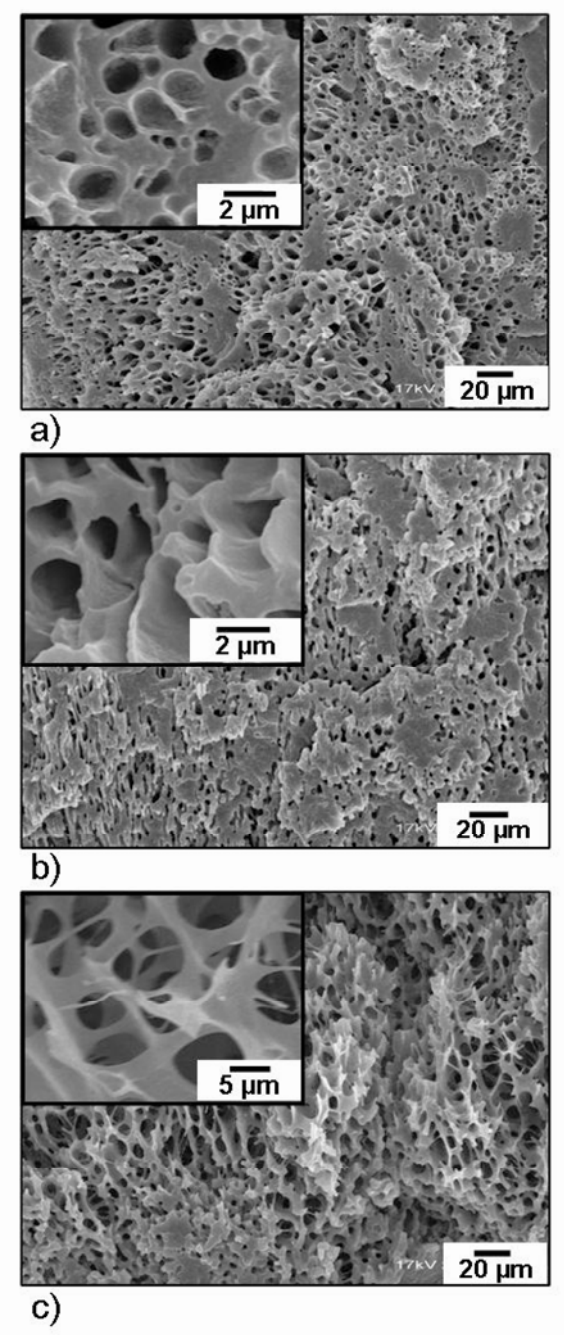

Figure 3.5. SEM micrographs of PP/SEBS (70/30) blend foams at 10 MPa: (a) 155°C (ρ_f = 0.82), depressurized in 10 s (b) 158°C depressurized in 10 s (ρ_f= 0.76) and (c) 158°C, depressurized in 60 s (ρ_f= 0.55), (ρ_s = 0.92).

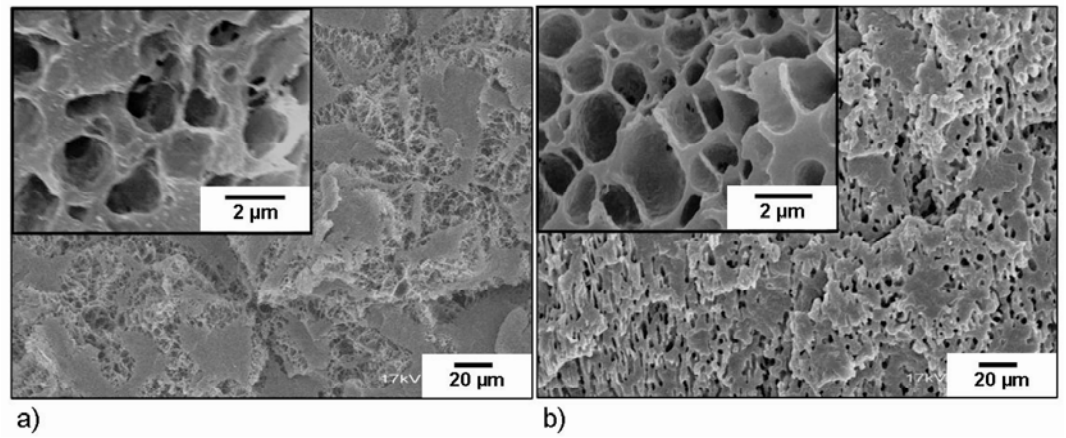

Figure 3.6. SEM micrographs of PP/SEBS (90/10) blend foams at 10 MPa and depressurized in 10s. Foaming temperature: (a) 155°C (ρ_f= 0.7) and (b) 158°C (ρ_f= 0.85), (ρ_s = 0.94).

3.3.3 CO_2-induced Reinforcement of Mechanical Properties

CO_2- induced PP crystallization can enhance the crystallinity and thicken the crystalline lamellae, as shown by the results presented in the previous section. Because the dual melting peaks could be observed even in both foams of PP and PP/SEBS blends, it can be assumed that bubble nucleation and growths predominantly occurred in the amorphous phase and in the dispersed SEBS domains and that foaming did not deteriorate the crystalline structure and thickness. Thus, the CO_2- induced crystallization reinforcement could be applied to nanocellular foams.

Figure 3.7 shows strain-stress (S-S) curves for the solid and foamed PP samples. PP foams were prepared by releasing CO_2 approximately at 1 MPa·s^{-1} from 10 MPa at 158°C. The cell size and the cell density of the resulting foams were difficult to measure because of their microfibril and spider- net- like cell structure, as shown in Figure 3.5. As

can be seen in Figure 3.7, the yield and ultimate stresses of PP foams were made larger than before foaming.

The same behavior was observed in the strain-stress (S-S) curves of PP/SEBS blend foams. Figure 3.8 shows the S-S curves of solid and foamed PP/SEBS (70/30). The foams were prepared with two different depressurization rates, 1 and 0.17 MPa·s^{-1}, and two different annealing temperatures, 155 and 158°C in 10 MPa CO_2. The resulting cell structures, cell size and cell density, are illustrated in Figure 3.9. The yield and ultimate stresses were increased to a higher level than those of the solid as long as the cell size was kept smaller than 2 μm.

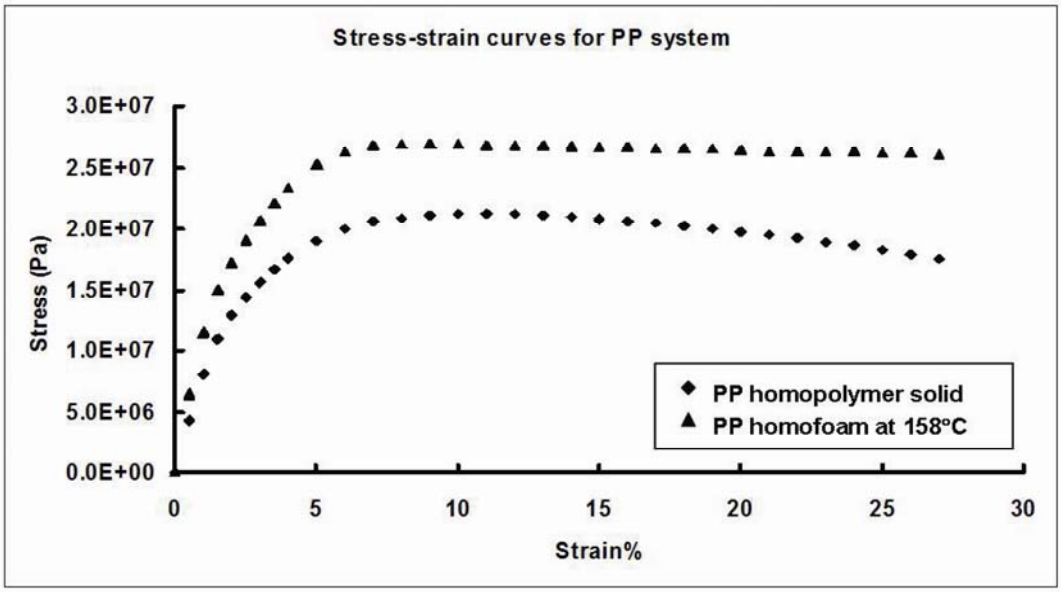

Figure 3.7. Stress-strain curve of the PP homopolymer system.

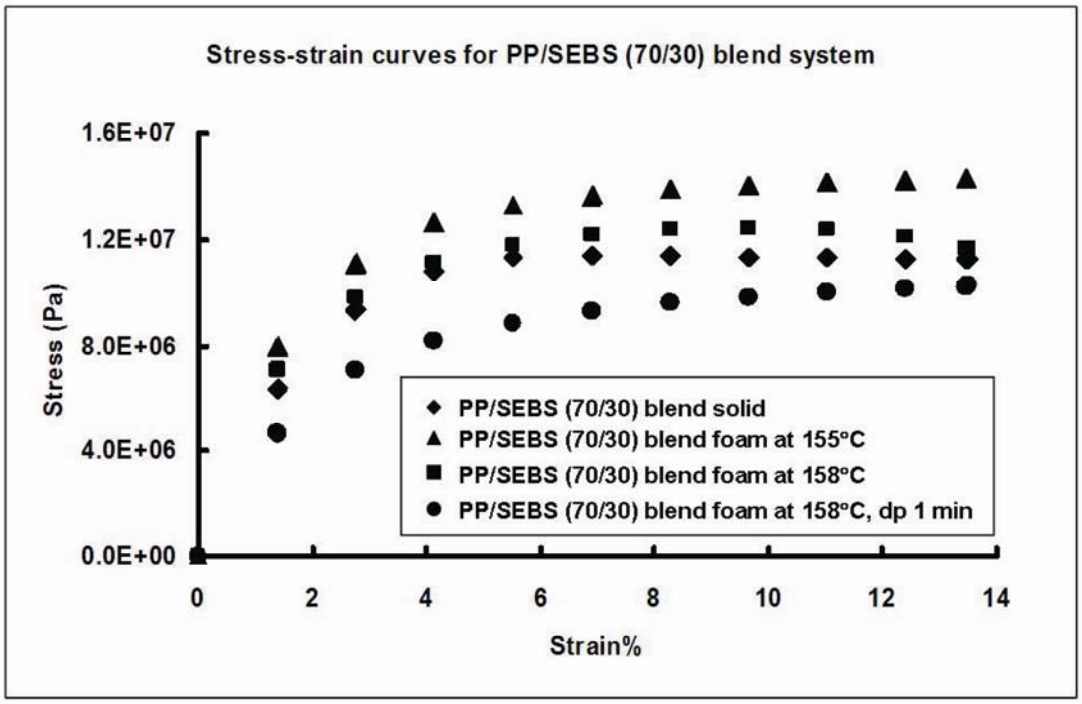

Figure 3.8. Stress-strain curves for the PP/SEBS (70/30) blend system.

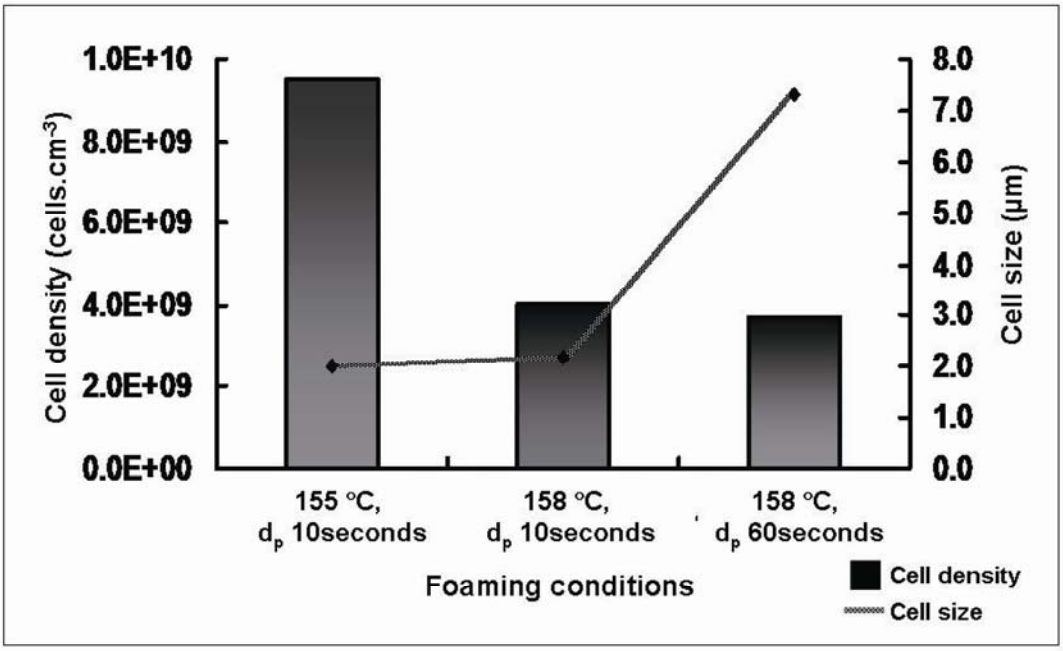

Figure 3.9. The cell density and cell size of PP/SEBS (70/30) blend foams under different foaming conditions.

Figure 3.10 shows that the PP/SEBS (90/10) foamed by releasing pressure at 1 $MPa \cdot s^{-1}$ after annealing at 158°C for 6 hours in 10 MPa CO_2. As can be seen, the yield and ultimate stresses were higher than those of PP/SEBS (70/30) blend foams. The cell size of PP/SEBS (90/10) was somewhat smaller than that of PP/SEBS (70/30). However, the major reason for the stress increase was the increase in the PP contents, as well as the increase in the non foamed part, which can be seen in the SEM micrographs of the foams (Figure 3.6). A quantitative measurement of the non foamed part in the foamed samples was conducted by meshing the SEM pictures and counting the mesh numbers where no bubbles existed. The non foamed portion of PP/SEBS (70/30) and PP/SEBS (90/10) foams was 13 and 29%, respectively. This result implies that the yield strength of the foam was dominantly determined by the PP content and the crystalline structure of PP.

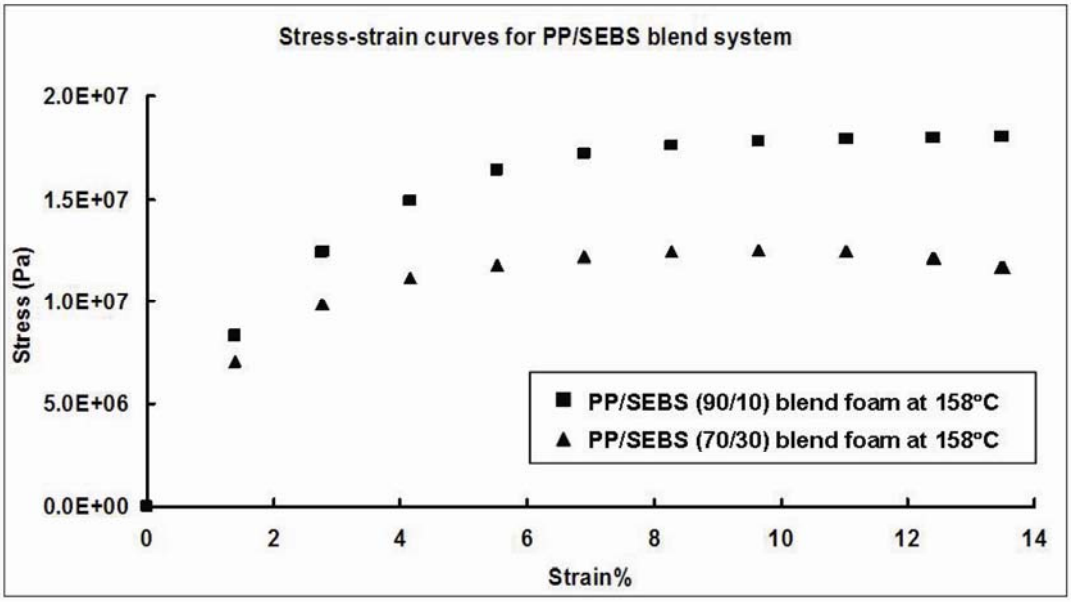

Figure 3.10. Stress-strain curves of PP/SEBS (70/30) and PP/SEBS (90/10) blend foams.

All PP/SEBS blend foams except a PP/SEBS (70/30) foam sample in this experiment showed the foam density in the range of 0.5 to 0.8. When the PP/SEBS (70/30) samples were foamed with a slow release rate, 0.17 $MPa \cdot s^{-1}$ after annealing at 158°C in 10 MPa CO_2. The cell size was increased to 8 μm as illustrated in Figure 3.5. Then, the tensile strength of the PP/SEBS (70/30) was lowered from that of the solid. This clearly indicated that the cell size was one of the most important factors in determining the yield and the ultimate stresses of the foams.

To clarify the cell size effect on the mechanical properties, we prepared a nanocellular foam of the PP/SEBS blend with a 80/20 weight ratio so as to obtain a cell structure 200 nm in size while keeping the crystallinity at the same level as the solid and the single melting peak. The sample polymer film was prepared with a 200 μm thickness, a 100 mm length, and a 100 mm width from PP (grade FY4, Japan Polypropylene Corporation) with a weight-average molecular weight of 2.53 x 10^5 and SBR (grade DR1320P, JSR Corporation). The sheet preparation was conducted by melt- extrusion. To improve the compatibility and make the dispersed SEBS domain as small as possible, we used a different twin-screw extruder (K-38-25T, φ25 mm, L/D= 38, TECHNOVEL CORP., Osaka, Japan) at a higher screw rotation rate of 120 rpm. Then, the sheet sample was placed in the high-pressure vessel. The vessel was kept at 25°C and pressurized by CO_2 to 20 MPa. CO_2 was dissolved into the sample for 1 hour while keeping the temperature constant. After establishing an equilibrium state, the pressure in the vessel was released at a rate of 1 $MPa \cdot s^{-1}$ without foaming the sample. Then, the sample was rapidly immersed in an ethylene glycol bath, holding the temperature at 120°C. To keep the crystallinity as well as crystalline morphology of the solid even after foaming, we

dissolved CO_2 into the samples at a low temperature (25°C). This procedure was the same one that was used in our previous study.

Figure 3.11 shows an SEM micrograph of the resulting foam. The cell size was 250 nm on average and the cell density was approximately 7.2 x 10^{13} cm^{-3}. Figure 3.12 illustrates the DSC curve of the foam and the solid sheet of PP/SEBS (80/20). The dual melting peaks were not observed in both solids and foams. The crystallinity was slightly increased from 29.6 to 32.4% by annealing in 25°C in 20 MPa CO_2. Figure 3.13 shows the S-S curve of the foam and the solid. As can be seen, the ultimate stress and the yield stress of the foam are very much similar to those of solid sample. It can be said that the nanocellular foam with a cell size less than 250 nm could maintain the ultimate stress of the solid without utilizing the CO_2 crystallization effect. In other words, the mechanical property of PP/SEBS blends can be improved by foaming with annealing in pressurized CO_2 because the cell size can be reduced to the nanoscale.

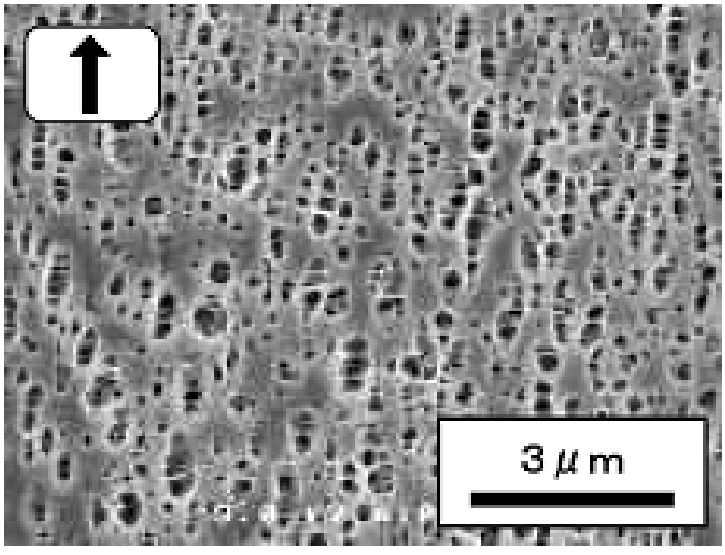

Figure 3.11. SEM micrograph of PP/SEBS (80/20) foams.

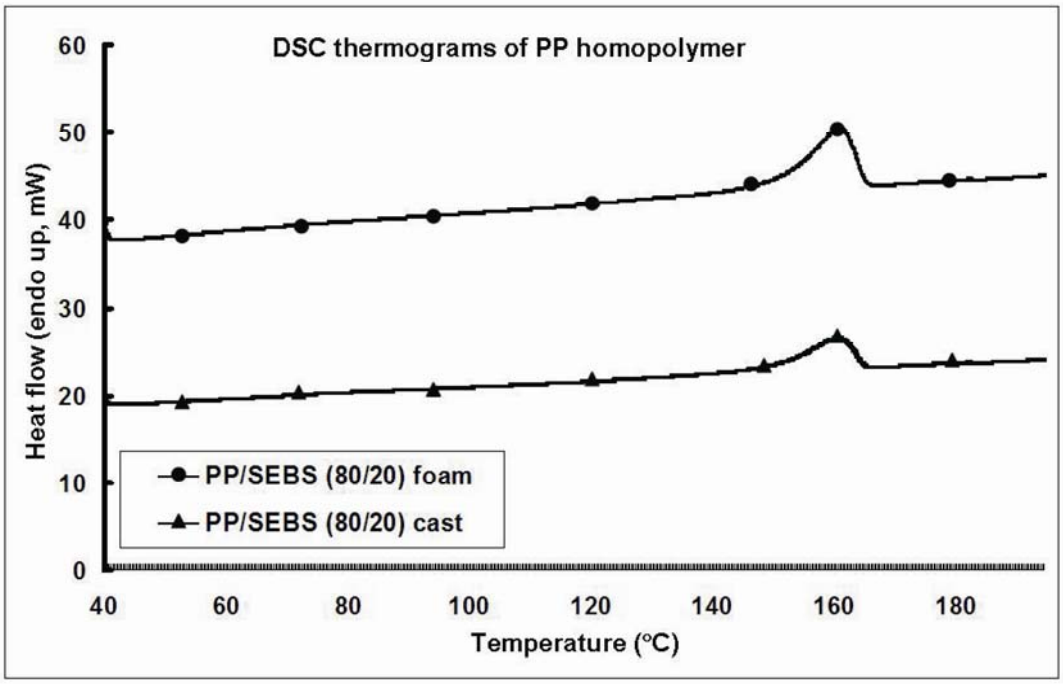

Figure 3.12. DSC curves of solid and foam PP/SEBS (80/20).

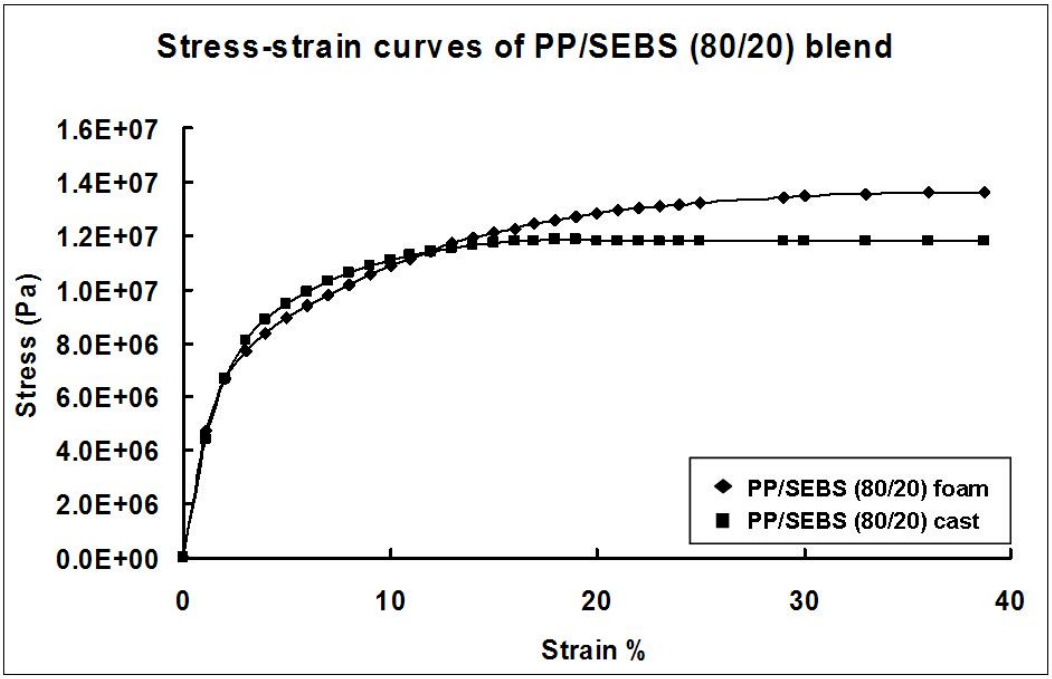

Figure 3.13. Stress-Strain curves of solid and foam PP/SEBS (80/20) without CO_2-induced crystallization.

In the previous studies on microcellular PP foam or semi crystalline microcellular foams, annealing in pressurized CO_2 was conducted. Thus, the foams underwent the CO_2 crystallization effect. However, because the cell sizes of these foams were normally approximately 10 μm, the CO_2- induced reinforcement of the mechanical properties did not occur.

3.4. Conclusion

The possibility of improving the mechanical properties of polymer foam was investigated. Using the effects of CO_2 on PP crystallization and a nanocellular foam technique, we were able to prepare the foam so that the yield and ultimate stresses were higher than those of the solid. Annealing the PP and PP/SEBS samples in pressurized CO_2 changed the crystallinity and the crystalline morphology. SEBS was used to improve the uniformity of the cell structure and to provide a preferential bubble nucleation site to enhance bubble nucleation but not bubble growth. As shown in this study, high strength, uniform nanocellular foam can be achieved by reducing the cell size to the nanoscale using CO_2 annealing to induce crystallization of the semicrystalline polymer. The elongation at break, which is also an important mechanical property, was deteriorated in this study by foaming. This could be due to the presence of collapsed bubbles on the surface of cut-out test piece, which played a role of notch for the tensile test. Controlling the skin layer on the sample surface could be much important and effective to improve the elongation at break. The technique of CO_2- induced mechanical properties could be applied to any semicrystalline matrix containing polymer and elastomers blended in a dispersed domain systems.

3.5. References

[1] J. L. Hedrick, K. R. Carter, R. Richter, T. P. Russell, M. Sanchez, R. Dipietro, S. Swanson, D. Mecerreyes, R. Jerome, *Polym. Prepr.* **1996**, 37, 156.

[2] A. Kabumoto, *Seikei Kako Journal* **1999**, 11, 966 (in Japanese).

[3] J. E. Martin, N. P. Suh, F. A. Waldman, *U.S Patent 4* **1984**, 473, 665.

[4] J. S. Colton, N. P. Suh, *Polym. Eng. Sci.* **1987**, 27, 485.

[5] J. S. Colton, N. P. Suh, *Polym. Eng. Sci.* **1987**, 27, 493.

[6] I. A. Al-Raheil, A. M. Qudah, M. Al-Share, *J. of App. Polym. Sci.* **1998**, 67, 1267.

[7] J. S. Colton, *Materials and Manufacturing Processes* **1989**, 4 (2), 253.

[8] S. Doroudiani, C. B. Park, M. T. Kortsch, *Polym. Eng. Sci.* **1996**, 36, (11), 2645.

[9] S. Doroudiani, C. B. Park, M. T. Kortshot, *Polym. Eng. Sci.* **1998**, 38, (7), 1205.

[10] Z. M. Xu, X. L Jiang, T. Liu, G. H. Hu, L. Zhao, Z. N Zhu, W. K Yuan, *J. of Supercritical Fluids* **2007**, 41, 299.

[11] X. L. Jiang, T. Liu, Z. M. Xu, G. H. Hu, W. K. Yuan, *J. of Supercritical Fluids* **2009**, 48 (2), 167.

[12] E. Beckman, R. S. Porter, *J. Polym. Sci., Part B: Polym. Phys*. **1987**, 25, 1511.

[13] Y. P. Handa, S. Lampron, M. L. O'Neill, *J. Polym. Sci.,Part B: Polym. Phys.* **1994**, 32, 2549.

[14] K. Mizoguchi, T. Hirose, Y. Naito, Y. Kamiya, *Polymer* **1987**, 28, 1298.

[15] Y. P. Handa, Z. Zhang, B. Wong, *Macromolecules* **1997**, 30, 8499.

[16] N. S. Kalospiros, G. Astarita, M. E. Paulaitis, *Chem. Eng. Sci.* **1991**, 48 (1), 23.

[17] M. Takada, M. Tanigaki, M. Ohshima, *Polym. Eng. Sci.* **2001**, 41, 1938.

[18] M. Varma-Nair, P. Y. Handa, A. K. Mehta, P. Agarwal, *Thermochimica Acta* **2003**, 396 1-2, 5.

[19] Y. T. Shieh, Y. H. Li, C. C. Huang, T. L. Wang, *The Journal of Supercritical Fluids,* **2010**, 55 (1), 373.

[20] B. Krause, R. Mettinkhof, N. F. A. Van Der Vegt, M. Wessling, *Macromolecules* **2001**, 34, 874.

[21] Y. P. Handa, Z. Y. Zhang, *Cell. Polym.* **2000**, 19 ,77.

[22] Y. Fujimoto, S. S. Ray, M. Okamoto, A. Ogami, K. Yamada, K. Ueda, *Macromolecular Rapid Communications* **2003**, 24, 457.

[23] T. Nemoto, J. Takagi, M. Ohshima, *Macromolecular Mater. Eng.* **2008**, 293 (7), 574.

[24] T. Nemoto, J. Takagi, M. Ohshima, *Macromol. Mater. Eng*. **2008**, 293 (12), 991.

[25] T. Nemoto, J. Takagi, M. Ohshima, *Polym. Eng. Sci.* **2010**, 50 (12), 2408.

[26] X. Wang, W. Hou, J. Zhou, L. Li, *Colloid Polym. Sci.* **2007**, 285 (4), 449.

Chapter IV

Preparation of microcellular thermoplastic elastomer foams from polystyrene-b-polybutadiene-b-polystyrene (SEBS) and their blends with polypropylene

4.1 Introduction

Recently, rubber foaming has been intensively studied by many researchers because of its great demand.[1-3] Chemical blowing agents (CBA) have typically been used for foaming rubbers. CBAs are chemicals that release a gas (such as CO_2 and N_2) when decomposed by heating. The released gas dissolves into the rubber or directly leads to bubble nucleation and the formation of a cellular structure in the rubber. The current major problem with the use of CBA in the foaming process is the emission of harmful substances and the contamination of foam products with residual CBA, which makes recycling difficult.

To solve the recycling issue, several researchers have conducted intensive studies on the physical foaming of rubbers and elastomers. They used non-toxic and lower global-warming-potential foaming agents, such as N_2 and CO_2, as physical blowing agents. For example, Kim *et al.*[4] studied the foamability of thermoplastic vulcanizates with various physical blowing agents (PBA). They reported that CO_2 was a good blowing agent to prepare lower density foams (high expansion foams), while N_2 was the best agent for preparing foams with a finer cell structure. Sahnoune *et al.*[5] prepared an elastomer foam using water as a non-toxic blowing agent.

When elastomers and rubbers were physically foamed, shrinkage and dimensional stability of the foam products became a critical issue. Rubbers are difficult to foam because they behave elastically and are less rigid. Sometimes, rigid fillers and short glass fibers are added to rubbers to reinforce their foams.[6] Vulcanization is commonly conducted to increase the rigidity and the stability of the foam. Vulcanization controls the chain mobility of rubber by introducing crosslinking agents, such as sulfur. Therefore, in rubber foaming with CBA, vulcanization and CBA decomposition reactions must be simultaneously controlled to retain both the viscoelastic properties of rubber and the gas liberation rate at appropriate levels. The compounding technique and the vulcanization conditions affect the parameters of the final cellular structure, such as the cell size, cell density and cell uniformity. For example, when the vulcanization reaction proceeds faster than the gas liberation rate, cell growth is prevented, and higher expansion foam is not obtained. When the gas liberation rate proceeds faster than the vulcanization reaction rate, the foam is not stabilized. There have been many reports on rubber foaming with vulcanization.[7-9] Tai *et al.*[10] investigated the effect of the crosslink density of a metallocene elastomer (m-POE) by varying the loading of the cross linking agent. Ariff *et al.*[11] reported that rubbers with higher degrees of crosslink density produce stiffer cell walls and provide greater restriction to expansion.

As a substitute technique for vulcanization, high- energy irradiation techniques have been proposed for the production of cross linked networks.[12-16] The technique has attracted attention because it is fast and clean, it requires less energy and it has the potential to improve chemical resistance.[17] Liu *et al.*[14] used the irradiation cross linking technique to control the physical and mechanical properties of silicone rubber foam.

Dubey *et al.*[15] reported that a significant improvement in the mechanical properties of an Styrene-butadiene rubber (SBR)- Etylene propylene diene rubber (EPDM) blend was achieved by the irradiation technique. However, the use of this technique has been restricted because direct irradiation is hazardous to human health;[18] furthermore, the technique is not applicable to certain polymers because of their poor resistance against radiation and poor impact resistance at low temperature.[19]

Because of vulcanization and the residual CBA, most elastomer or rubber foams are difficult to recycle. Thermoplastic elastomers (TPE), often called thermoplastic rubbers, are a class of copolymers or physical mixes of polymers (usually a plastic and a rubber) that possess both thermoplastic and elastomeric properties. Therefore, TPEs have advantages of both rubbery and plastic materials. The crosslinking in TPE is a weaker dipole or hydrogen bond, which is de-bonded by heating, while the crosslink created during the vulcanization of a rubber or elastomer is a covalent bond. These properties make TPEs recyclable; consequently, they are suitable for recyclable microcellular rubber foams. Although great success has been made in the production of microcellular foams from thermoplastic polymers, a limited number of reports have been made on microcellular TPE foams. Zhai *et al.*[20] prepared microcellular poly(ethylene-co-octene) (PEOc) foam using CO_2 as a physical blowing agent and reported that the increase of the PEOc molecular weight increased the matrix modulus and melt viscosity and tended to stabilize the cell structure at high foaming temperatures.

In this study, hydrogenated polystyrene-b-polybutadiene-b-polystyrene (SEBS) was investigated for physical foaming with CO_2. SEBS is a type of TPE that consists of a soft midblock of ethylene-butylene (EB) and hard polystyrene end-blocks. The end-blocks

(styrene) form a physical crosslink and provide a rubber-like elasticity. With the increase of styrene block percentage, the storage modulus and melt viscosity can be increased, and the diffusivity of CO_2 can be decreased. Two SEBS with different styrene contents were foamed at three different foaming temperatures to determine the effect of the styrene content on the microcellular structure. Furthermore, because PS and PP have higher elasticities and CO_2 diffusivities as compared to SEBS, blending approach can be utilized to tune the modulus and CO_2 diffusivity of SEBS. Adding PS or PP into SEBS probably controls the foam shrinkage through enhancement in elasticity as well as reduction in CO_2 permeability in SEBS blend samples.

The use of different polymers in controlling the foam shrinkage is also studied. Polymers are differed by their physical properties. Due to the difference in physical properties, one polymer may have additional benefits over other polymer. These physical properties also may be a constraint for polymer to perform well in one process. For example in foaming process, the bubble growth of PS can only be controlled below its T_g. This study focused on the relationship between the T_g and the T_m of PS and PP, respectively, on the controllability of foam shrinkage in SEBS. SEBS is blended with PS and PP to enhance the elasticity through crosslink their chains. Below T_g, PS remained glassy and formed entanglement network with styrene chains. This entanglement network is deformed above the T_g of PS which reduced the controllability of foam shrinkage in SEBS. Pressure quench batch foaming were carried out on SEBS/PS and SEBS/PP blends to compare their controllability on foam shrinkage.

Research overview: This study is divided into two major tasks:

1) Investigate the potential of using a thermoplastic polymers; PS and PP in reducing

foam shrinkage of SEBS by taking their advantages of high elasticity and lower CO_2 diffusivity.

2) Study the effect of T_g and T_m of PS and PP on controllability of foam shrinkage in SEBS foam.

4.2 Experimental

4.2.1 Materials

Two SEBS copolymers with different styrene contents (H1062 and H1043) were kindly provided by Asahi Kasei Elastomer. H1062 is composed of 18 wt% styrene blocks and 82 wt% ethylene-butylene blocks, and its average molecular weight is 70,000 g mol^{-1}. H1043 possesses a higher styrene content of 67 wt%, an EB content of 33 wt% and a molecular weight of 45,000. Polystyrene (PS) (Mw=192,000 g/mol, Aldrich) and polypropylene (PP) (Mw= 410,000 g/mol, Mitsubishi) were also used as received.

4.2.2 Blend Sample Preparation

Please refer to preceding chapter.

4.2.3 Solubility and Diffusivity Measurement

A magnetic suspension balance (MSB; Robotherm and Bel Japan) was used to measure the solubility and diffusivity of CO_2 in two SEBS copolymers and their PS blends. When CO_2 dissolves in a polymer, the weight of the polymer increases because of the weight of the dissolved CO_2. Thus, weighing the polymer under pressurized CO_2 allows us to determine the solubility and diffusivity of CO_2. The MSB makes it possible to weigh samples under high pressures and temperatures. The details of this measurement

scheme are described elsewhere.[21] When CO_2 dissolves in the polymer, it causes the polymer to swell. Because the buoyancy caused by the swelling affects the solubility measurements, the specific volume of the polymer/CO_2 mixture must be estimated accurately to conduct a correction of buoyancy and obtain the true transport properties. The specific volume at a given temperature and pressure was calculated by the Sanchez-Lacombe equation of state (S-L EOS) and a mixing rule with a binary interaction parameter, k_{12}.[21,22] The characteristic parameters of the S-L EOS for each polymer blend were determined from the Pressure-Volume-Temperature (*PVT*) data (Figure 4.1). The resulting parameter values are listed in Table 1. The solubility of CO_2 in PS, SEBS and their blends was measured at pressures ranging from 5 to 18 MPa. CO_2 of 99.9% purity (Showa Tansan, Japan) was used.

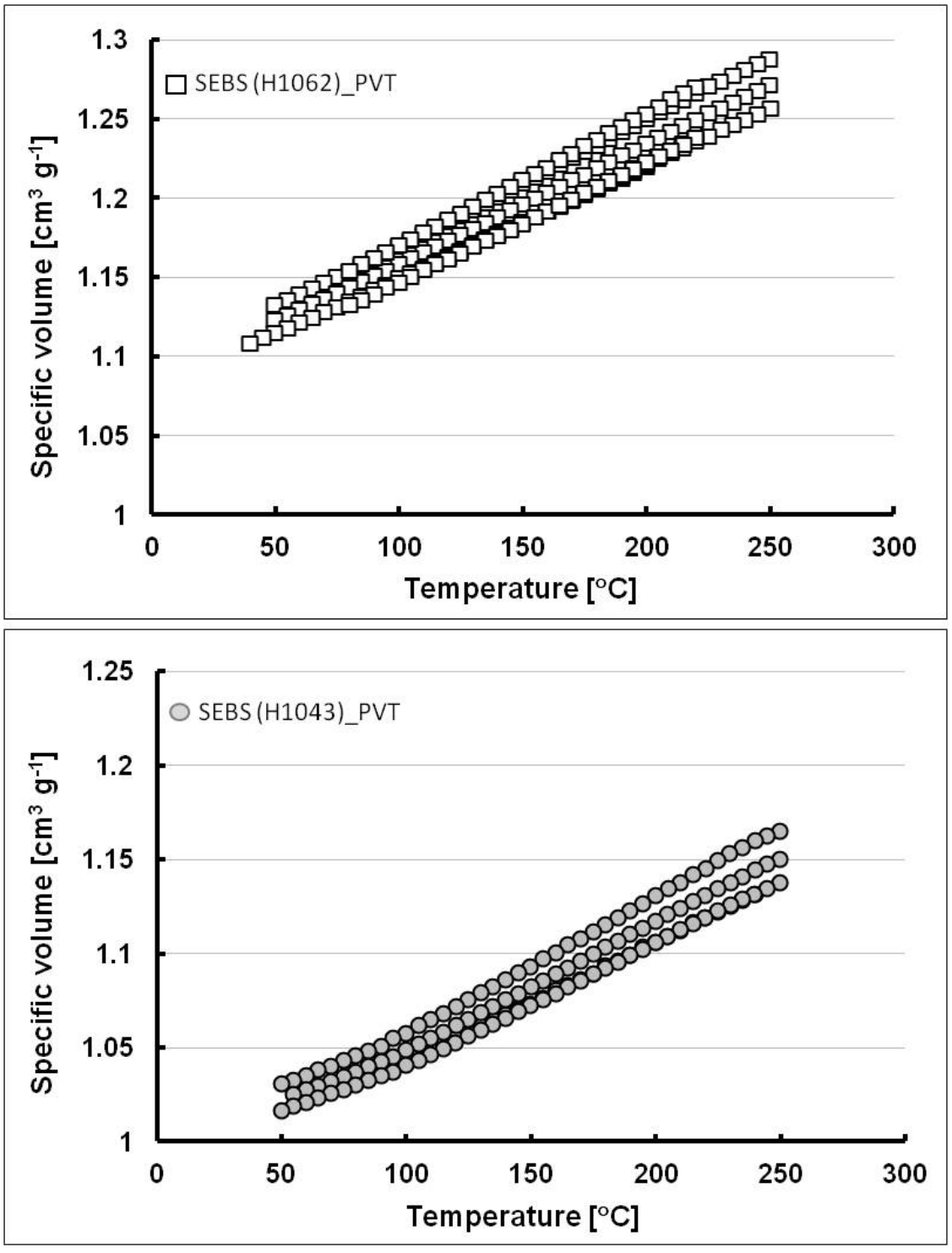

Figure 4.1 *PVT* data of SEBS (H1062) and SEBS (H1043).

To estimate the specific volume of polymer/CO_2 single phase mixture, the Sanchez-Lacombe equation of state (SL EOS) was used in the following way. The SL-EOS was derived from a lattice model to describe the relationship among the specific volume (density), pressure and temperature and it is given by

$$\tilde{\rho}^2 + \tilde{P} + \tilde{T}\left[\ln(1-\tilde{\rho}) + \left(1-\frac{1}{r}\right)\tilde{\rho}\right] = 0 \qquad (4.1)$$

where $\tilde{T}, \tilde{P}$ and $\tilde{\rho}$ are the reduced temperature, pressure and density, respectively. *r* is the size parameter, which represents the number of lattice sites occupied by one polymer chain.

The reduced parameters and size parameter are defined by

$$\tilde{P} = \frac{P}{P^*}, \tilde{\rho} = \frac{\rho}{\rho^*}, \tilde{T} = \frac{T}{T^*}, r = \frac{P^*}{RT^*}\left(\frac{\overline{M}_w}{\rho^*}\right) \qquad (4.2)$$

where *R* is the gas constant and $\overline{M}_w$ is the weight average molecular weight, and P^*, T^* and ρ^* are characteristic parameters.

When the SL equation of state is used for a single component, such as for neat polymer or CO_2 alone, the characteristic parameters can be obtained either from the literature or by fitting Eq. (4.1) to *PVT* experimental data of the neat polymer or CO_2. To estimate the specific volume of a polymer blend/CO_2 mixture, a mixing rule is employed to modify the characteristic parameters in Eq. (4.1) for blend system. The mixing rule used for our blend/CO_2 mixture was given by Eqs.(4.1)-(4.10) [21,23-26], where the subscript 1 and 2 stand for parameters of CO_2 and polymer respectively.

$$P^* = \phi_1 P_1^* + \phi_2 P_2^* - \phi_1\phi_2 (P_1^* + P_2^* - 2(1-k_{12})(P_1^* P_2^*)^{0.5}) \qquad (4.3)$$

$$T^* = \frac{T_1^*\phi_1 + \left(\frac{v_1^*}{v_2^*}\right)T_2^*\phi_2}{\phi_1 + \left(\frac{v_1^*}{v_2^*}\right)\phi_2} - \phi_1\phi_2\left[\frac{\left(P_1^* + P_2^* - 2(1-k_{12})\left(P_1^*P_1^*\right)^{0.5}\right)\left(\phi_1^0 v_1^* + \phi_2^0 v_2^*\right)}{R}\right] \tag{4.4}$$

$$\phi_i^0 = \frac{\phi_i}{\left(\phi_i + \frac{v_1^*}{v_2^*}\phi_2\right)} \tag{4.5}$$

$$\frac{1}{\rho^*} = \frac{1}{\left(\frac{m_1}{\rho_1^*} + \frac{m_2}{\rho_2^*}\right)} \tag{4.6}$$

$$r = x_1\left(\frac{W_1}{\rho_1^*\left(\frac{RT_1^*}{P_1^*}\right)}\right) + (1-x_1)\left(\frac{W_2}{\rho_2^*\left(\frac{RT_2^*}{P_2^*}\right)}\right) \tag{4.7}$$

$$x_i = \frac{\left(\frac{W_i}{\overline{M}_{w,i}}\right)}{\left(\frac{W_i}{\overline{M}_{w,i}} + \frac{W_2}{\overline{M}_{w,2}}\right)} \tag{4.8}$$

$$\phi_i = \frac{\left(\frac{m_i}{\rho_i^*}\right)}{\left(\frac{m_i}{\rho_i^*}\right) + \left(\frac{m_2}{\rho_2^*}\right)} \tag{4.9}$$

$$m_i = \frac{W_i}{W_i + W_2} \tag{4.10}$$

where T_i^*, P_i^*, ρ_i^* and r_i are characteristic parameters of *i-th* component, W_i, m_i and x_i are weight, weight fraction and mole fraction of the *i-th* component in the mixture, respectively and k_{ij} is the binary interaction parameter between the *i-th* and the *j-th* components.

An orthodox method of obtaining the SL EOS for the SEBS/PS/CO_2 system is to use the mixing rule regarding the system as a ternary system: the characteristic parameters of CO_2, SEBS, and PS are determined individually each *PVT* data. Then, two interaction parameters between polymers (SEBS and PS) and CO_2 are determined from MSB measurement of each polymer/CO_2 binary system. The third interaction parameter between SEBS and PS is determined by fitting Eq. (4.1) to MSB measurement of SEBS/PS/CO_2 ternary systems with two predetermined interaction parameters of polymer/CO_2 binary systems. However, in this study, assuming that each SEBS/PS blend can be treated as one grade of polymer and SEBS/PS/CO_2 can be treated as a polymer/CO_2 binary system, we applied the following simple method for calculating the specific volume of mixtures of SEBS/PS/CO_2 with blend ratios of SEBS/PS at 80/20 and 50/50. Therefore, the characteristic parameters of SEBS/PS blend were determined by fitting Eq. (4.1) to the *PVT* data of the blend. The molecular weight of the blend was determined by weight average of the molecular weight of SEBS and PS:

$$\overline{M}_w = m_1 \overline{M}_{w,1} + (1 - m_1)\overline{M}_{w,2} \tag{4.11}$$

where $\overline{M}_{w,1}$ and $\overline{M}_{w,2}$ are the molecular weights of SEBS and PS, respectively.

4.2.4 Rheological Characterization

The linear dynamic storage modulus, G', was measured by a rheometer (ARES, TA Instrument Japan) at a strain of 0.1%. A dynamic temperature ramp test was also performed in a rectangular torsion mode in the temperature range from 30 to 120°C. The strain was maintained at 0.1% with a frequency of 1 rad s^{-1}. The heating rate was 2°C min^{-1} for all tests. The frequency sweep test was also carried out at two different

temperatures (60 and 100°C) with a fixed 0.1% strain in the frequency range from 0.1 to 100 rad s^{-1}.

4.2.5 Foaming Experiment

Please refer to preceding chapter.

4.2.6 Morphology Characterization

Cell morphology of the foamed samples was analyzed by SEM (Tiny-SEM, Technex CO. Ltd., Japan), after cryo-fracturing by liquid nitrogen and gold coating with 20 seconds processing time. The solid and foam densities were measured using densimeter (Mirage, MP-200S).

4.3 Results and Discussion

4.3.1 Solubility and Diffusivity of CO_2 in SEBS

Figures 4.2 and 4.3 show the solubility and diffusivity data, respectively, of CO_2 in the two SEBS copolymers in the range from 6 to 18 MPa and temperatures of 60, 100, and 155°C, which covers the foaming temperatures in this study. The resulting binary interaction parameters, k_{12}, are listed in Table 1. In the given pressure range, the solubility of CO_2 in all polymers increases proportionally with CO_2 pressure and follows Henry's law. With the increase of the styrene content, the solubility decreased.

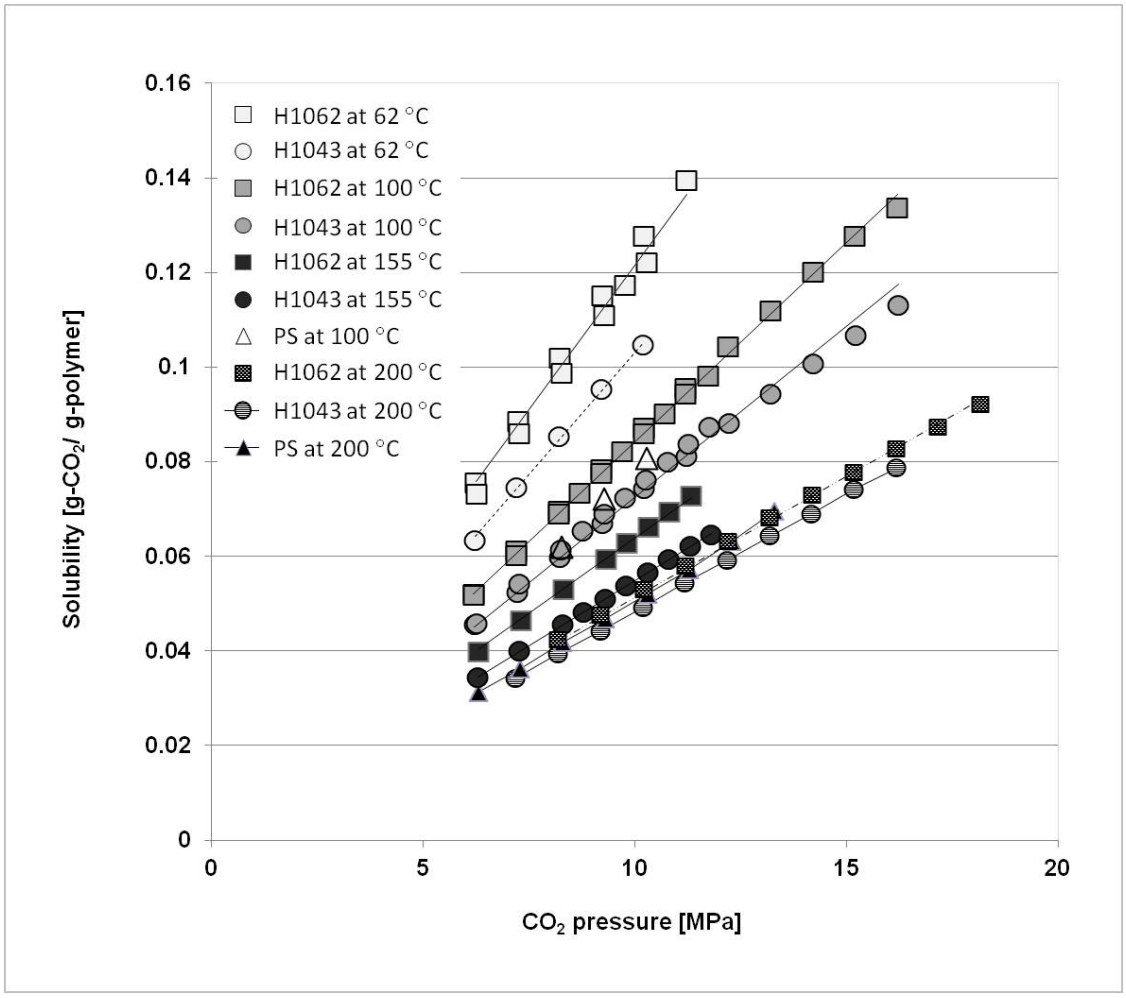

Figure 4.2 Solubility of CO_2 in SEBS and blends at different temperatures.

Figure 4.3 plots the logarithmic mutual diffusion coefficient against the inverse of the temperature (1/T). The diffusivity coefficients were calculated by taking the average values measured in the pressure range from 7 to 12 MPa.

The solubility increases and the diffusivity decreases as the temperature decreases in accordance with Henry's law. Furthermore, the diffusivity and solubility of CO_2 in SEBS (H1043) are lower than those in SEBS (H1062). The difference in the diffusivity of CO_2 between H1062 and H1043 is large, especially at the lower temperature of 62°C. Thus,

the CO_2 permeability (which is the product of the solubility and the diffusivity) of SEBS (H1043) is lower than that of SEBS (H1062) at any investigated foaming temperature.

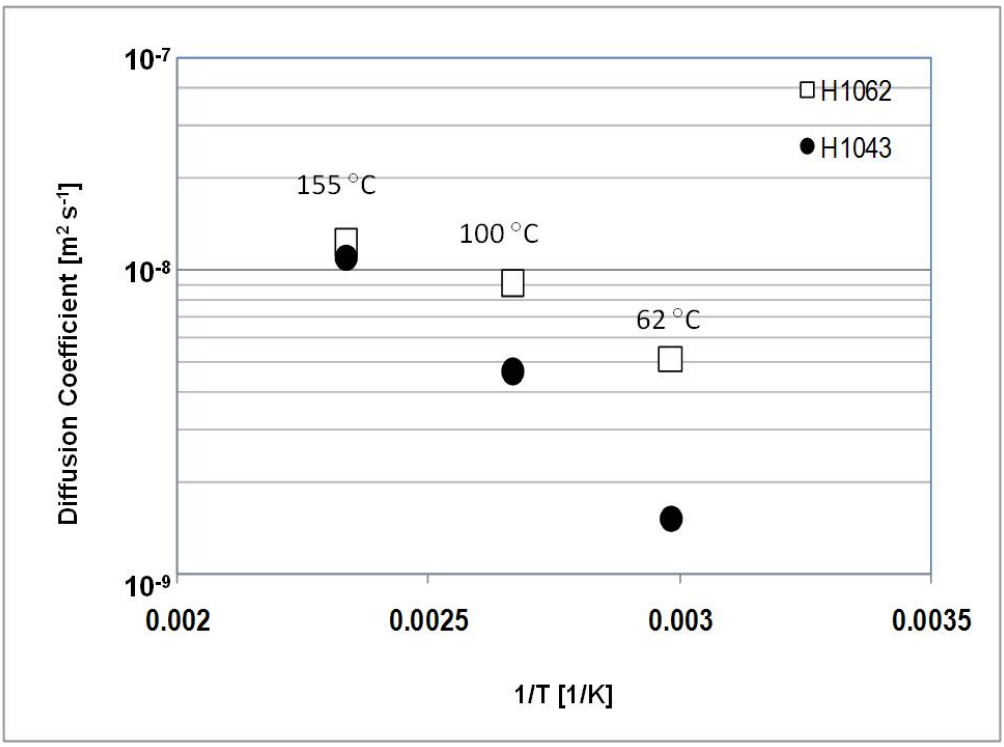

Figure 4.3 Temperature dependency of the diffusion coefficient of CO_2 in SEBS.

TABLE 4.1 Characteristic parameter of Sanchez- Lacombe Equation of state.

	H1062	**H1043**	**PS**	**H1062/PS**		**H1043/PS**	
				80/20	**50/50**	**80/20**	**50/50**
T^* [K]	6.5599E+02	6.7455E+02	6.9512E+02	6.5209E+02	6.7335E+02	6.9216E+02	6.9512E+02
P^* [K]	3.1685E+08	3.4094E+08	3.1123E+08	3.2507E+08	3.1909E+08	3.0777E+08	3.1123E+08
ρ^* [kg/m^3]	9.3939E+02	1.0319E+02	1.0338E+03	9.6967E+02	1.0144E+03	1.0338E+03	1.0338E+03
Mw [kg/mol]	7000	45000	192000	94400	131000	74400	118500
k_{12}_62°C	0.1309	0.1299					
k_{12}_100°C	0.1349	0.1320	0.1266	0.1332	0.1351	0.1337	0.1317
k_{12}_155°C	0.1412	0.1382					
k_{12}_200°C	0.1523	0.1333	0.1526				

Figure 4.4 shows the solubility and diffusivity of CO_2 in the SEBS blends at a temperature of 100°C under 10 MPa CO_2 pressure. As the PS content increased in the H1043/PS blend, the diffusivity decreased and the solubility increased compared with those in neat H1043. This is because the solubility and diffusivity of CO_2 in PS is respectively higher and lower than that in the neat H1043.

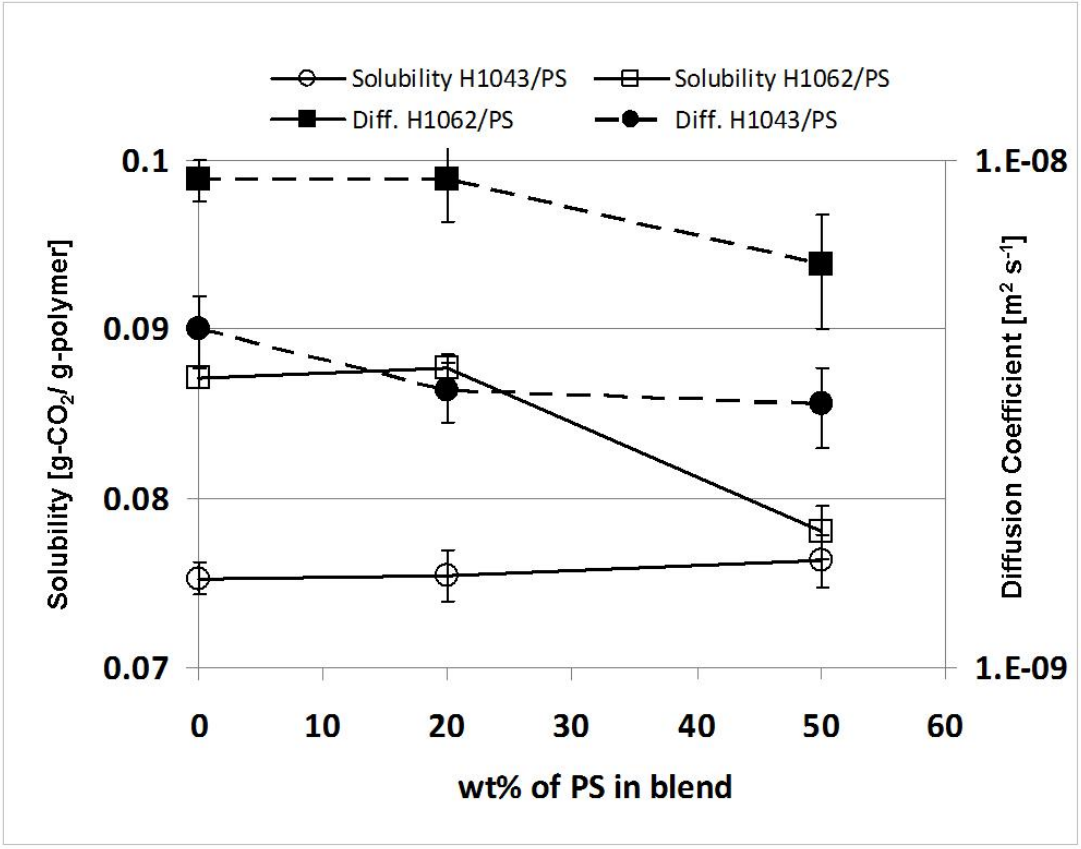

Figure 4.4 Solubility and Diffusivity of CO_2 in polymer blends with different PS %.

The changes in the solubility and diffusivity were detectable at 20 wt% PS content in H1043/PS blend. However, for H1062/PS blends, the changes in the solubility and diffusivity at 20 wt% PS contents were too subtle to be differentiated from experimental measurement errors. They became prominent when PS content was increased to 50 wt%

in the blend. Considering the fact that both diffusivity and solubility of CO_2 in PS were lower than those in H1062 as shown in Figures 4.2 and 4.4, it is natural to speculate that the solubility and diffusivity of CO_2 in H1062/PS decreases with the increase of PS content in the blend but the changes in diffusivity and solubility at 20 wt% PS content could not be prominent due to interaction (miscibility) between EB block of H1062 and PS.

The permeability of SEBS (H1062)/PP blends are estimated using Gusev and Lusti model[25] for supporting the reduction of CO_2 diffusivity in SEBS with the addition of thermoplastic polymer PS. The estimation on the permeability of SEBS (H1062)/PP was done by considering the case of circular disk filler type. This case is considered to represent PP as dispersed domain in SEBS matrix. Permeability is the product of solubility and diffusivity; $P = DS$. The penetrant (CO_2) solubility in SEBS matrix is given by

$$S = S_0(1-\phi) \tag{4.12}$$

where S_0 is the penetrant solubility coefficient in the pure polymer matrix and ϕ is the volume fraction of particles dispersed in the matrix.

The diffusion coefficient of penetrant by accounting the tortuosity factor, f

$$D = D_0 f \tag{4.13}$$

Combining the above equations gives

$$P = DS = (1-\phi)S_0 D_0 f = (1-\phi)P_0 f \tag{4.14}$$

By considering the particle geometry of circular disk of diameter, d and thickness, t, the following equation is used

$$(P_0 / P)(1-\phi) = (1+\alpha\phi/3)^2 \qquad (4.15)$$

Where $\alpha = d/t$

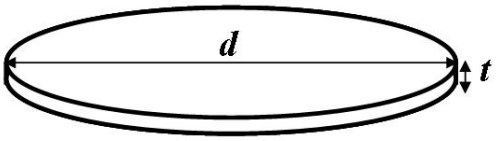

Figure 4.5 shows the plot of SEBS (H1062)'s permeability as a function of PP content (wt%). The permeability of SEBS (H1062) decreased with the increased of PP content. The result indicates that the CO_2 diffusivity of SEBS (H1062) is decreased with PP content.

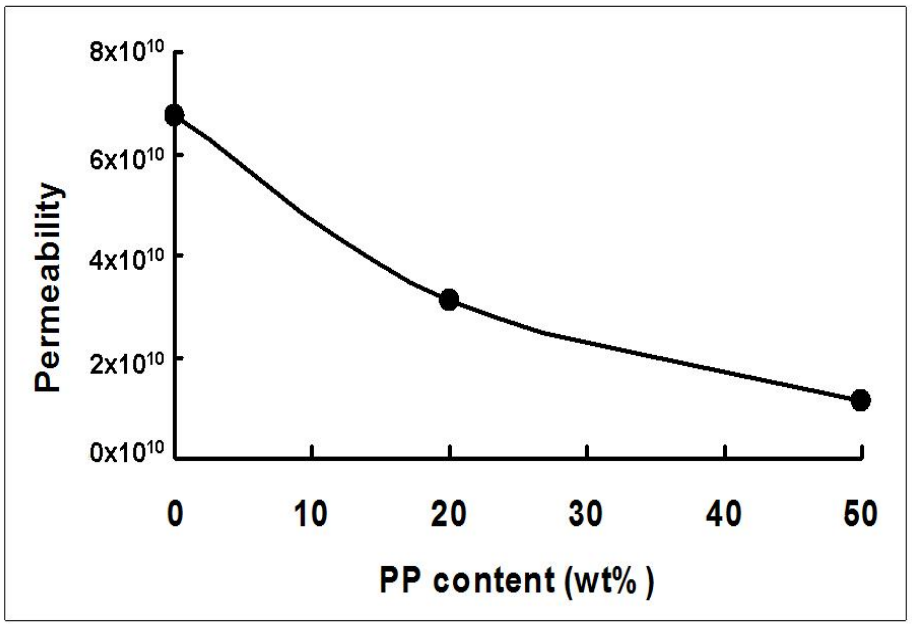

Figure 4.5 Permeability of SEBS (H1062) as a function of PP content.

4.3.2 Rheological Characterization of SEBS and SEBS/PS blend

Figure 4.6-a shows the temperature dependence of the storage modulus, G', and the loss modulus, G", of PS and the two SEBS copolymers. The measurements were conducted at a strain of 0.1% and a frequency of 1 rad s^{-1}. These data indicate that the G' of PS is highest, that of SEBS (H1043) is second, and that of SEBS (H1062) is lowest in the temperature range from 40 to 100°C, which is below the T_g of polystyrene. Based on the temperature at which tan δ shows the peak value, T_g values of PS, H1062 and H1043 are identified to be 105, 75 and 95°C, respectively as shown in Figure 4.6-b.

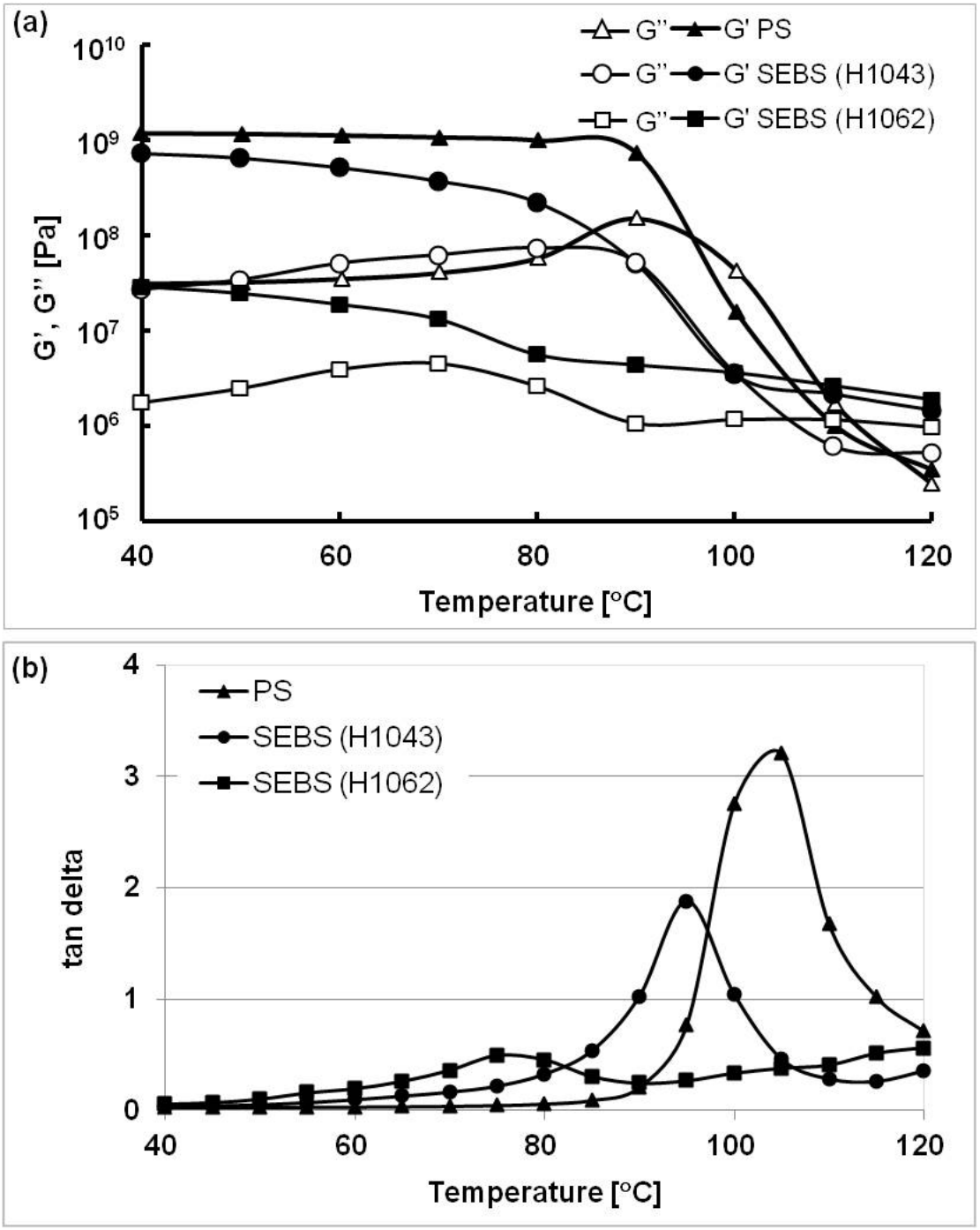

Figure 4.6 Rheological characterization of PS and SEBS; (a) G' and G''; and (b) tan delta.

Figures 4.7 and 4.8 show G’ and G”, respectively, of the SEBS (H1062)/PS and SEBS (H1043)/PS blends with two different blend weight ratios, 80/20 and 50/50. Blending PS with SEBS (H1062) at 20 wt% reduced both G’ and the absolute values of complex viscosity from those of neat PS. At temperatures below 80°C, their values were lower than those of SEBS (H1062). But, they became higher than SEBS (H1062) alone at temperatures higher than 80°C. The 50 wt% PS blends did not show any viscosity reductions from the value of neat SEBS. They exhibited the increases in both G’ and complex viscosity, which were higher than those of SEBS (H1062) and approaching to those of PS. The blend of PS with SEBS (H1043) did not reduce G’ from the value of SEBS (H1043) alone at any temperatures or any investigated blend ratios. G’ value of SEBS (H1043)/PS blends slightly increased as the amount of PS increased in the range of 90 to 100°C, as shown in Figure 4.8.

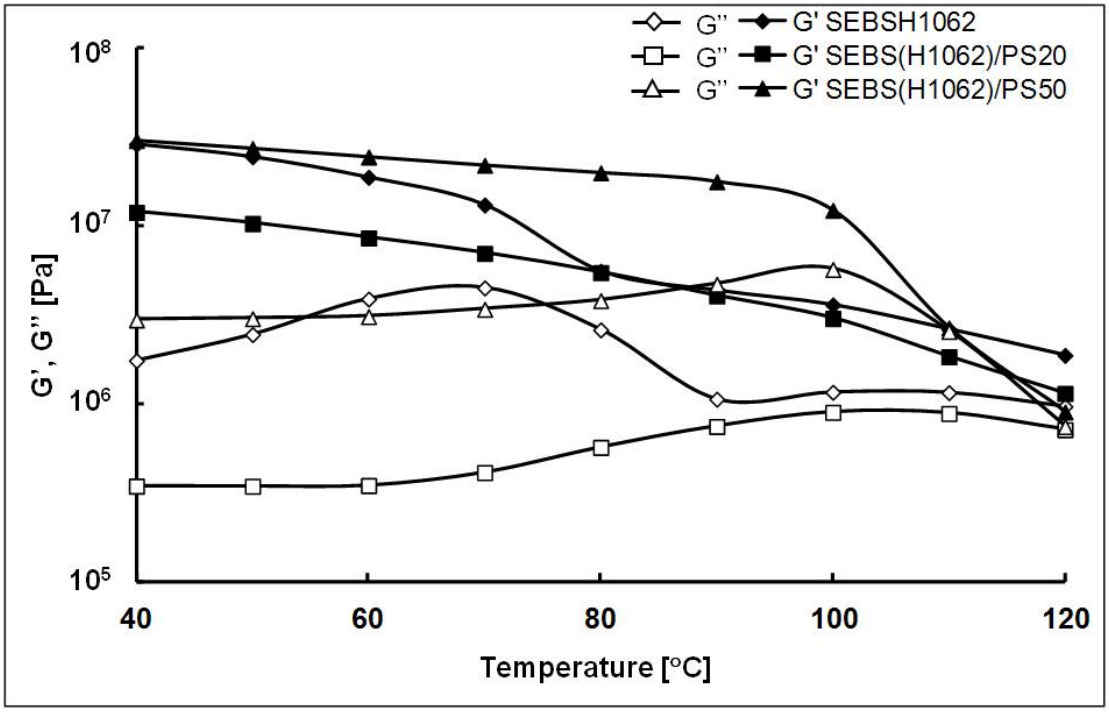

Figure 4.7 G’ and G’’ of SEBS (H1062) and its blend with PS.

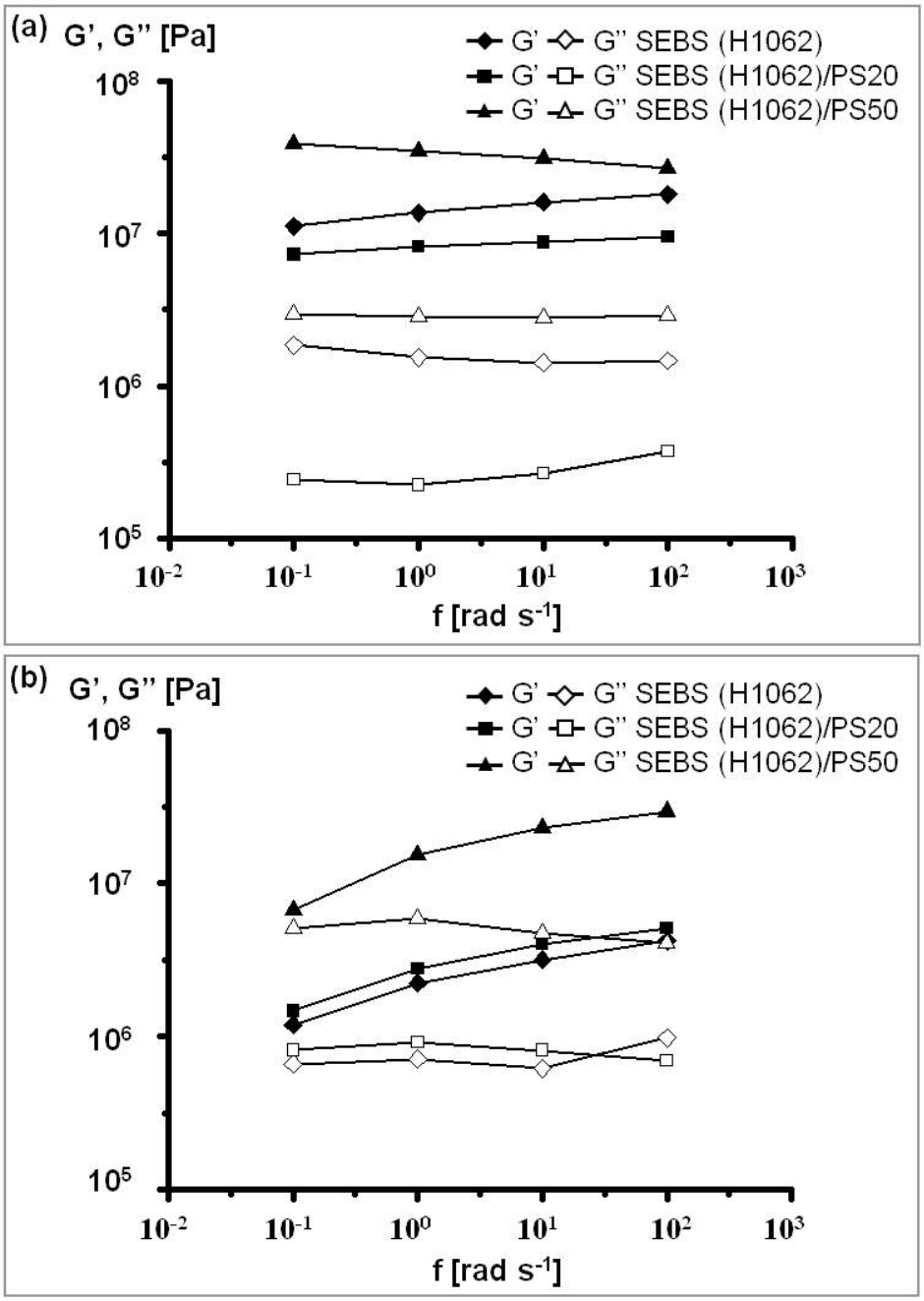

Figure 4.8 G' and G'' of SEBS (H1062) and its blend with PS as a function of frequency.

To confirm that the viscosity of the SEBS (H1062)/PS (80/20) blend reduces at temperatures below 80°C and increases at a temperature of 100°C, the frequency dependency of the storage and loss moduli was measured at both 60 and 100°C for SEBS (H1062) alone and its blends. Figures 4.9-a and 4.9-b show the G' and G'' of the SEBS (H1062) and blends as a function of frequency at 60 and 100°C. The storage moduli, G' of SEBS (H1062)/PS (80/20) blend decreased slightly at 60°C, but it became larger than the value of SEBS (H1062) alone at 100°C. Furthermore, at 60°C, the 50 wt% PS blended samples exhibited slight increase in G' at low frequency, which resembles the behavior of a cross-linked polymer.

Figure 4.10 (a) shows the G' and G''of SEBS (H1062) and its blend with PP. At 60°C, SEBS (H1062)/PP (80/20) shows a slight drop of G' and G'' from the SEBS (H1062) alone. The G' and G'' of SEBS (H1062)/PP (50/50) however, were increased up to 10^8 and 10^7 Pa, respectively. The increased of both moduli in SEBS (H1062) with 50 wt% PP at all temperature ranges shows the behavior of crosslinked polymer as SEBS (H1062)/PS (50/50) blend. Figures 4.10 (b) displays a plots of G' and G'' versus temperature for SEBS (H1043) and SEBS (H1043) blends at 20 and 50 wt% PP. It was observed that G' and G'' of blend samples are higher than that of SEBS (H1043) alone at temperature above the T_g of styrene.

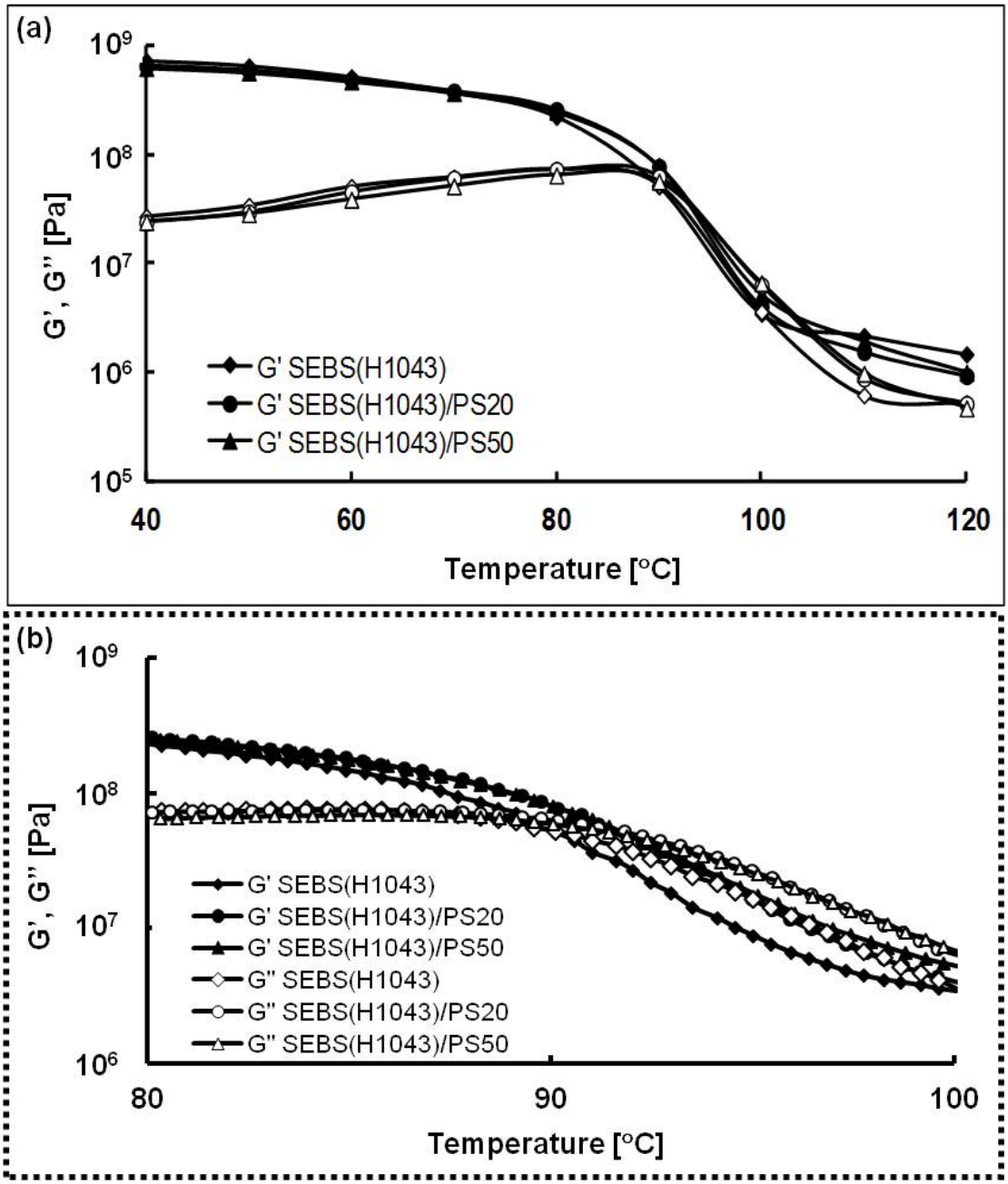

Figure 4.9 G’ and G’’ of SEBS (H1043) and its blends.

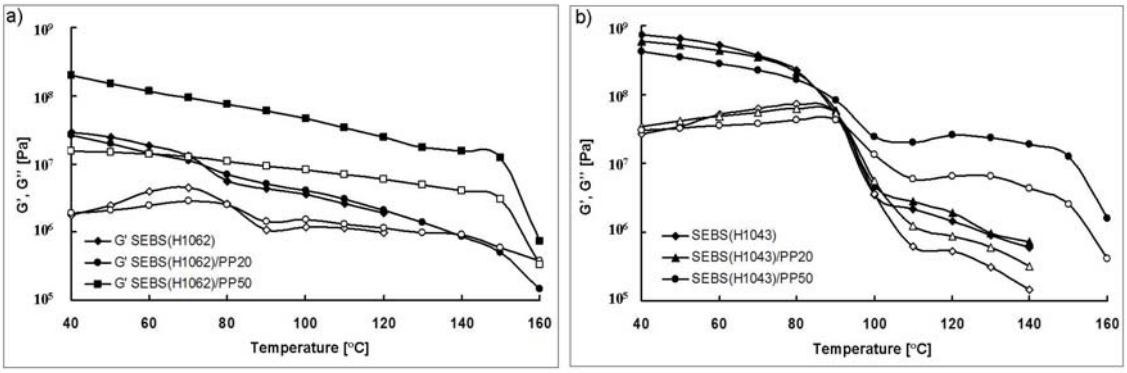

Figure 4.10 Elastic and viscous moduli of SEBS (H1062) and (H1043) and their blends at different temperature.

Figures 4.11-a and (b) show the G' and G'' obtained from frequency sweep for the SEBS (H1062)/PP (50/50) and SEBS (H1043)/PP (50/50) blend samples at 200°C and 0.1% strain. As seen in Figure 4.11-a, the G' of SEBS (H1043)/PP (50/50) blend is higher as compared to G'' which implies that the sample behaves as solid (elastic) at high frequency and behaves as rubber- like at lower frequency. It is demonstrated that high elasticity in SEBS (H1043)/PP (50/50) resembles the restriction of chain mobility. Figure 4.11-b however, displays that SEBS (H1062)/PP (50/50) blend shows the apparent liquid-like behavior (viscous) where the G' was smaller than the G'' at almost all frequencies. Complex viscosity (η^*) of SEBS (H1062)/PP (50/50) is higher than that of SEBS (H1043)/PP (50/50) blend at high frequency but dropped at lower frequency. This result demonstrates the tendency of the entangled chains in SEBS (H1062)/PP (50/50) blend to deform and resemble the highly-crosslinked polymer behavior.

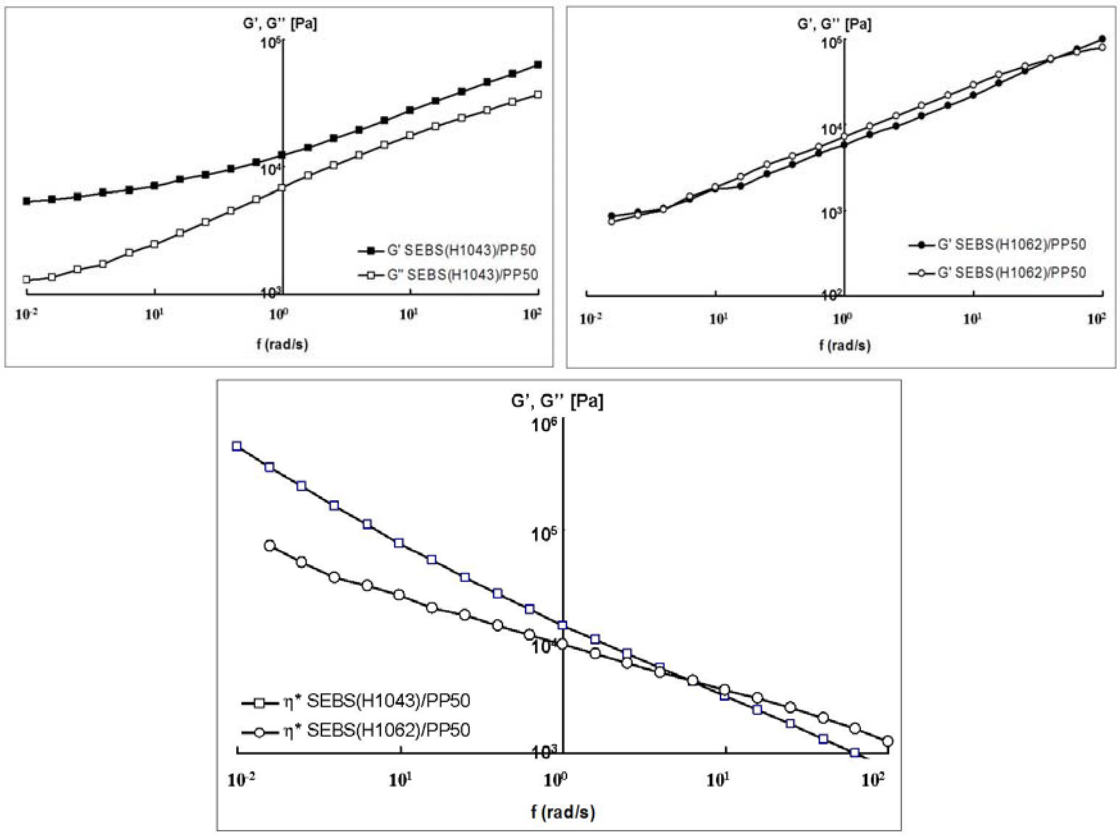

Figure 4.11 Rheological characterizations of samples measured by frequency sweep test at 200°C and at 0.1% strain.

The polymer chain of SEBS consists of styrene and EB blocks. The micro-phase separation occurs and forms sea-island morphology, where the end segment (styrene block) forms cubic domains in the EB continuous phase.[27] Wang *et al.*[28] claimed that high interfacial tension between styrene and EB blocks brings about the micro-phase separation. In 80/20 SEBS (H1062)/PS, due to interaction between styrene block of SEBS and PS polymer, the sea-island morphology was still formed but the size of styrene disperse domain seemed to increase slightly (Figure 4.12-a) comparing with the disperse domain in EB continuous matrix in 50/50 blend (Figure 4.12-b). The slight increase in

size of the styrene-disperse domain could reduce the G' and G'' values at 80/20 SEBS (H1062)/PS blend from those of SEBS (H1062) alone at temperatures below 80°C.

As observed, the 80/20 SEBS (H1062)/PS blend did not show so much difference in the CO_2 solubility and diffusivity from those of SEBS (H1062) alone. This might be caused by preservation of micro-phase separation in the blend. When the added PS content increased to 50 wt% in the blend, the aggregation behavior of PS progressed, the size of PS domain increased to micro-scale and the morphology changed from micro-phase separation to the morphology where PS formed micro-scale large domains as shown in Figure 4.12-b. Then, the effect of presence of stiff PS on viscosity would become stronger and viscosity increased at 50/50 SEBS (H1062)/PS blend.

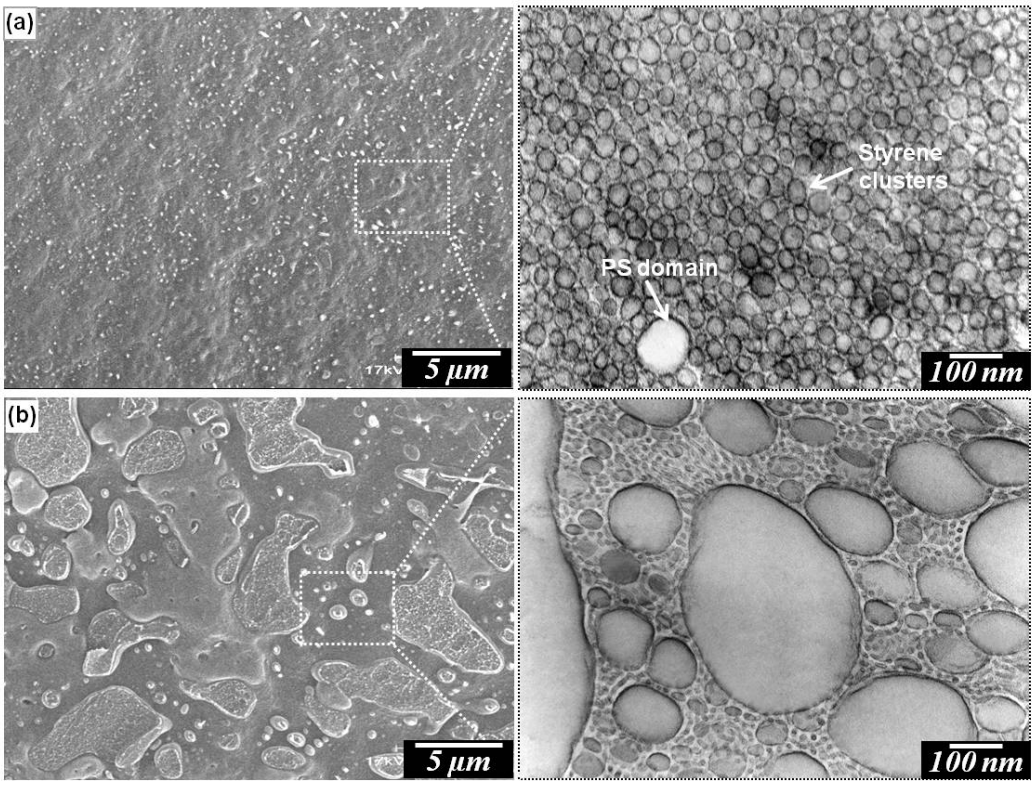

Figure 4.12 Blend morphology of SEBS (H1062)/PS blends at different ratio: (a) 80/20 and (b) 50/50.

The same phenomenon was observed when SEBS (H1062) was blended with PP where sea and island structure was obtained in stained SEBS (H1062)/PP (80/20) blend. The resulted morphology indicates the presence of interaction between EB segment and PP polymer (Figure 4.13-b). The change from sea and island structure to co-continuous structure was apparently when the amount of PP was increased to 50 wt% as shown in Figure 4.13-c.

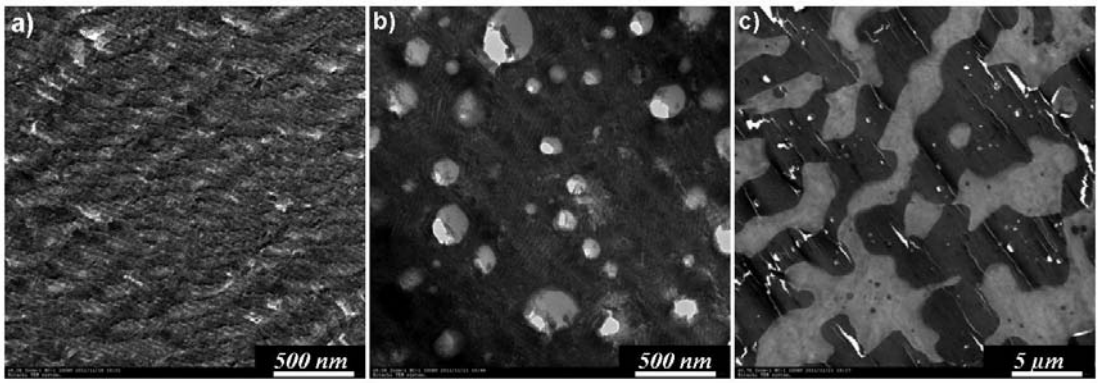

Figure 4.13 SEM micrographs of $RuCl_4$-stained fracture surface: (a) SEBS (H1062); (b) SEBS (H1062)/PP20 and (c) SEBS (H1062)/PP50.

4.3.3 Foaming Behavior of SEBS (H1062) and (H1043)

Figure 4.14 compares the cell structures of the foamed SEBS (H1062) and (H1043) alone. Three different foaming temperatures, 60, 100 and 155°C, were investigated under the same 10 MPa saturation pressure of CO_2. Both H1062 and H1043 were foamed. Their foam expansion ratios increased with the increase of the foaming temperature. SEBS (H1043) developed spherical pores, even though its foamability was not as high as that of SEBS (H1062). This effect was caused by the higher G' of SEBS (H1043). Because of the large dimensional instability with foam shrinkage, pores were not clearly observed in

the SEBS (H1062) foams at any foaming temperatures, as shown in the images in the upper row of Figure 4.14.

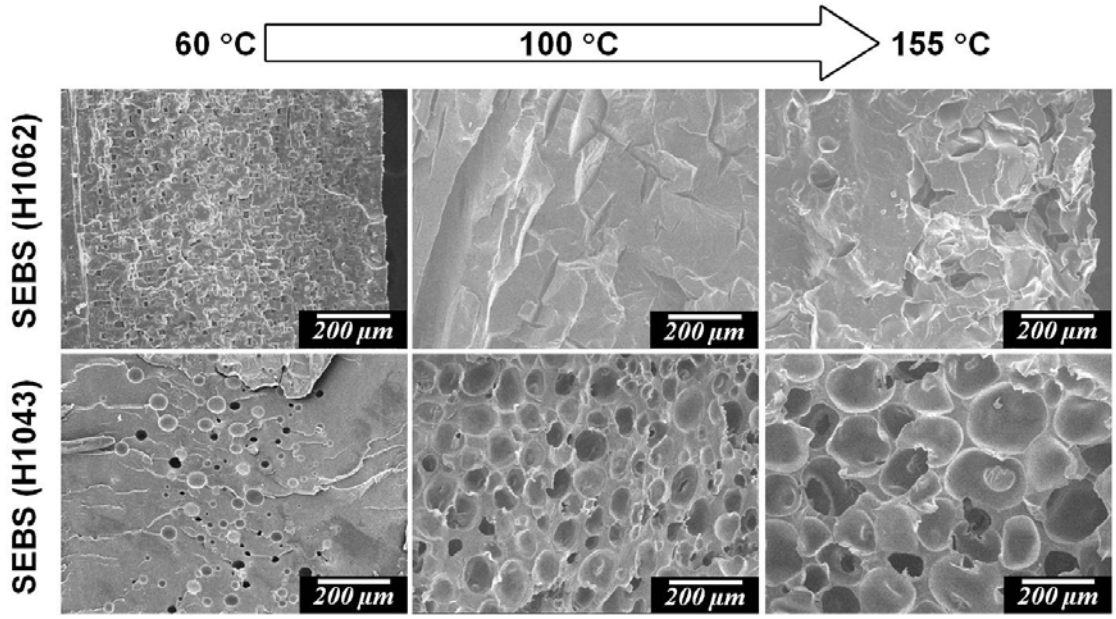

Figure 4.14 Cell structure of SEBS (H1062 and H1043) foams at three different temperatures: (a) 60°C, (b) 100°C and (c) 155°C.

Figure 4.15 shows the change in foam density as a function of time after the conclusion of foaming. After the SEBS copolymers were foamed at 60, 100 and 155°C, the foams were maintained at room temperature and atmospheric pressure, and the density of the foams was occasionally measured by the densimeter. The SEBS (H1062) foam exhibited a drastic increase in density over time (instability of foam) at 60°C. When the SEBS (H1062) was foamed at 155°C, the change in its density was too fast to be recorded, and the foam eventually exhibited a higher density (lower expansion ratio). This densification occurred because of the increase in the diffusivity and the decrease in G' with the increase of the foaming temperature. SEBS (H1062) was not rigid enough to prevent the

foams from shrinking against the excess forces exerted by elastic deformation and the rapid gas loss from the cells.

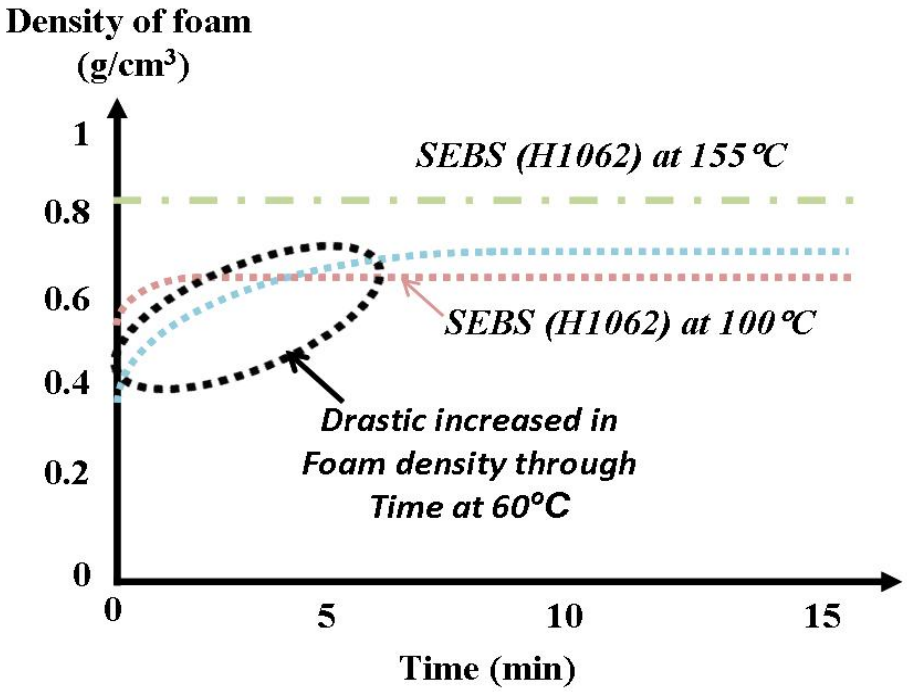

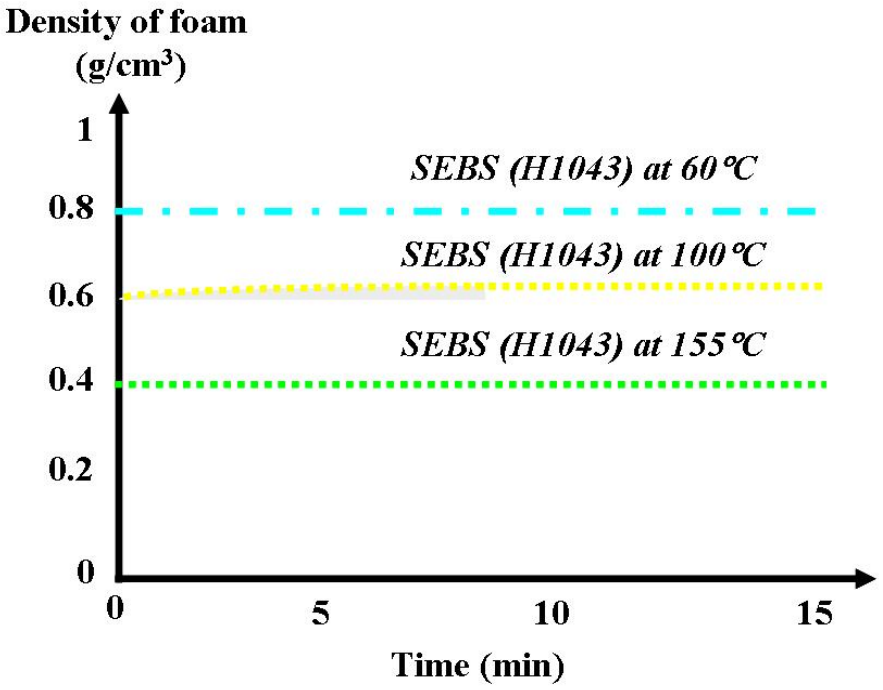

Figure 4.15 Shrinkage of SEBS (H1062 and H1043) foams (foam density-time curves).

In the SEBS (H1043) foams, the shrinkage was not as drastic as that of H1062 at both foaming temperatures. Because of the higher storage modulus, the expansion ratio was low at a foaming temperature of 60°C, but it was improved when the foaming temperature was increased to 155°C. The higher instability of the cell structure of the SEBS (H1062) foams could be explained by the higher diffusivity of CO_2 (Figures 4.3 and 4.4) and the lower storage modulus of the polymer (Figures 4.6 and 4.7). By comparison of the results of both H1062 and H1043, it can be observed that the increase in the styrene content of the SEBS decreased the CO_2 diffusivity and solubility while simultaneously increasing the storage modulus and the complex viscosity, which stabilized the cell structure.

4.3.3 Foaming Behavior of SEBS (H1062)/PS and SEBS (H1043)/PS blends

To control the storage modulus and CO_2 diffusivity, PS was blended with both SEBS copolymers. The SEBS (H1062)/PS and SEBS (H1043)/PS blends were prepared at different weight ratios (80/20 and 50/50) and foamed at different temperatures (60, 100 and 120°C). Figures 4.16 and 4.17 show SEM micrographs of the SEBS (H1062)/PS and SEBS (H1043)/PS blend foams, respectively. Figures 4.18 and 4.19 show the change in the foam density over time after foaming.

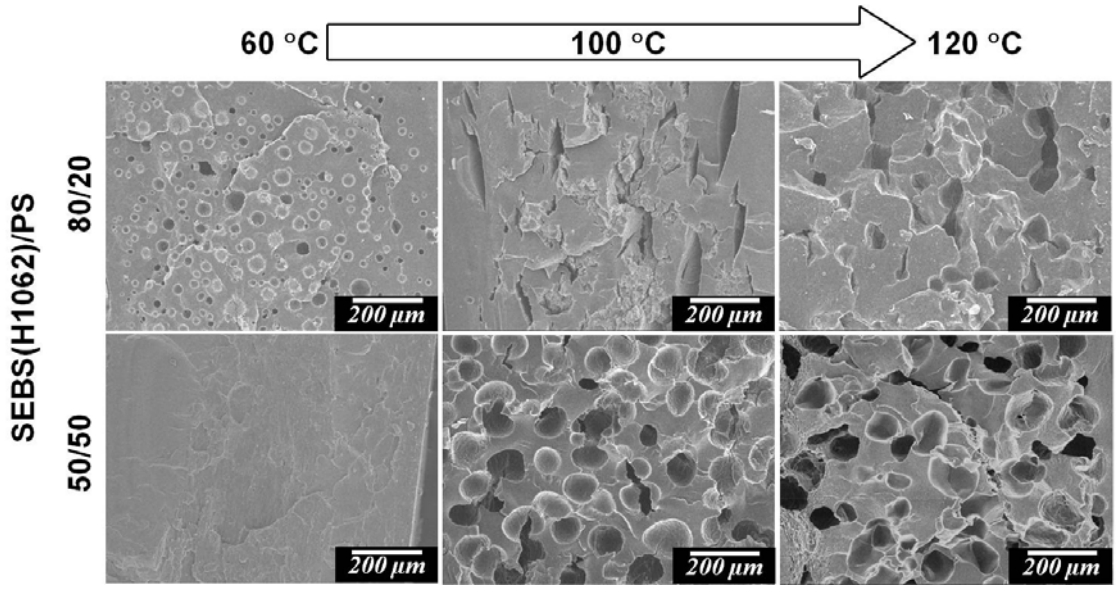

Figure 4.16 SEM micrographs of SEBS (H1062)/PS foams with weight ratios of 80/20 and 50/50 at different foaming temperatures.

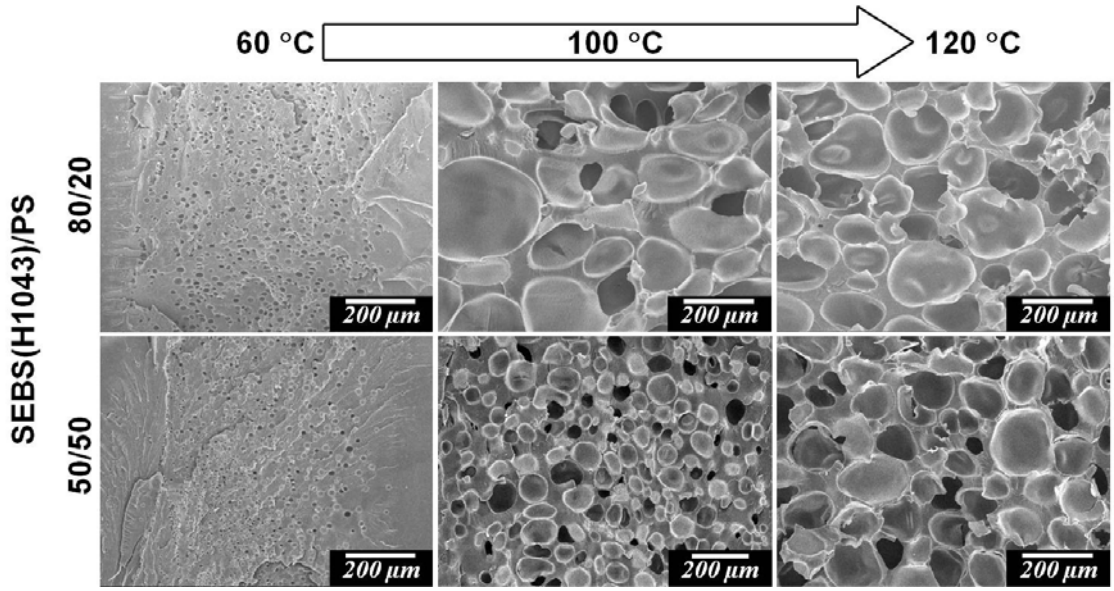

Figure 4.17 SEM micrographs of SEBS (H1043)/PS foams with weight ratios of 80/20 and 50/50 at different foaming temperatures.

In the SEBS (H1062)/PS (80/20) foams, the cell size increased with elevated foaming temperature (Figure 4.16), but the foam density did not increase (Figure 4.18). As shown in Figure 4.18, the foam density (expansion ratio) reached its minimum (maximum) when the SEBS (H1062)/PS (80/20) was foamed at 100°C. The storage modulus and complex viscosity decreased with the increase of temperature, as shown in Figure 4.6. This viscosity reduction caused the cell growth to occur faster and the cell size to become larger. In addition, the CO_2 diffusivity increased as the temperature increased. These changes made the gas loss increase and reduced the expansion ratio at 120°C. By increasing the PS blend ratio to 50 wt%, the CO_2 diffusivity was lowered, as shown in Figure 4.4. Then, even though the foamability was not good at 60°C because of the higher storage modulus, it was improved by increasing the foaming temperature, as shown in Figures 4.16 and 4.18.

For the case of the SEBS (H1043)/PS foams, the cell size increased as the foaming temperature increased at blend ratios of both 80/20 and 50/50. The difference in the foaming behavior from that of the SEBS (H1062)/PS blends was induced by the lower CO_2 diffusivity and the higher storage modulus. Blending PS with the SEBS produced a polymer matrix that was rigid enough to prevent the cell from shrinking.

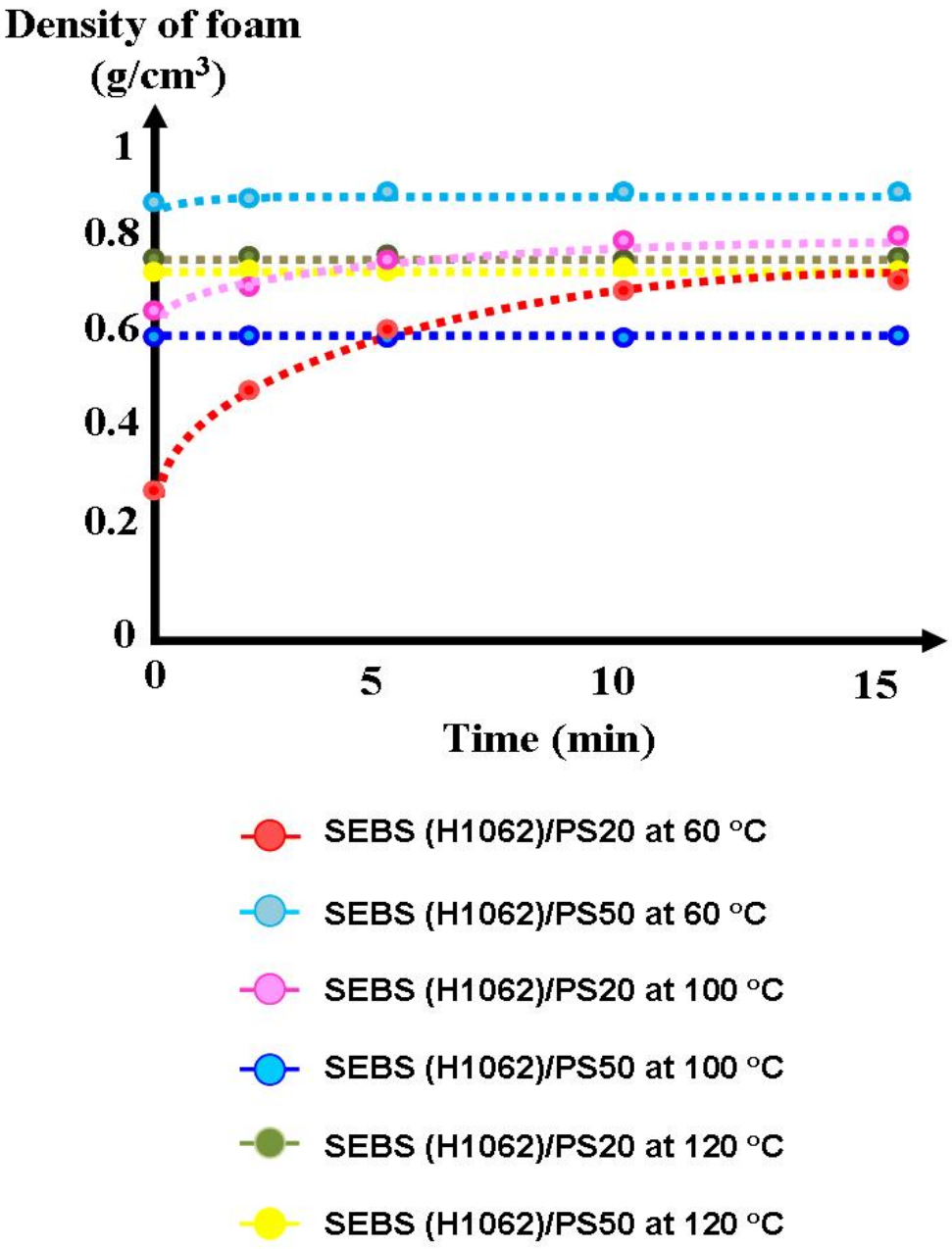

Figure 4.18 Shrinkage of SEBS (H1062)/PS with blend ratios of 80/20 and 50/50 at different foaming temperatures.

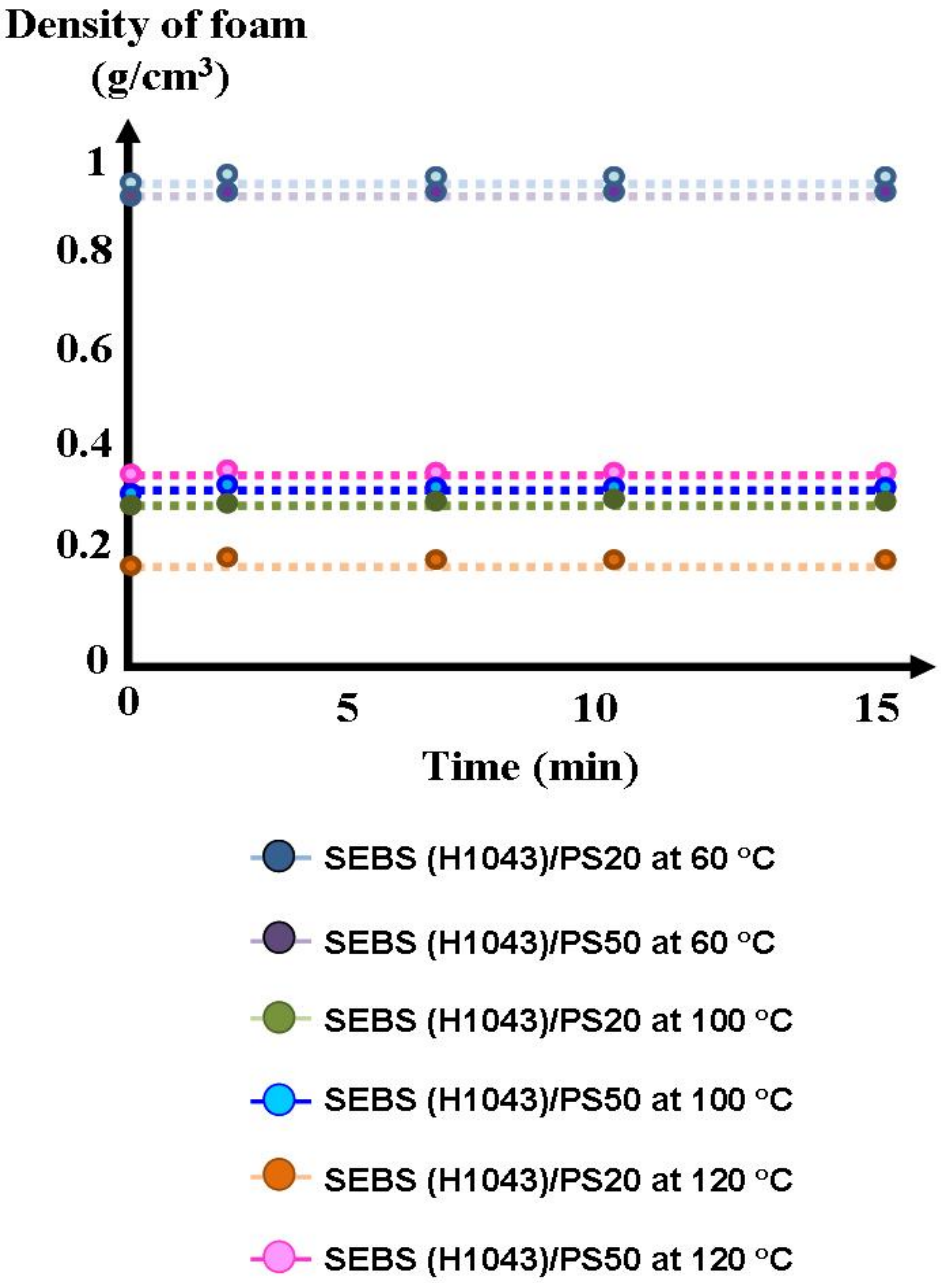

Figure 4.19 Shrinkage of SEBS (H1043)/PS with blend ratios of 80/20 and 50/50 at different foaming temperatures.

4.3.5 Foaming behavior of SEBS (H1062)/PP and SEBS (1043)/PP blends

Figure 4.20 shows the cell structures of SEBS (H1062) foams after adding 20 and 50 wt% of PP at 60 and 155°C. At 60°C, the cell properties of SEBS (H1062)/PP (80/20) blend foam were improved in terms of cell size and cell density as compared to SEBS (H1062) foam. Eventhough the G' and G'' of SEBS (H1062)/PP (80/20) were decreased at 60°C, the dimensional stability of the foam could be maintained due to its slower CO_2 permeability compared to SEBS (H1062). However, no bubble was obtained in SEBS (H1062)/PP (50/50) blend after foaming at corresponding temperature. When the foaming temperature was increased to 155°C, large bubble was obtained in SEBS (H1062)/PP (80/20) while in SEBS (H1062)/PP (50/50) blend, small cell size and high cell density foam was produced.

In addition to high G' and G'', the reason of why no bubble was formed in SEBS (H1062)/PP (50/50) is due to high crystalline fraction in PP that restricted CO_2 diffusion into the sample and thus prevented bubble nucleation. The result also shows that the SEBS (H1062) blending with high concentration of PP could reduce the cell expansion at elevated foaming temperature. Thus, the controllability of foam shrinkage in SEBS (H1062) at high temperature is enhanced with PP as compared to with PS.

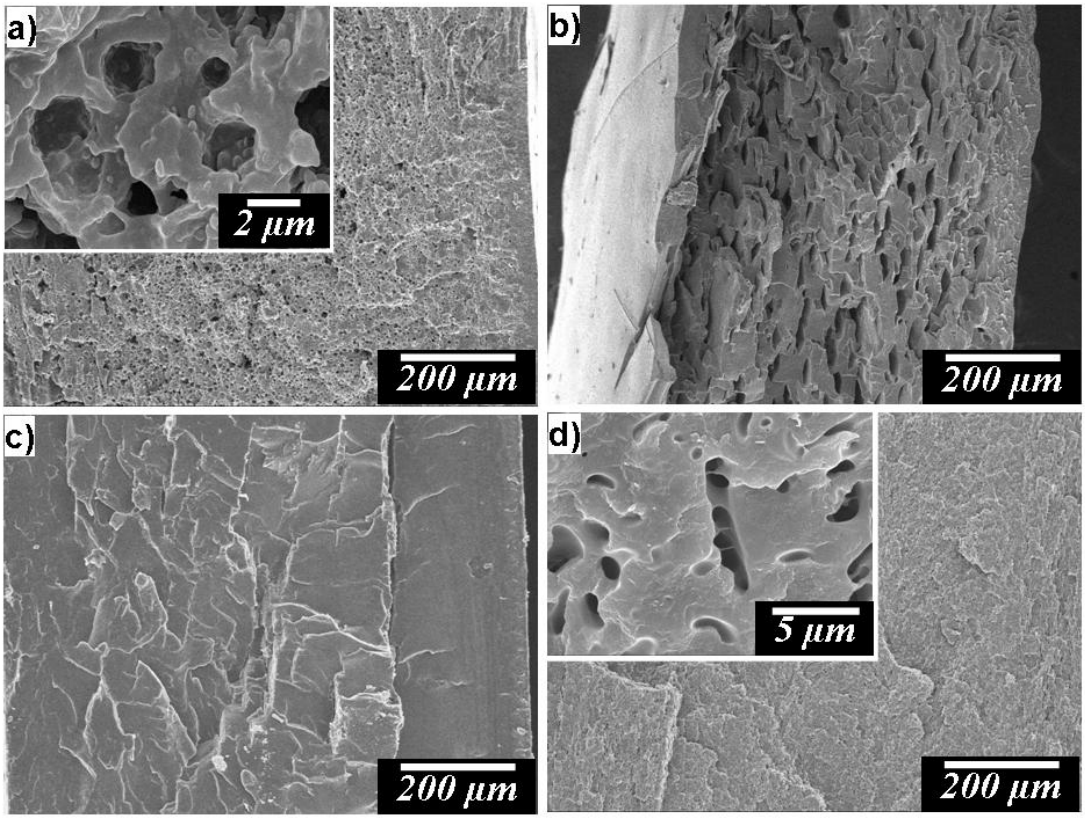

Figure 4.20 SEM micrographs showing SEBS (H1062) blend foams (a) and (c) SEBS (H1062)/PP (80/20) at 60 and 155°C, respectively; (b) and (d) SEBS (H1062)/PP (50/50) at 60 and 155°C, respectively.

Figure 4.21 shows the foam density of SEBS (H1062) blends as a function of time at 60 and 155°C. At 60°C, rapid increased in foam density of SEBS (H1062)/PP (80/20) was observed. High CO_2 diffusivity and low elasticity are identified as the main factors contribute to the foam shrinkage. The addition of 50 wt% PP reduced the foam shrinkage in SEBS (H1062) by increasing the elasticity and decreasing the CO_2 diffusivity. This reduction of shrinkage is clearly shown by no changes in foam density through time.

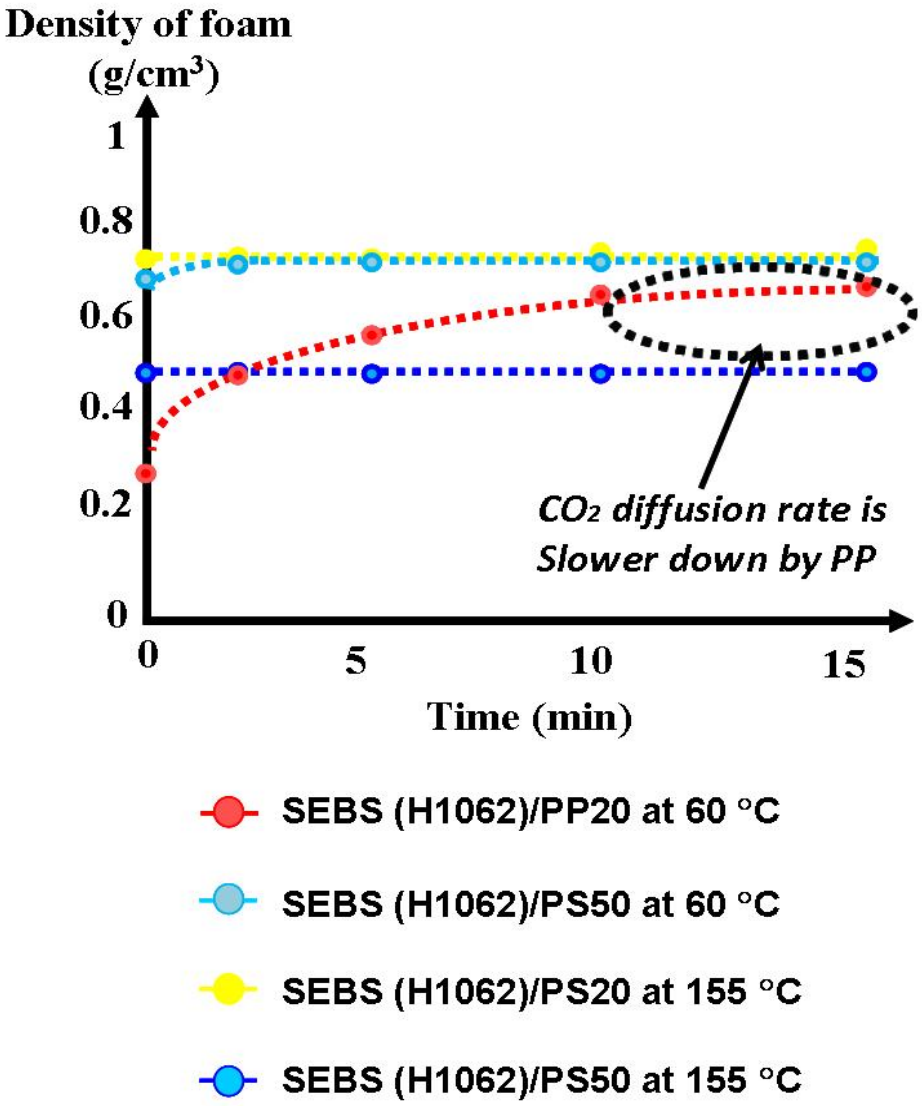

Figure 4.21 Shrinkage of SEBS (H1062) foam and SEBS (H1062)/PP blend foams.

This study was further investigated by utilizing SEBS with longer styrene segment. SEBS (H1043) with styrene as the main constituent is more rigid and behaves as a solid. Thus, it was believed that SEBS will have higher elasticity when the styrene% is increased. A comparison of foaming behavior between SEBS (H1062) and SEBS (H1043) based on different elasticity and diffusivity was performed by blending both grades of SEBS with PP and further foamed the blend samples at 60 and 155°C. Figure 4.22 shows the resulted cell structures of SEBS (H1043)/PP (80/20) and SEBS (H1043)/PP (50/50) foams after 6 hours sorption in $scCO_2$ at 10 MPa. SEBS (H1043)/PP (80/20) was foamed at 60°C. SEBS (H1043)/PP (50/50) however not foamed at corresponding temperature. Its foamability however, was improved as the foaming temperature was increased to 155°C. Foam with small cell size and high cell density was obtained in SEBS (H1043)/PP (50/50). This result indicates that bubble was probably nucleated in SEBS and cell expansion was restricted by PP's crystalline phase. As the foaming temperature increased to 155°C, SEBS (H1043)/PP (80/20) foam showed the increment of cell size. However, SEBS (H1043)/PP (80/20) foam remained stable even it was highly expanded at 155°C as illustrated in Figure 4.22.

Figure 4.23 shows the estimated degree of shrinkage of SEBS (H1043) blend based on change in foam density through time. All foam samples show no significant change in density against time, reflected by no foam shrinkage occur at all foaming temperatures.

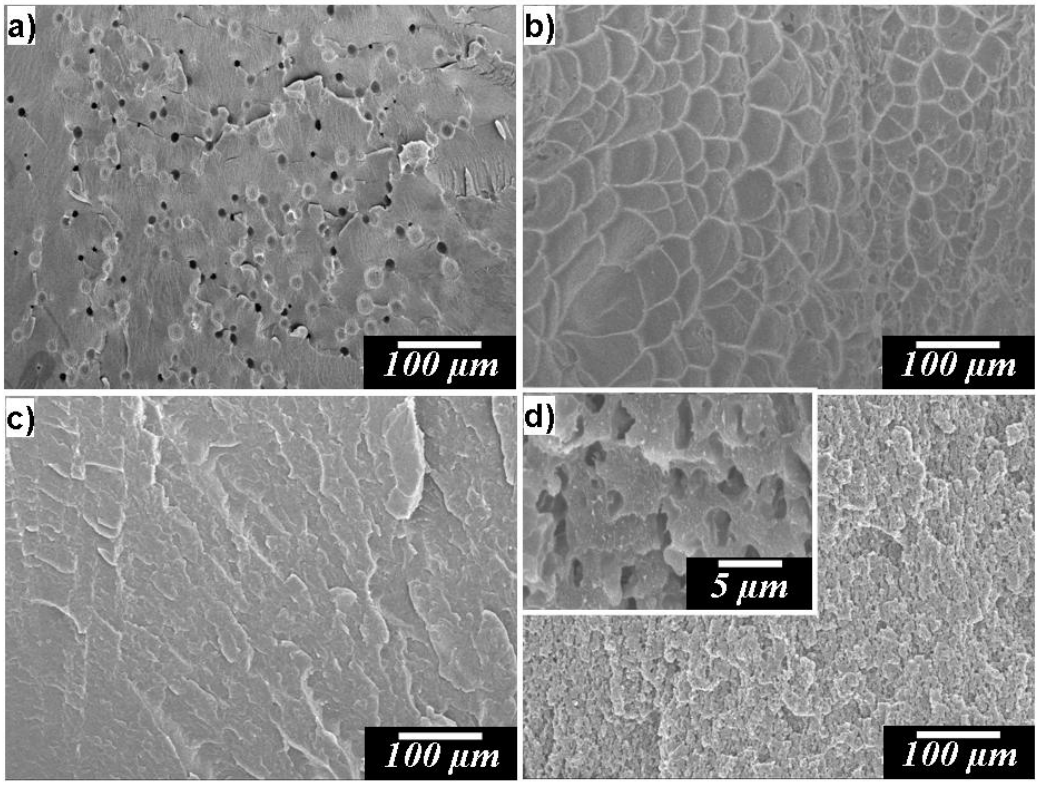

Figure 4.22 SEM micrographs showing SEBS (H1062) blend foams (a) and (b) SEBS (H1043)/PP20 at 60 and 155°C, respectively; (c) and (d) SEBS (H1043)/PP50 at 60 and 155°C, respectively.

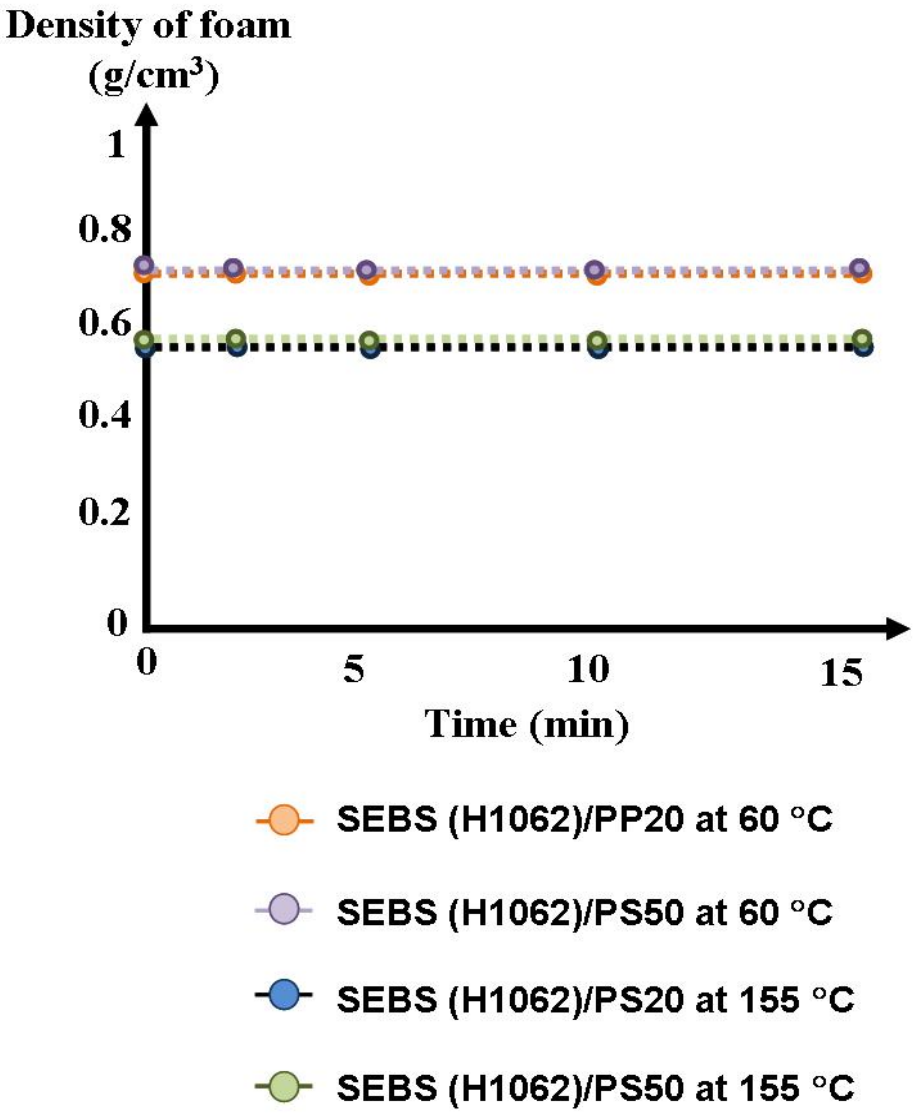

Figure 4.23 Graph of density of foam as a function of time for SEBS (H1043) foam and SEBS (H1043)/PP blend foams.

4.3.6 Effect of T_g and T_m of PS and PP on The Controllability of Foam Shrinkage in SEBS (H1062)

The effect of T_g and T_m of PS and PP, respectively, was further studied on the controllability of foam shrinkage in SEBS (H1062). Foaming experiments were carried out on SEBS (H1062)/PS blend at temperature above the T_g of PS (120°C) and SEBS (H1062)/PP blend at temperature slightly lower than T_m of PP (158°C).

As observed, at 120°C, the foam shrinkage was occurred in SEBS (H1062)/PS at any blend ratio. The result indicates the controllability of foam shrinkage with the presence of PS is reduced at temperature above its T_g. This is because PS is in rubbery state has high chain mobility. As the chain mobility increases, the elasticity decreases while CO_2 diffusivity increases. Thus, the controllability of foam shrinkage by PS is ineffective as its elasticity is reduced while CO_2 diffusivity is increased.

The effect of entanglement network on foaming behavior of SEBS/PP (50/50) blend was further investigated by foaming the sample at temperature near to the melting point of PP. Figure 4.23 shows the resulted cell structure where open cell was obtained at foamed part of sample. Besides, there are also containing some non foamed part in sample. Basically, the crystalline region and non- crystalline region coexist in PP. The entanglement network however, only formed in the non- crystalline region below T_m[17] as shown in the schematic diagram (Figure 4.24). At temperature near to T_m of PP or above, the entangling chain is deformed. This is because, the tendency of chain disentanglement increases with the increases of temperature[18]. Therefore, it is necessary to lower down the foaming temperature profile below the T_m of PP to ensure the crosslinked chains is remain entangled. Thus, the controllability of foam shrinkage still can be attained.

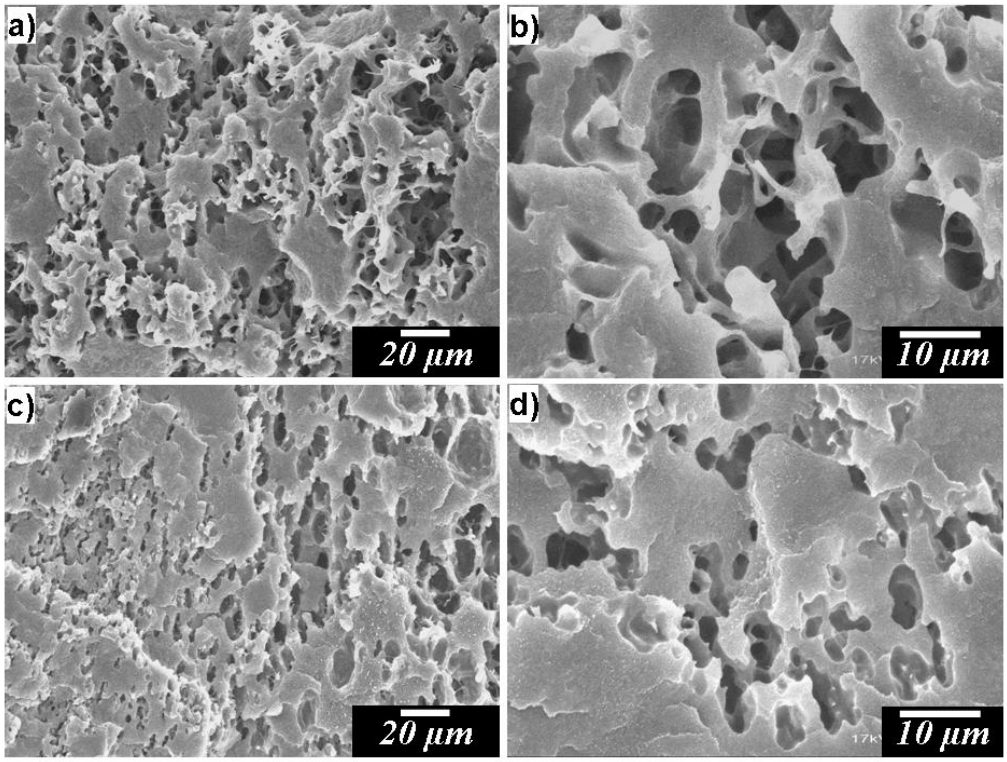

Figure 4.24 SEM micrographs showing SEBS/PP blend foams at 158°C (a) and (b) SEBS (H1062)/PP50; (c) and (d) SEBS (H1043)/PP50.

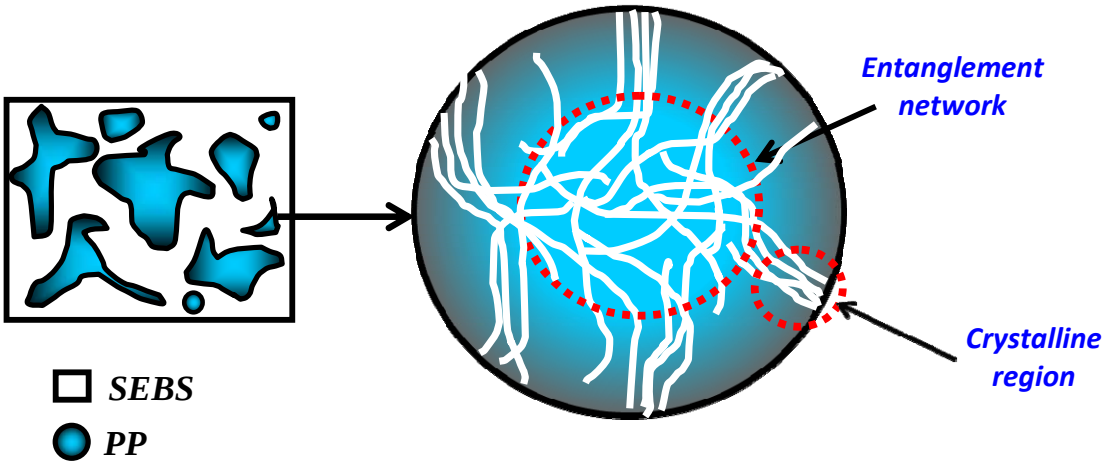

Figure 4.25 Schematic representation of entanglement network in PP.

Even though the foam shrinkage in SEBS was successfully reduced by adding PS and PP, there is a limitation of using those thermoplastic polymers. The controllability of foam shrinkage is highly dependent on cross linked chains between SEBS and PS or PP. The controllability of this foam shrinkage however is become ineffective due to disentanglement of those cross linked chains at temperature above the T_g and T_m of PS and PP, respectively.

The effect of cross linked chains on the controllability of foam shrinkage in SEBS/PS and SEBS/PP blends was investigated by foaming the samples at temperature above the T_g of PS and near to T_m of PP. The cell structures of SEBS/PS blends foamed at 120ºC verified the decreased in controllability of PS on the foam shrinkage. For the case of SEBS/PP (50/50) foamed at 158ºC, the limitation of controlling the foam shrinkage was due to the deformation of rigid entanglement network between amorphous and crystalline phase in PP itself. The results showed that the limitation in controlling the foam shrinkage is based on the T_g and T_m of PS and PP.

4.3.7 Discussion

In accord with the foam shrinkage of SEBS (H1062) at elevated temperatures, adding thermoplastic polymer like PP and PS into SEBS (H1062) appears advantageous. They provided better control of cell growth through enhancement elasticity and reduction CO_2 diffusivity of sample. For the case of blending with PS, the controllability of foam shrinkage is reduced at temperature above the T_g of PS. In order to have better controllability on foam shrinkage at higher foaming temperature, blending with PP is preferable. It is expected that blending SEBS with PP improved the elasticity which in

turn leads to the reduction of foam shrinkage. High concentration of PP was successfully reduced the foam shrinkage of SEBS (H1062) at 155ºC.

Another concern regarding to the controllability of foam shrinkage is the permeability of gas inside the cell. SEBS (H1062) cell was shrunk at any foaming temperature used in this study and thus, narrowing the foaming window for SEBS (H1062). Foam density of SEBS (H1062) showed a rapid increased within 5 minutes and it was remained unchanged after 5 minutes. However, SEBS (H1062) blend foams showed improved foamability and lower foam shrinkage as compared to SEBS (H1062) alone. This result is verified by the increment of foam density after 5 minutes. Thus, it was indicated that the presence of PS and PP slower down the shrinkage as well as improved the foamability due to longer retention of gas in the cell. As shown in the plots of diffusivity and permeability of SEBS (H1062) as a function of PS and PP contents, respectively, the CO_2 diffusivity of SEBS (H1062) was reduced by blending.

Low permeation of blowing gas in cell helps to stabilize the polymer foam. This is because imbalance in pressure inside and outside the cells results to the dimensional stability problem.[23] Rubbery polymer for example, possesses higher diffusion rates to penetrating gas molecules compared to glassy polymer. This is because the energy required to produce microcavity for gas molecules to diffuse into is relatively low. Therefore, blending SEBS (H1062) with glassy polymer like PS is one of the effective approaches to improve the gas retention in cell and thereby minimize the foam shrinkage. For the case of SEBS (H1062)/PP blends, the permeation rate of CO_2 was also reduced due to the presence of crystalline phase. The compact polymeric chain of crystalline domains hindered the transport of CO_2 gas out from the cell.[24]

Through manipulation of blend composition, temperature and rheological properties, foam shrinkage could be controlled whereby dictates the final cell properties of crosslinked material. As shown by foaming results, high elasticity and low diffusivity are essential for controlling the cell expansion. The optimum viscoelasticity is generally a compromise between sufficient plasticity for bubble growth and sufficient elasticity to stabilize the foam once it has expanded. This study proposes an ideal foaming process of thermoplastic elastomer by controlling the elasticity and CO_2 diffusivity. If the elasticity is too high, the chain mobility is highly restricted. Thereby, cell cannot be generated or grow due to over elasticity. However, if the elasticity is too low due to the disentanglement of physical crosslink, cell growth will be dominant and resulted to cell collapse. In between of this state, the ideal foaming process could be achieved to allow the foaming process is progressing well.

Thus, it is worth mentioning that the preparation of stable SEBS foam is possible perhaps, through the utilization of thermoplastic polymer like PP and PS as well as increasing the styrene% in the SEBS. This is essential to reduce the foam shrinkage and to enhance the cell properties, which reflected by high elasticity as well as low CO_2 diffusivity.

4.4 Conclusion

With regards to the shrinkage of SEBS (H1062) cell at high foaming temperature, simple blending with 50 wt% of PP allows the controllability of bubble nucleation and growth by considering the enhancement of its elasticity and reduction of diffusivity. Moreover, the viscoelastic nature of thermoplastic PP serves the SEBS (H1062) with an appropriate resistance to control the bubble growth by its crystalline phase, and thereby

facilitates a technique to reach fine cell properties of thermoplastic elastomer foam product. Such systems can easily been exerting by controlling the foaming temperature, rheological behavior and blend composition. As blending technique improved the elasticity as well as the interface between two phases induced heterogeneous bubble nucleation, the cell growth can be controlled and cell coalescence is reduced. Instead of blending with thermoplastic polymer, the enhancement of thermoplastic elastomer foamability could also be achieved through increasing the styrene chain segment. High styrene% in SEBS (H1043) improves the controllability of cell growth over the SEBS (H1062) through its higher elasticity and plasticity by restricting the cell expansion.

4.5 References

[1] P. G. Pape, *J. of Vinyl & Additive Tech.*, **2000**, 6 (1), 49.

[2] A. K. Pikaev, *High Energy Chemistry*, **2002**, 36 (3), 135.

[3] K. A. Dubey, Y. K. Bhardwaj, C. V. Chaudhari, S. Bhattacharya, S. K. Gupta, S. Sabharwal, *J. of Polym. Sci.*, **2006**, 44, 1676.

[4] N. Barie, M. Rapp, H. J. Ache, *Sensors and Actuators B*, **1998**, 97, 103.

[5] D. Nwabunma,K. J. Kim, Y. Lin, L. C. Chien, T. Kyu, *Macromolecules*, **1998**, 31, 6806.

[6] A. Kajii, S. Okumura, K. Taki, *Proceedings of the 67th SPE Annual Technical Conference*, **2009**,

[7] P. Liu, D. Liu, H. Zhou, P. Fan, W. Xu, *J. of App. Polym. Sci.*, **2009**, 113, 3590.

[8] R. Giri, M. S. Sureshkumar, K. Naskar, Y. K. Bharadwa, K. S. S. Sarma, S. Sabhrwal, G. B. Nando, *Adv. in Polym. Tech.*, **2008**, 27 (2) 99.

[9] N. N. Najib, Z. M. Ariff, A. A. Bakar, C. S. Sipaut, *Materials and Design*, **2011**, 32, 505.

[10] Z. M. Ariff, Z. Zakaria, L. H. Tay, S. Y. Lee, *J. of App. Polym. Sci.*, **2008**, 107, 2531.

[11] R. L. Fan, Y. Zhang, F. Li, Y. X. Zhang, K. Sun, Y. Z. Fan, *Polym. Testing*, **2001**, 20, 2001.

[12] A. Sahnoune, *J. of Cellular Plastics*, **2001**, 37, 149.

[13] M. S. Kim, C. C. Park, S. R. Chowdhury, G. H. Kim, *J. Of App. Polym. Sci.*, **2004**, 94, 2212.

[14] H. J. Tai, *J. of Polym. Research*, **2005**, 12, 457.

[15] R. Gendron, C. Vachon, *J. of Cellular Plastics*, **2003**, 39, 117.

[16] R. Gendron, C. Vachon, *J. of Cellular Plastics*, **2003**, 39, 71.

[17] S. Takahashi, H. A. Goldberg, C. A. Feeney, D. P. Karim, M. Farrell, K. O. Leary, D. R. Pau, *Polymer*, **2006**, 47, 3083.

[18] Y. Zhao, H. X. Huang, Y. K. Chen, *Polym. Bull*, **2010**, 64, 291.

[19] S. Li, P. K. Jarvela, P. A. Jarvela, *Polym. Eng. and Sci.*, **1997**, 37, 18.

[20] W. A. Kaplan, R. L. Tabor, *J. of Reinforced Plastics and Composites*, **1994**, 13, 155.

[21] J. A. de Sales, P. S. O. Patricio, J. C. Machado, G. G. Silva, D. Windmoller, *J. of Membrane Sci.*, **2008**, 310, 129.

Chapter V

General Conclusion

Most commercial polymer foam products acquire desirable properties like tensile strength, flame retardance, toughness, reduced cost, improved cell properties, and etc. The two systems considered in previous researches are mainly on polymer blend (polymer/polymer), nanocomposite (polymer/inorganic particle) and polymer/block copolymer systems where the addition of those secondary constituents into polymers gives a profound impact on cell properties and cell structures. The primary motivation of adding secondary constituent into polymer is to produce high cell density foam through inducing heterogeneous nucleation. Various types of inorganic particles as nucleating agents in polymer foaming have been reported in literature. For example, the use of inorganic particle like clay in polymer foaming reveals the significance success in increased cell density over homopolymer foam. However, this system can have some drawbacks. As reported from previous studies, the use of inorganic particles as nucleating agents seemed ineffective due to their aggregations in some cases.

As regards to this problem, this study is focusing on the foaming of incompatible polymer blend system. Prior to foaming process, the main objective is to distribute the dispersed domain uniformly as well as to produce dispersion of small domain size on polymer matrix. In this work, the controllability of bubble location and nucleation based on polymers' physical properties is studied to investigate how this factor influences the foaming behavior of selective blend systems and discuss the significant impact of controlling the bubble nucleation and location on cell properties as well as cell structures

that benefit from the use of polymer blend systems. As reported in previous chapters, the location of bubble is controlled in the following phases:

i. Chapter 2- at polymer interface
ii. Chapter 3- in dispersed domain
iii. Chapter 4- in matrix phase

5.1. Controlling Bubble Nucleation at Polymer Interface (Chapter 2)

The motivation of this chapter is to enhance the cell properties of PS and PMMA foams in solid-state foaming. The cell properties that can be improved include cell size, cell density and cell size distribution. The reason of blending PS and PMMA with PP is to induce heterogeneous nucleation at polymer interface as an alternative system to inorganic particle/polymer blend system. The advantages of using polymer/polymer system as compared to inorganic particle/polymer system are:

i. Distribution of dispersed domain on polymer matrix can be controlled by viscosity and temperature;
ii. bubble nucleation is controllable in any phases based on physical properties' of polymers such as viscosity and CO_2 solubility and diffusivity; and
iii. appropriate foaming conditions can be chosen by referring to the T_g or T_m of polymers used.

In chapter 2, two pairs of polymer blends are studied namely PS/PP and PMMA/PP where PS and PMMA formed a matrix phases while PP formed a dispersed domain. The unique cell structures of PS/PP and PMMA/PP foams reveal the role of PP dispersed domain as nucleating agent in the PS and PMMA solid-state foaming, as evidenced by

the increased cell densities in both blend foams. The use of PP is preferable because its dispersibility on polymer matrix is controllable. In addition, due to higher CO_2 solubility and diffusivity, PP could act as CO_2 reservoir and releaser.

Figure 5.1 shows the cell structure of PMMA/PP foam at 100ºC and 10 MPa. The cell structure clearly shows that bubble was successfully located at the interface, while PP remained as particle. PP acted as nucleating agent due to its high stiffness, and maintained its original shape during foaming is carried out.

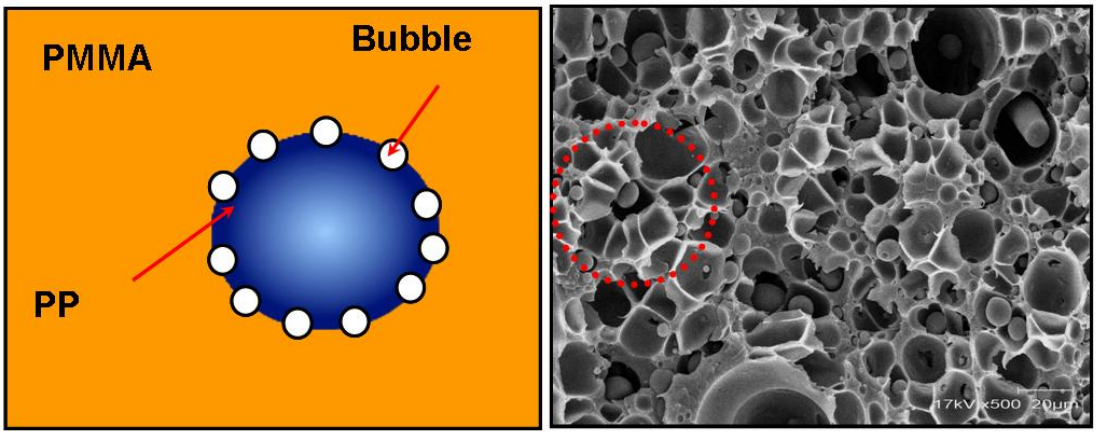

Figure 5.1 Schematic representation of bubble nucleated at polymer interface of PMMA/PP blend foam.

High interfacial tensions between PS/PP as well as PMMA/PP can affect the location of nucleated bubble in both blend systems. Based on the generalization made with respect to the change in the bubble nucleation sites by the relative values of the various interfacial tension;

If both $\gamma_A < \gamma_B + \gamma_{AB}$ and $\gamma_B < \gamma_A + \gamma_{AB}$ are hold,

The bubble nucleation is more favorable to be located at the interface. Regarding to the above-mentioned formula, the stabilities of bubbles in polymer A (PP) and polymer B (PS or PMMA) were lower as compared to at the interface between polymer A and B, which reflected by low energy needed to nucleate the bubble in both polymers. Thus, bubble was more stable at the interface of PS/PP and PMMA/PP as depicted schematically in Figure 5.2.

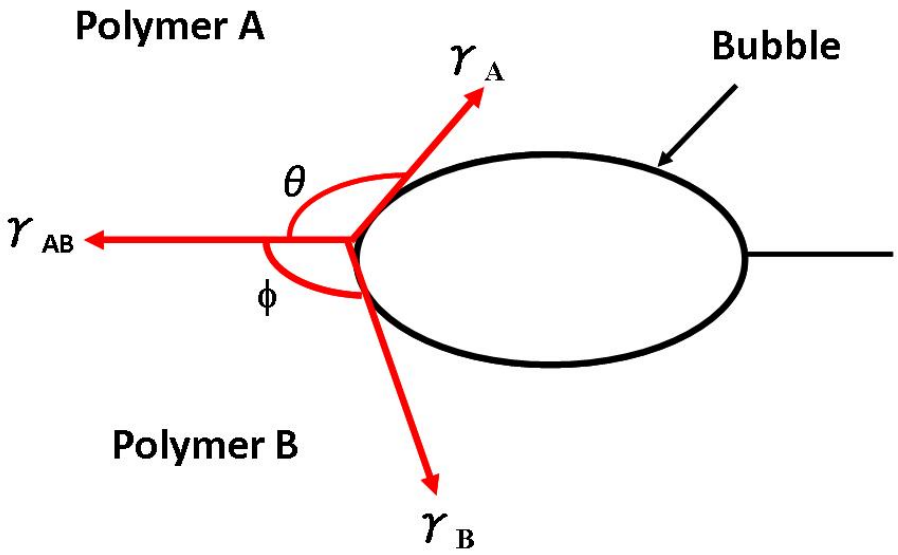

Figure 5.2 Schematic nucleation model in polymer blend.

Although bubble was successfully controlled at the interface due to high interfacial tension between matrix and dispersed domain phases, other impact of high interfacial tension on the cell structure was identified. In both PS/PP and PMMA/PP blend systems, the formation of spaces between PS/PP and PMMA/PP was resulted from the diffusion of CO_2 from the matrix and the dispersed domain into the weak adhere interfaces. This

process was taken place after heterogeneous nucleation, depicted schematically for illustrative purpose in Figure 5.3.

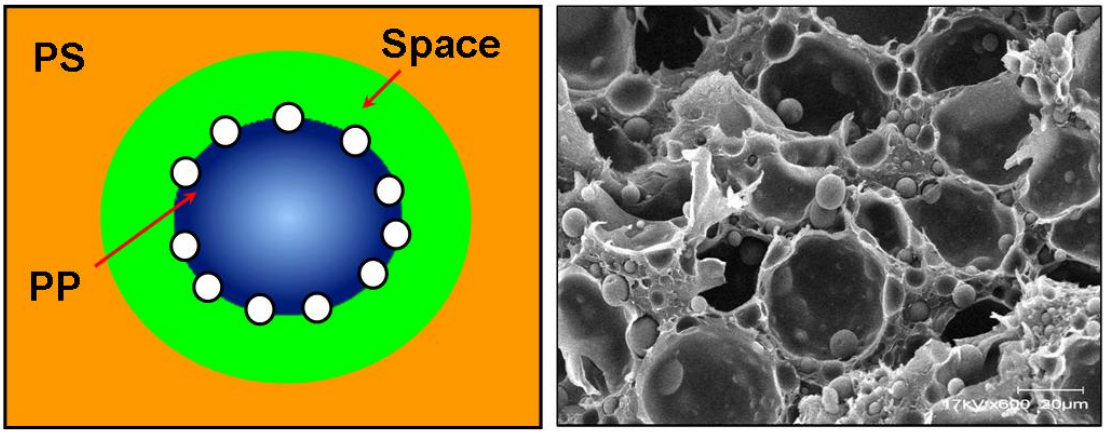

Figure 5.3 Schematic representation of void space formation in PS/PP foam.

Overall, this chapter demonstrates the impacts of high interfacial tension on the cell structures of PS/PP and PMMA/PP blends. It is important to recognize that high interfacial tension can significantly influences the nucleation of bubble at the interface and the formation of the space between matrix and dispersed domain. Although the aim of this study is to control the bubble nucleation at the interface was succeed, further work is clearly needed to control the formation of the space. This is because the formation of this space reduced the availability of CO_2 for bubble nucleation. Since high interfacial tension is the key factor in controlling both nucleation and space formation, compatibilization of the weak adhere interface capable of controlling the adhesibility between two phases in the presence of compatibilizer such as block or graft copolymers.

5.2. Controlling Bubble Nucleation in Dispersed Domain (Chapter 3)

The objectives of this chapter are to improve the cell properties of PP foam by exploiting SEBS nanoscaled dispersed domain in templating the foaming of PP/SEBS blend, as well as to enhance the mechanical properties of PP foam in terms of yield and ultimate stresses by inducing PP crystallization with CO_2.

This work utilizes microphase-separated block copolymer/ polymer blend system with the size of dispersed domain approximately 500 nm in diameter. The expected properties that can be improved in PP foam through exploitation of this SEBS nanoscaled dispersed domain include cell size, cell uniformity, cell density and foaming window for PP foaming. The use of low elasticity SEBS dispersed domain in the preparation of PP foam is beneficial because bubble is easily nucleated in dispersed domain than in PP matrix. Figure 5.5-a shows the schematic representation of the preparation of microcellular or nanocellular foam based on viscoelasticity and CO_2 solubility of polymers. By considering sea and island morphology which consists of two polymers with different viscosity and CO_2 solubility, higher concentration of CO_2 as well as lower viscoelasticity in island (dispersed domain) as compared to in sea (matrix phase) make bubble is easily nucleated at island. This idea of creating a microcellular or nanocellular foams was utilized in this study to control bubble nucleation in SEBS dispersed domain. By controlling the dispersion of SEBS dispersed domain on PP matrix, high cell uniformity could be achieved, depicted schematically in Figure 5.5-b. The addition of SEBS improves the cell uniformity because of its tiny size and highly dispersed in PP matrix leads to small cell size without eliminating the effect of CO_2-induced crystallization.

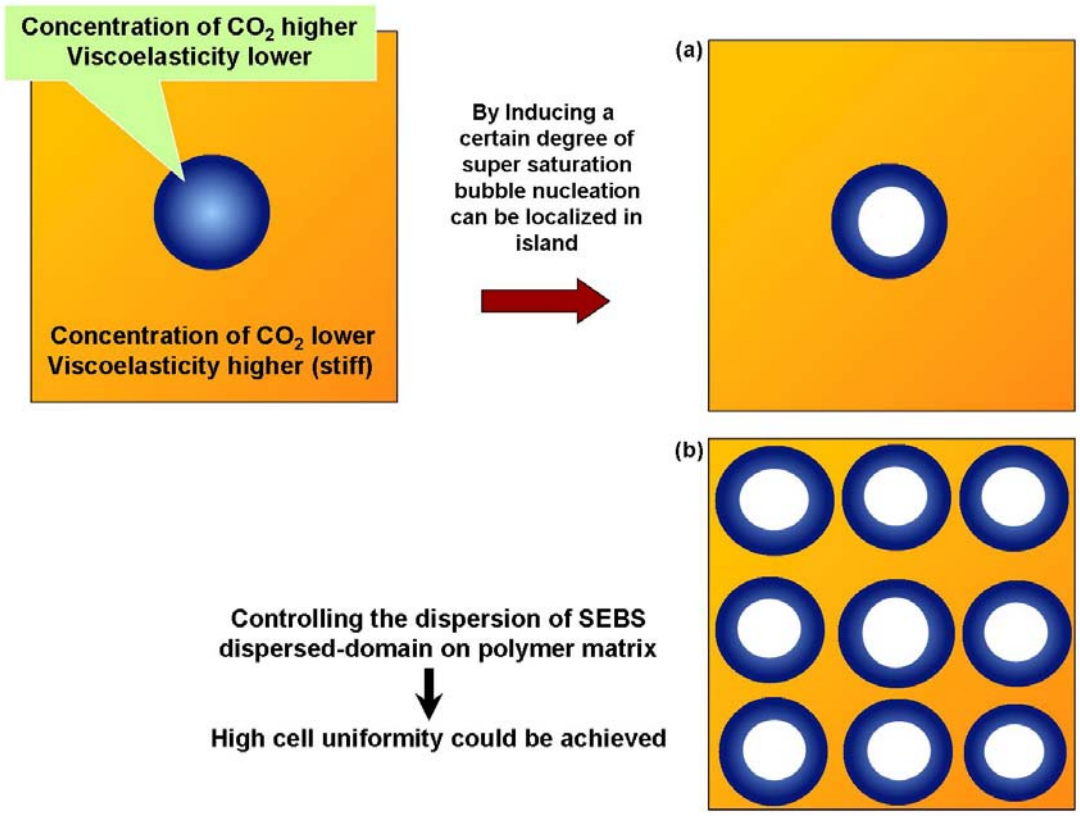

Figure 5.4 Schematic representation of preparation of microcellular/nanocellular foams.

Nanocellular foaming requires the presence of well-dispersed nanoscaled species like block or graft copolymers as dispersed domain in polymer matrix. During depressurization, by inducing a certain degree of supersaturation, the resulted size of cell nucleated in dispersed domain probably would have a size typically 100 nm to <10 μm as compared to in microcellular foam in the range of >10 μm to <1mm. Some literatures have been repeatedly show that CO_2 capable to induce crystallization in a wide variety of homopolymer systems. This study therefore, utilizes CO_2- induced crystallization approach together with nanocellular foaming to prepare high strength polyolefin-based nanocellular foam. This is because CO_2 annealing can improves PP crystallinity through

promoting the change in PP crystallization. CO_2 molecules act as lubricating agents that increases chain mobility, thereby allowing the thickening of the crystalline lamellae.

Crystallization of neat PP and PP/SEBS blend after annealing with CO_2 has been examined by differential scanning calorimetry (DSC) and X-ray diffractomer (XRD). Exposure the samples to CO_2 by annealing process resulted in the formation of new γ-form crystal as well as formation of the thickened crystalline lamellae (Figure 5.5). DSC thermograms of the neat PP and the blend PP after annealing revealed the formation of these two features as illustrated in Figure 5.6. The endotherm indicates T_m values (~175ºC) higher than that of neat PP (160ºC). The results of DSC thermograms also confirmed that changes in PP crystallinity and crystalline morphology are highly affected by CO_2 sorption temperature where annealing the PP/SEBS blend at ambient temperature resulted to no change in PP crystallization. This is confirmed by no formation of new peak as well as no shifting in T_m peak.

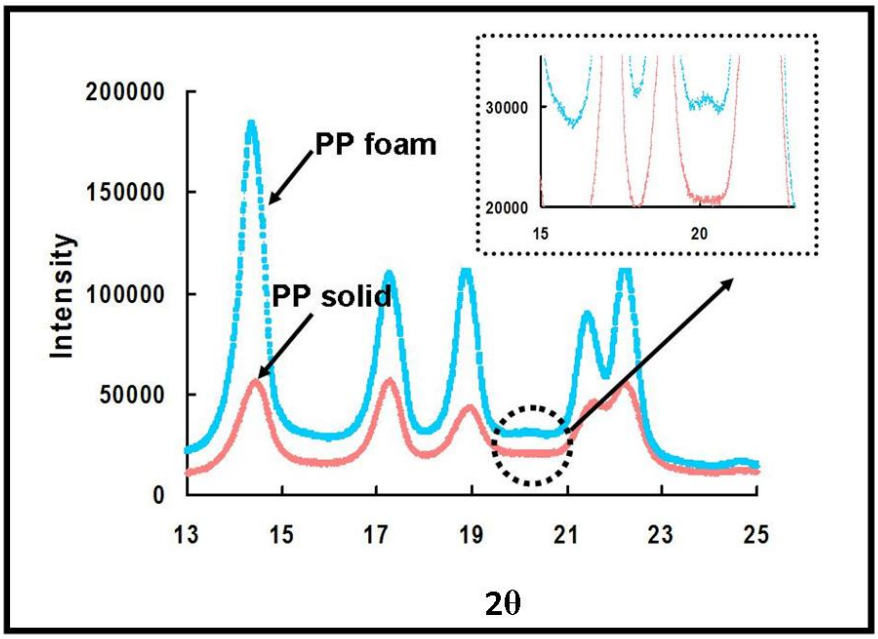

Figure 5.5 XRD patterns of PP solid and PP foam.

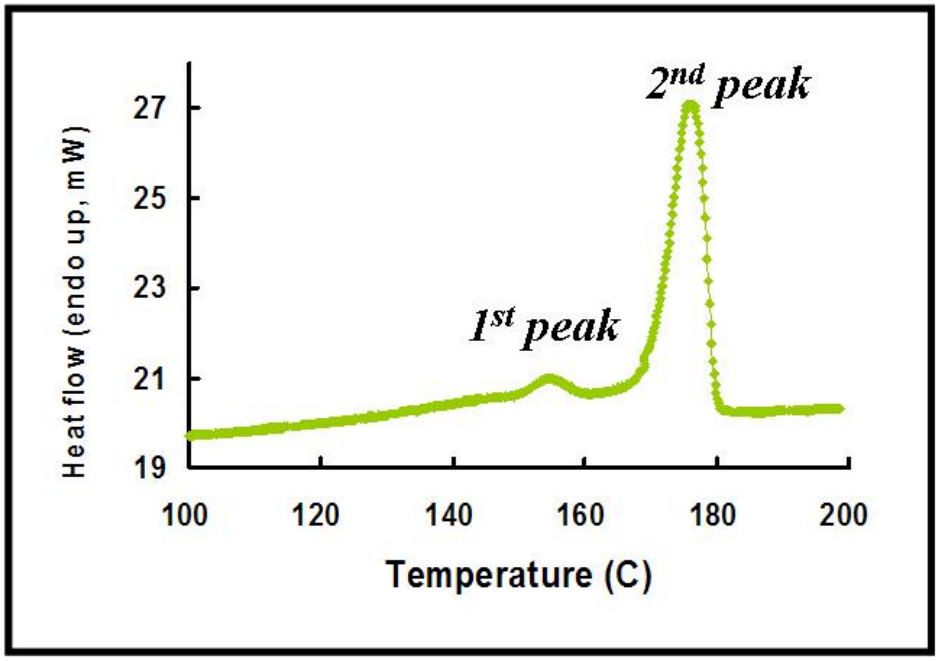

Figure 5.6 DSC thermogram of PP foam.

In general, this study shows that CO_2-induced crystallization improves the mechanical properties of PP foam over the solid PP. This enhancement was also observed in PP/SEBS blend foam. Blending process does not eliminate the effect of CO_2-induced PP crystallization, and thus the enhancement of mechanical properties could also be achieved in blend sample. In addition to CO_2-induced crystallization effect, controlling the bubble nucleation in SEBS dispersed domain, foam product with small cell size, high cell density, high cell uniformity and high strength can be prepared.

5.3. Controlling Bubble Nucleation in Matrix Phase (Chapter 4)

The primary motivation of chapter 4 is to prepare stable SEBS blends microcellular foam by controlling their shrinkages. This study considers polymers' physical properties include elasticity, CO_2 solubility and diffusivity as critical factors for controlling the foam shrinkage in SEBS blends foaming. Thus the bubble nucleation is aimed to be located in SEBS matrix. The addition of high elastic PS and PP polymers as a dispersed domain makes bubble is easily nucleated in SEBS matrix (Illustrative figure shown in Figure 5.7).

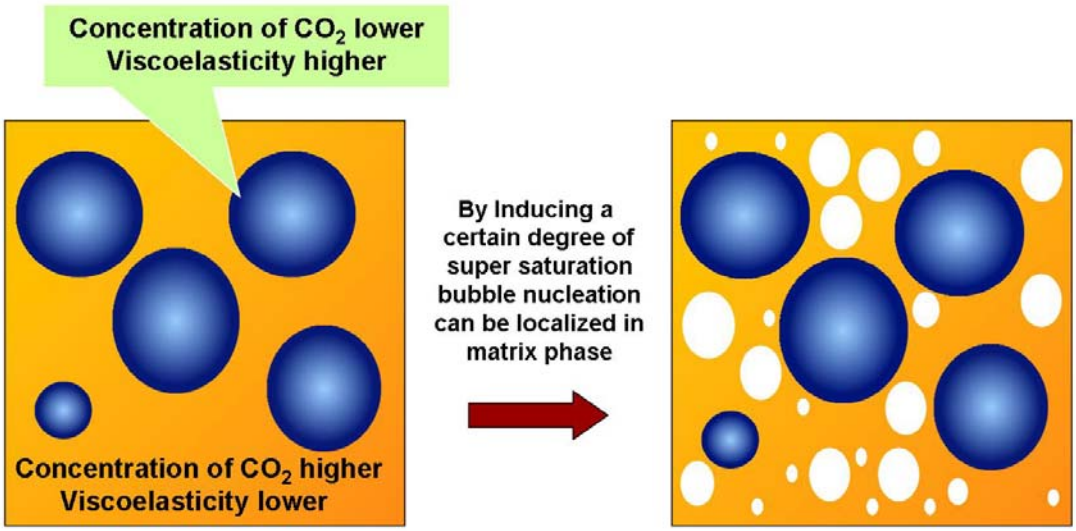

Figure 5.7 Schematic representation of bubble nucleation in matrix phase based on viscoelasticity and CO_2 solubility.

Experimental evidences such as rheological behavior and CO_2 diffusivity measurements of neat PS, PP and SEBS confirmed that blending process can substantially decrease the degree of shrinkage in SEBS blend foams by increasing the

elasticity and reducing the CO_2 diffusivity. For instance, the reduction of CO_2 diffusivity with increasing PS and PP contents resulted in a significant reduction of the foam shrinkage. This is because, PS or PP dispersed domains hindered the transport of CO_2 gas and thus, increased the CO_2 gas trapped within the SEBS closed cell as illustrated in Figure 5.8.

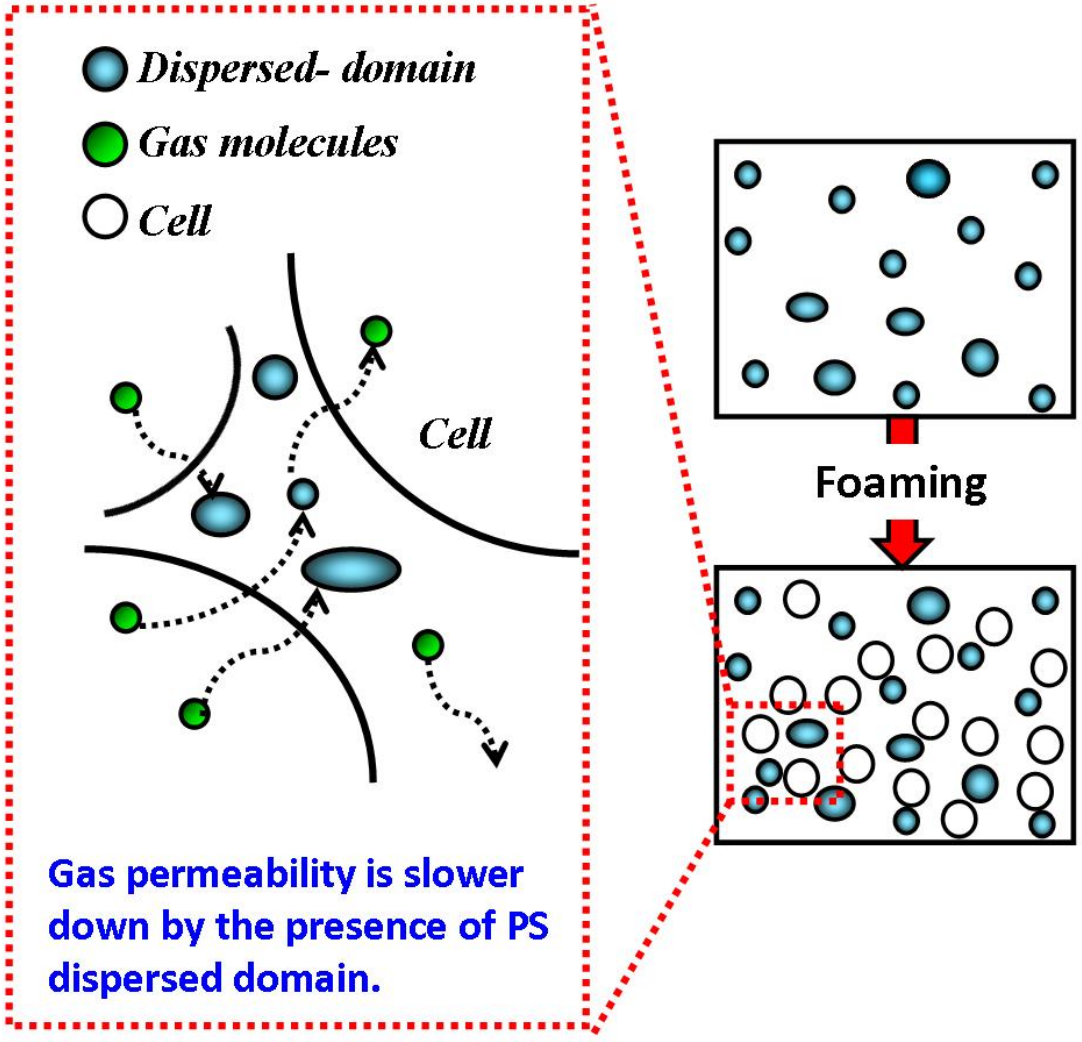

Figure 5.8 Schematic representation of gas diffusion through SEBS cell with the presence of dispersed domains.

Instead of controlling the CO_2 diffusivity, elasticity was also an important factor in controlling the foam shrinkage. Regarding to the foam shrinkage which was occurred in SEBS, it was believed that low elasticity of SEBS resulted to dimensional instability problem. In order to control the foam shrinkage in SEBS blends, controlling the elasticity was very essential in reducing the foam shrinkage. Figure 5.9 shows the schematic diagram of ideal foaming of crosslinked polymer blend such as SEBS/PP and SEBS/PS based on controlling the elasticity. If the elasticity was too high, bubble could not be nucleated. However, if the elasticity was too low, there will be a tendency to have bubble collapse. The optimum elasticity was required in order to have fine cell properties. Therefore, the ratio of blending is essential to take into consideration to ensure that the optimum elasticity for ideal foaming process of crosslinked blend polymers is achieved

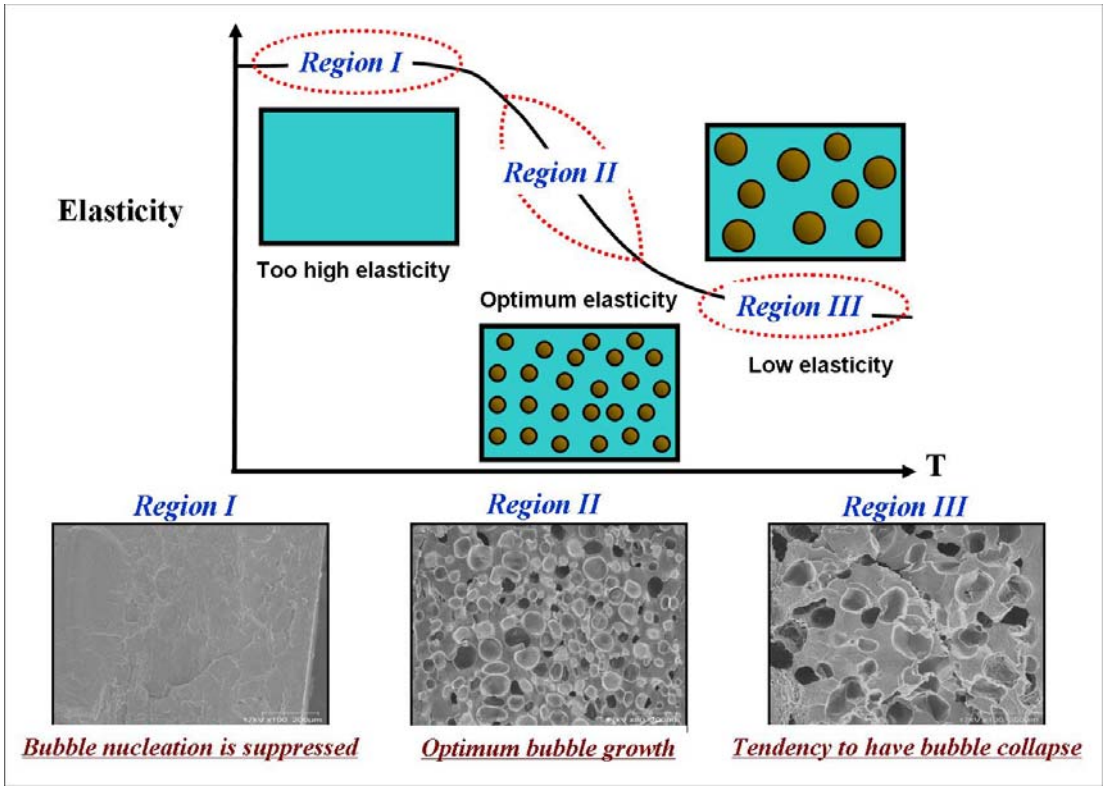

Figure 5.9 Schematic diagram of ideal foaming of crosslinked polymer blend.

The improved foamability and reduced foam shrinkage of SEBS blends upon CO_2 foaming have been attributed to enhancement of elasticity and reduction of CO_2 diffusivity of the blend samples. Blends of SEBS with PS and PP have been successfully foamed into structures with a stable cell dimensions at temperatures below their T_g and T_m, respectively. The formation of unstable dimension cells in SEBS/PS and SEBS/PP foams at temperature above the T_g of PS and near to T_m of PP indicates that there is a limitation in using thermoplastic polymer for controlling the foam shrinkage. Since foam shrinkage in SEBS with PS is difficult to be controlled at high temperature because its low elasticity and high CO_2 diffusivity, SEBS with PP affords a favorable blending alternative as far as the foaming temperature is below its T_m.

5.4. Conclusion

The controllability of bubble nucleation is very important. This is because bubble nucleation which becomes the critical process in foaming is highly determines the cell properties of final foam products. The idea of utilizing nucleating agent to increase the bubble nucleation rate has been well practiced in conventional foaming process. The key factor to produce high cell density foam is forming an interface in the polymer/gas solution by adding foreign body known as nucleating agent. High nucleation rates have been achieved through the heterogeneous nucleation induced by nucleating agent. However for some cases, the uses of inorganic nucleating agents such as talc or clay for enhancing cell density were ineffective due to agglomeration problem. Considering the fact that some inorganic nucleating agents unable to well-distribute in polymer matrix, the use of polymer/polymer system has been considered as an alternatives by taking the advantages of polymer are easily obtainable, good dispersibility in polymer matrix and its viscosity is controllable by temperature.

In this dissertation, a concept of controlling bubble location and nucleation based on polymers' physical properties and processing parameters was introduced for improving the cell properties and cell structure of polymer blend foams. Various pairs of polymer blends are foamed by using supercritical CO_2 and their foaming behavior are controlled by manipulating the processing parameters like temperature, pressure and pressure drop rate as well as the physical properties of polymers. In each chapter, the key factors in controlling the foaming behavior were summarized as follows.

In chapter II, the improvement of cell properties in PS/PP and PMMA/PP blend foams has been identified due to the presence of PP dispersed domain as a nucleating

agent for PS and PMMA solid-state foaming. The interfaces between PS/PP and PMMA/PP led to the reduction of activation energy barrier for bubble nucleation due to heterogeneous nucleation and also led to the formation of space between matrix and dispersed domain phases. PP was a good candidate as nucleating agent for PS and PMMA foaming because it is easily obtainable, its dispersibility could be controlled by viscosity and temperature, and it could act as CO_2 reservoir and releaser.

Chapter III related to the study of CO_2-induced PP crystallization reinforces the mechanical properties of polyolefin-based nanocellular foam. Using the effects of CO_2 on PP crystallization and nanocellular foaming technique, foam with higher yield and ultimate stresses as compared to the solid one was successfully prepared. The crystalline lamellaes of PP and PP/SEBS samples in pressurized CO_2 were thickened during CO_2 annealing. As a result, their yield and the ultimate stresses were increased. The combination technique of CO_2-induced crystallization and nanocellular foaming provides new approach to enhance the mechanical strength of foam sample compared to the solid ones.

In chapter IV, blending SEBS with high elastic thermoplastic polymer like PP and PS improved the permeability of CO_2 as well as elasticity which are among the most important factors in controlling the cell stabilization. Foam shrinkage which is the main problem in SEBS foaming could be reduced by controlling the diffusivity of CO_2 to keep the total pressure inside the cell and thus improved the cell stabilization. The experimental results indicated the addition of PP and PS into SEBS reduces the CO_2 permeation rate and increases the elasticity through blending is beneficial for controlling the foam shrinkage.

Polymer blend is a common process in polymer processing area. However, controlling bubble location and nucleation in polymer blend is not widely reported in literature. In parallel to explore the potential of polymer blend foaming, this study was carried out to enhance control over the cellular structure based on polymers' physical properties and processing parameters. This study aimed to provide a novel concept of controlling the bubble nucleation and location for the purpose of enhancing cell properties and cell structures. Thus, it is expected that this study will contributes to the development of polymer blend foaming research area and also contributes to a continued growth of foamed polymer blend into new markets.

5.5. Future Outlook

The study of PP as a nucleating agent for PS and PMMA solid-state foaming focused on the effects of weak adhere interface (represented by high interfacial tension) on the cell structures of PS/PP and PMMA/PP foams. The experimental results showed that the weak adhere interface induced heterogeneous nucleation and also acted as channel for CO_2 diffusion, which resulted to the formation of space between matrix and dispersed domain phases. Regarding to this space formation, it was probably due to CO_2 from matrix and dispersed domain were diffused into the interface. Thus, it is needed to verify this phenomenon by controlling the adhesibility of this interface. Block or graft copolymers as compatibilizers can be utilized to control the adhesibility of polymers' interfaces. A better adhesibility between PS and PP as well as PMMA and PP might be achieved by blending with block copolymer containing the PS and PMMA core components for example. To study the effect of polymer's adhesibility on CO_2 diffusion, the ratio of core components can be verified.

List of Figures

List of Tables

Acknowledgement

I acknowledge Kyoto University, University of Technology MARA and Ministry of Higher Education, Malaysia.

I would like to express my sincere gratitude and appreciation to my advisor, Professor Masahiro Ohshima for giving me a valuable opportunity to work in foaming research area, for his encouragement, support, expert guidance and mentorship. Special thanks and respects to, Associate Professor Shinsuke Nagamine and Assistant Professor Kentaro Taki for their endless support, guidance and fruitful discussion. I would also like to thank Professor Minoru Miyahara and Professor Ryoichi Yamamoto for reading this dissertation and offering valuable comments.

My beloved parents, brothers and sisters. I appreciate your support throughout the whole life.

Not to be forgotten, dearest friend who all shared ideas and inspirations.

To all of you, I humbly say,

THANK YOU VERY MUCH.

List of Publications

Chapter 2

R. W. Sharudin, A. Nabil, K. Taki, M. Ohshima, Polypropylene- Dispersed Domain as Potential Nucleating Agent in PS and PMMA Solid-State Foaming, Journal of Applied Polymer Science, **2011**, 119(2), 1042-1051.

Chapter 3

R. W. Sharudin, M. Ohshima, CO_2-induced Reinforcement of the Mechanical Properties in Polyolefin-based Nanocellular Foams, Macromolecular Materials and Engineering, **2011**, 296(11), 1046-1054.

R. W. Sharudin, M. Ohshima, CO_2-induced Reinforcement of the Mechanical Properties in Polyolefin-based Nanocellular Foams, Best of Macromolecular Journals **2011**, 48- 56 (one of the 12 selected paper from 1200 papers published in the Macromolecular Journals in 2011).

Chapter 4

R. W. Sharudin, M. Ohshima, Preparation of Microcellular Thermoplastic Elastomer Foams from Polystyrene-b-polybutadiene-b-polystyrene (SEBS) and their Blends with Polystyrene. (accepted)

Other Relevant Publication

1. M. Ohshima, R. W. Sharudin, T. Nemoto, J. Takagi, Nanocellular Foams Prepared from Polymer blends, Magazine for the Polymer Industry, Rubber Fiber Plastics (RFP) International/ RADO Gummi GmbH, **2011**, 28-31.

2. M. Ohshima, R. W. Sharudin, T. Nemoto, J. Takagi, Nanocellular Foams Prepared from Polymer blends, [Polymerblend-Schaumstoffe mit einer Zellstruktur im Nanogroβ enbereich] Gummi, Fasern, Kunststoffe, **2011**, Volume 64, Issue 9, 554-558.

3. M. Ohshima, H. Shikuma, R. W. Sharudin, Preparation of Nanocellular Foams, Japan Plastics, **2012**, 2, 11- 15.

International Conferences

1. R. W. Sharudin, N. Abacha, K. Taki, M. Ohshima, Solid-State Foaming of Binary Polymer Blend: Can a Dispersed Domain of Semicrystalline Polymer be Used as a Bubble Nucleating Agent?, FOAMS 2009- 7th International Conference on Foam Processing and Technology, New Jersey, USA (2009).

2. R. W. Sharudin, M. Ohshima, PP/PS/PMMA (80/10/10) Ternary Blend Foaming: Morphology and Cell Structure, Asian Workshop on Polymer Processing, Penang, Malaysia (2009).

3. R. W. Sharudin, M. Ohshima, CO_2- Induced Reinforcement of Mechanical Properties in Polyolefin-Based Nanocellular Foams, The 27th World Congress of the Polymer

Processing Society (PPS-27), Marrakech, Morocco (2011).

4. T. Nemoto, R. W. Sharudin, M. Ohshima, Preparation of Nanocellular Foams (NCF) from Polymer Blends- NCF Provide a Higher Performance than Conventional Foams, The 1st International Conference on Materials Engineering and The 3rd AUN/SEED-Net Regional Conference on Materials, Yogyakarta, Indonesia (2011).

5. M. Ohshima, H. Shikuma, R. W. Sharudin, Preparation of Nanocellular Foams and their Properties, Bayreuth Polymer Symposium, Bayreuth, German (2011).

National Conferences

1. R. W. Sharudin, N. Abacha, K. Taki, M. Ohshima, Foam of PP/PS/PMMA Ternary Blend System- Morphology and Cell Structure, Sekei-Kako, Tokyo, Japan (2009).

2. R. W. Sharudin, N. Abacha, K. Taki, M. Ohshima, PP Dispersed Domain as Nucleating Agent for PS and PMMA Solid-State Foaming, Kyoto Institute Polymer Symposium (KIPS), Kyoto, Japan (2009).

3. R. W. Sharudin, M. Ohshima, CO_2- Induced Reinforcement of Mechanical Property in Polyolefin-Based Nanocellular Foams, Workshop of Material Chemistry Systems Engineering, Kyoto, Japan (2010).